Proceedings

Seminar on

UNCERTAINTIES RELATED TO THE DESIGN AND CONSTRUCTION OF OFFSHORE JACKET STRUCTURES

Copenhagen, May 22, 1986

DANSK VANDBYGNINGSTEKNISK SELSKAB

DANISH SOCIETY OF HYDRAULIC ENGINEERING

v/ H. F. Burcharth, AUC, Sohngårdsholmsvej 57, 9000 Aalborg. Tlf. 08 - 142333
Denmark

Proceedings

Seminar on

UNCERTAINTIES RELATED TO THE DESIGN AND CONSTRUCTION OF OFFSHORE JACKET STRUCTURES

Copenhagen, May 22, 1986

DANSK VANDBYGNINGSTEKNISK SELSKAB

DANISH SOCIETY OF HYDRAULIC ENGINEERING

v/ H. F. Burcharth, AUC, Sohngårdsholmsvej 57, 9000 Aalborg. Tlf. 08 - 142333

Denmark

PREFACE

In structural design one of the important tasks is to evaluate the uncertainties involved in the design procedure and the construction.

The level of uncertainty is closely related to the nature and the state of development of the various technical disciplines. Very often large deviations in levels are a reality, for example between the reliability of parameters related to soil mechanics as opposed to the reliability of some parameters related to structural members.

This volume contains the contributions of invited speakers to a seminar arranged by The Danish Society of Hydraulic Engineering in cooperation with The Danish Society for Structural Science and Engineering, Danish Offshore Technology Services, The Danish Geotechnical Society, and The Danish Society of Naval Architecture and Marine Engineering. The object was to explore the uncertainties related to the design and construction of a typical offshore jacket structure.

The organizers are most grateful to the speakers for their valuable contributions to the seminar.

H.F. Burcharth
President
The Danish Society of Hydraulic Engineering

CONTENTS

VBS Seminar May 1986

ON THE UNCERTAINTIES RELATED TO THE ESTIMATION OF EXTREME ENVIRONMENTAL CONDITION

by

H.F. Burcharth

INTRODUCTION

The calculation of the forces on the structural members of a structure in the sea is based on knowledge of the kinematics of the surrounding water and air. Therefore our goal is to establish some statistics for the related *velocity and acceleration fields.*

If we consider the sea such statistics can be established only with the knowledge of the joint probability density function (j.p.d.f.) related to *waves, current* and *sea level.*

Because waves and currents are described in terms of characteristic parameters as e.g. the significant wave height, H_s or H_{mo}, the mean zero-crossing period, T_z, the mean current velocity over the depth etc. we also need information on *parameter distributions* and *theories for particle kinematics* to make possible the calculation of the related velocity and acceleration fields.

With such information in hand one can in principle calculate the forces on a structural number and establish the j.p.d.f. of the force (moment, shear) and its direction, which again allow the estimation of extreme design values corresponding to some exceedence probability levels.

Besides this we need an evaluation of the uncertainty related to the extreme values.

The j.p.d.f. of waves, current and sea level can only be found with reasonable accuracy either by *direct measurements* on the location on question or by the use of *numerical models* based on meteorological data.

Due to lack of data the author is not able to evaluate the uncertainty related to extreme estimates on the combined wave-current-sea level effect.

In the following discussion of uncertainty only one parameter is dealt with, namely the wave height, which of course is a key parameter. Moreover, only the uncertainty related to estimates on extreme design waves is discussed. This means that uncertainty on long-term wave loads leading to fatigue failures is not included.

SOURCES OF ERROR ON WAVE ESTIMATES

The procedure for establishing the design data is shown in Figure 1. It also renders the many sources of errors. The figure indicates that although we can estimate a design wave in terms of height, period and direction we are still lacking information, physical understanding and theory for the estimation of the related velocity and acceleration fields. For this reason it is of course impossible to evaluate the uncertainties on this very important part of the procedure.

If we look only on the first part of the procedure which leads to the estimation of some extreme value of the significant wave height H_s the sources of errors can be listed as follows:

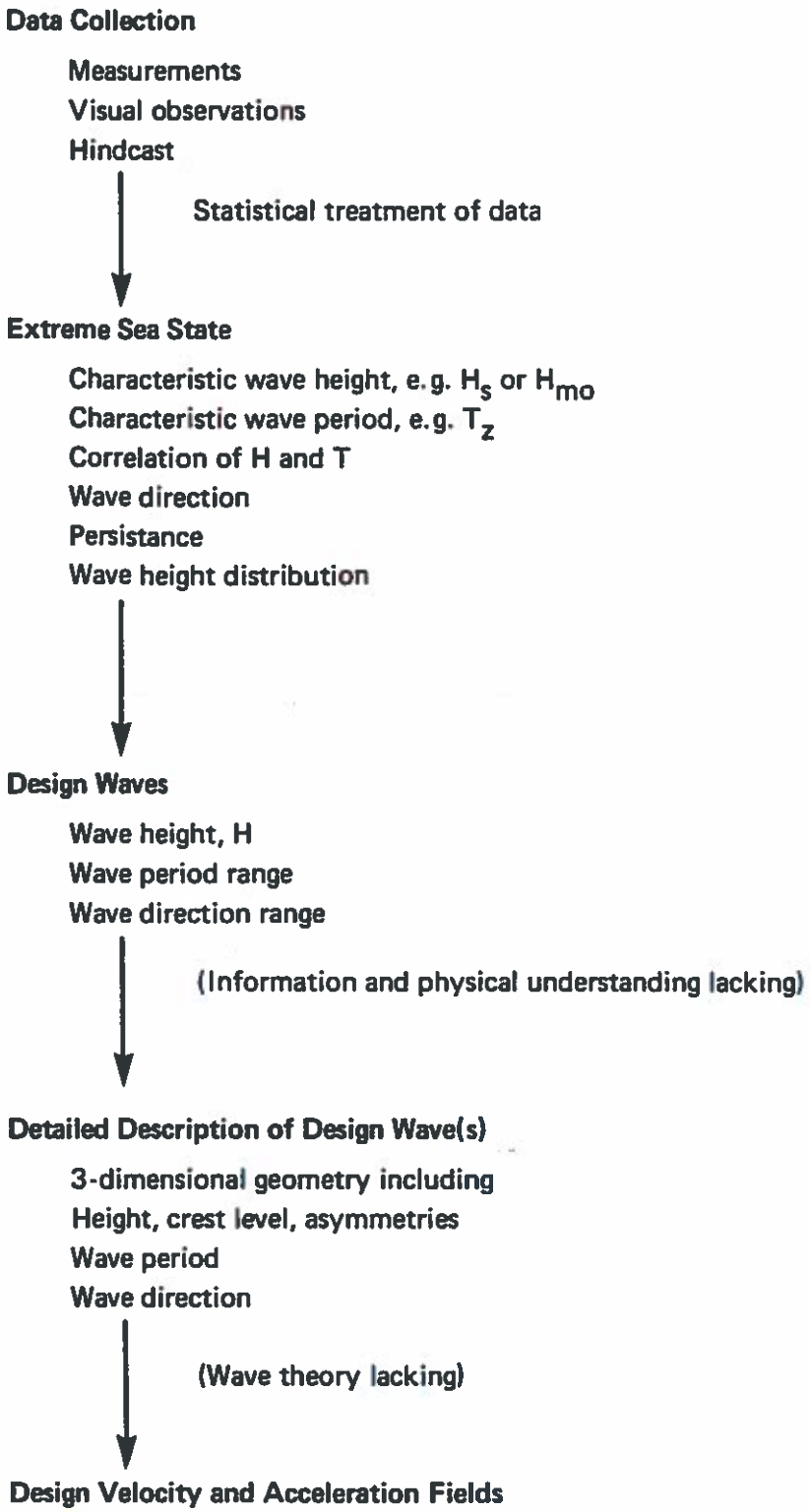

Figure 1. Procedure for establishment of extreme design wave kinematics.

A. Errors in measurements, visual observations or hindcasting of the wave data on which the extreme statistics are based.

B. Errors related to extrapolation from short samples to events of high return periods, i.e. low probability of occurrence.
Errors due to the choice of exceedence level.
Errors due to the method of fitting data to a chosen distribution.

C. Lack of knowledge about the underlying distribution for the extreme events.

D. Errors due to plotting positions.

E. Climatological variations.

ad A. Errors in wave data

Le Mehaute et al., 1984, discussed the uncertainties and systematic errors or bias related to the wave data under the assumption of errors being normally distributed. They reported the following "typical" normalized standard deviation σ' defined as the absolute standard variation divided by the expectation ("mean") value of H_s:

Direct wave measurement	$\sigma'_M = 0.05$	bias 0.00
Visual observations from ships	$\sigma'_M = 0.20$	bias 0.05
Hindcast (excluding hurricanes and other tropical storms)	$\sigma'_M = 0.15$	bias 0.05

It should be noted that the two last set of figures are applicable only when the sample populations are ranked statistically. A direct comparison in the time domain, i.e. comparison of individual sea states, generally shows larger discrepancies. Moreover the figures are average figures. For instance it is believed that wave data based on to-day's most advanced hindcast models applied to relatively restricted areas, such as the North Sea where high quality weather maps are available will show a smaller uncertainty.

Based on comparisons of hindcasts with measurements by Resio and Vincent, 1978; Holthuijsen, 1980; Ewing et al., 1981; Bouws et al., 1982, the following generalized conclusions were stated by Battjes, 1984:

" (a) The development of new wave models or modification of existing ones, in response to the advances made in understanding of the physics of wave generation and propagation, has not (yet) given rise to a correspondingly better performance of these models operatinally. At least two factors contribute to this paradoxical situation. One is the limited quality of the wind input. Another is the fact that models with less realistic modelling of the physics compensate for this with more empiricism. It is not surprising that such models, tuned so as to simulate not only observed growth rates but a condition of saturation as well, are cabable of fairly realistic predictions in the more or less common situations similar to those for which they were tuned. It is to be expected however that the physically better founded models will perform better in more demanding conditions.

(b) For the majority of the models, the overall r.m.s. relative difference between hindcast and observed H_s is in the range 0.2 to 0.3, but the error in the prediction of extreme conditions is smaller by approximately a factor 2 (apart from possible phase

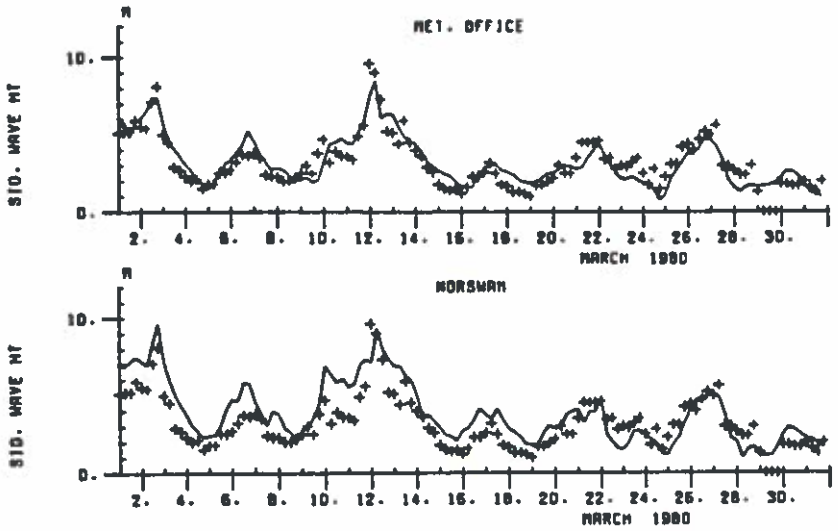

Fig. 4. Measured (+) and hindcast (——) significant wave height at Brent B (Ewing et al., 1981).

errors). An example is shown in Fig. 4 where results of a hybrid model (NORSWAM) and of a discrete model with nonlinear coupling (METOFFICE) are compared to observed H_s-values at the Brent B location. "

ad B. Errors due to short samples.

Estimates on events of low probabilities are often performed in the following two different ways:

1) The extrapolation of data from frequent measurements or observations. The data are often compiled at intervals Δt = 3, 6 or 24 hours, which gives a large sample, N events, even in the case of a short time of observation or record length Y in years. The order of magnitude of N is often 1000 - 10,000.

2) The extrapolation of relatively few data sets representing the max significant wave height H_s for a number of storms exceeding a certain level, H_s'. The data are often determined from hindcasts and the sample size N is typically within the range 10 - 30.

Wang et al., 1983, examined the uncertainties related to the first method. They considered the long term distribution of H_s to be of the exponential type which also includes the often used Weibull distribution,

$$P(H_s) \equiv P[H < H_s] = 1 - \exp\left(-\left(\frac{H_s - A}{B}\right)^{\gamma}\right) \qquad (1)$$

where A is signifying the background noise level or lower-bound, B is the scale parameter and γ is the shape parameter. All three characteristic variables are normally determined by best fitting to the observed data.

Assuming the data asymptotically normally distributed around the underlying probability distribution function, eq (1), the authors obtained for large N the normalized standard deviation,

$$\sigma_s' = \frac{1}{\gamma \ln(R\,\nu)} \left(\frac{R}{Y}\right)^{0.5} \qquad (2)$$

where R is the return period in years, ν is the number of observations per year compiled at interval Δt and Y is the number of years of observations. Formula (2) is valid only for low proba-

bility levels and only for large samples $N = \nu Y$ of uncorrelated data. The latter implies that Δt should exceed approximately 24 hours, but because of little sensitivity on the confidence bands for H_s smaller values, as for example $\Delta t = 6$ hours, are often used.

It is stressed that the data to be used must belong to the same statistical population as the extreme event in question, i.e. wave data must be separated with respect to origin, direction, shoaling effects etc. when relevant.

Example.

Taking R = 50 years, Y = 5 years, ν = 365 observations per year and $\gamma = 1.2$
gives $\sigma_s' = 0.27$

Changing R and Y to 100 years and 3 years respectively
gives $\sigma_s' = 0.46$

The second method mentioned above is relevant to situations where data have to be obtained from hindcasting, which, due to the costs involved, restricts the number of data.

Rosbjerg, 1981, considered this case, where only maximum values η of H_s for independent storms exceeding a chosen level H_s' are taken into consideration, cf. figure 2.

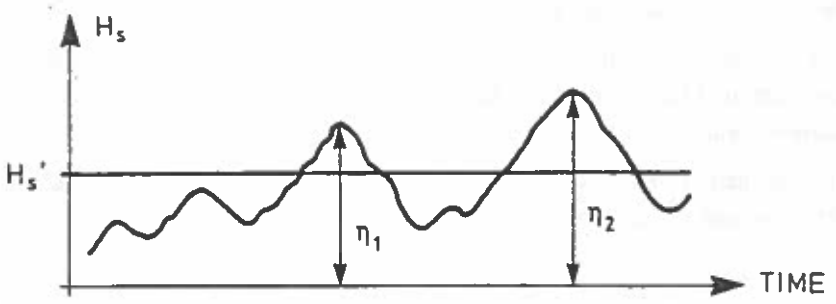

Figure 2. Data reduction by application of exceedence level, H_s'.

Rosbjerg assumed all the exceedences $\eta - H_s'$ to follow the exponential probability distribution,

$$P(H_s) \equiv P[\eta \leq H_s] = 1 - \exp(-\frac{H_s - H_s'}{\alpha}) \tag{3}$$

which is of the same type as the Weibull distribution, eq (1), with $\gamma = 1$.

The author also assumed the events η to occur at times corresponding to a Poisson-process with time dependent intensity. He arrived at the following expression for the R-year event defined as the value of η, which in average is exceeded once every R years,

$$H_s = H_s' + \alpha \ln \nu R \tag{4}$$

The corresponding absolute standard variation is

$$\sigma_s = \frac{\alpha}{(\nu Y)^{0.5}} (1 + (\ln \nu R)^2)^{0.5} \tag{5}$$

and the normalized standard deviation consequently

$$\sigma_s' = \frac{\sigma_s}{H_s} = \frac{\frac{\alpha}{(\nu Y)^{0.5}} (1 + (\ln \nu R)^2)^{0.5}}{H_s' + \alpha \ln \nu R} \tag{6}$$

The maximum likelihood estimate for α is

$$\hat{\alpha} = \bar{\eta} - H_s' \tag{7}$$

where $\bar{\eta}$ means average of η.

Nielsen et al., 1985, extended the analysis to include the Weibull distribution

$$P(H_s) = P[\eta \leq H_s] = 1 - \exp(-(\frac{H_s - H_s'}{\alpha})^{\gamma}) \tag{8}$$

and found the following

$$H_s = H_s' + \alpha(\ln \nu R)^{1/\gamma} \tag{9}$$

$$\sigma_s = (\ln \nu R)^{1/\gamma - 1}\left[\frac{\alpha^2}{\gamma^2 \nu Y} + (\ln \nu R)^2 \frac{\alpha^2}{\nu Y}\left(\frac{\Gamma(1+\frac{2}{\gamma})}{\Gamma^2(1+\frac{1}{\gamma})} - 1\right) + \frac{\alpha^2}{\gamma^4}(\ln \nu R)\cdot \ln(\ln \nu R))^2 \mathrm{Var}[\hat{\gamma}]\right]^{0.5} \tag{10}$$

ν is the average number of data per year and Γ the Gamma function.

The variance of $\hat{\gamma}$, $\mathrm{Var}[\hat{\gamma}]$, cannot easily be estimated, but by means of numerical simulation it is found that the term in (10) containing this quantity is highly dependent on the method for estimating the parameters in the Weibull distribution.

Petrauskas and Aagaard, 1971, found, by using a least square method, that the last term in (10) is insignificant. In this case the normalized standard deviation is

$$\sigma_s' = \frac{\sigma_s}{H_s} \cong \frac{(\ln \nu R)^{\frac{1}{\gamma}-1}\left[\frac{\alpha^2}{\gamma^2 \nu Y} + (\ln \nu R)^2 \frac{\alpha^2}{\nu Y}\left(\frac{\Gamma(1+\frac{2}{\gamma})}{\Gamma^2(1+\frac{1}{\gamma})} - 1\right)\right]}{H_s' + \alpha(\ln \nu R)^{1/\gamma}} \tag{11}$$

Nielsen et al., 1985, fitted the Weibull parameters by the method of moments, i.e. equating the first three moments of the distribution to those of the data, and found that the last term in (10) was of significance, namely in the order of 1/3 of the total standard deviation. The estimates on the parameter by the applied method of moments are given by

$$\frac{\Gamma(1+\frac{3}{\hat{\gamma}}) - 3\Gamma(1+\frac{2}{\hat{\gamma}})\Gamma(1+\frac{1}{\hat{\gamma}}) + 2\Gamma^3(1+\frac{1}{\hat{\gamma}})}{(\Gamma(1+\frac{2}{\hat{\gamma}}) - \Gamma^2(1+\frac{1}{\hat{\gamma}}))^{3/2}} = \frac{\overline{\eta^3} - 3\,\overline{\eta^2}\,\bar{\eta} + 2(\bar{\eta})^3}{(\overline{\eta^2} - (\bar{\eta})^2)^{3/2}} \tag{12}$$

$$\hat{\alpha}^2 = \frac{\overline{\eta^2} - (\bar{\eta})^2}{\Gamma(1+\frac{2}{\hat{\gamma}}) - \Gamma^2(1+\frac{1}{\hat{\gamma}})} \tag{13}$$

$$\hat{H}_s' = \bar{\eta} - \hat{\alpha}\,\Gamma(1-\frac{1}{\hat{\gamma}}) \tag{14}$$

$\overline{\eta^2}$ and $\overline{\eta^3}$ mean the average of sample values of η^2 and η^3, respectively, which are unbiased estimates of $E[\eta^2]$ and $E[\eta^3]$.

Eqs (1), (6) and (11) make it possible to determine the necessary sample length when a prediction for a given return period with a prescribed accuracy and confidence is required. If we assume that the dispersion of the sample variables is normal distributed around the underlying probability distribution function then it is possible to determine the control curves corresponding to various confidence limits, see e.g. Wang et al., 1983. The limits 0.84 σ_s', 1.28 σ_s', 1.65 σ_s' and 2.32 σ_s' define the *upper* bound of spread corresponding to a confidence level of 80%, 90%, 95% and 99% respectively. For instance, the prediction of an event with 90% confidence (i.e. 90% of the observations should fall below the upper bound control curve) and an uncertainty of no more than 0.20 implies that 1.28 $\sigma_s' \leqslant 0.20$. Inserting this in eqs (1), (6) and (11) gives the corresponding number of years of observation Y for given ν and R.

Example.
The accuracy of estimates based on a restricted number of hindcasted data sets might be illustrated by the following example. The Delft Hydraulics Laboratory made a hindcast study for a specific deep water location in the Mediterranean Sea and found for a 20 years period the following 17 most severe storms, Table 1:

Table 1. Example of hindcasted storm wave data for a 20 years' period.

Rank i	Max H_s ($= \eta$) metres	Peak period T_p seconds	Average wave direction degrees
1	9.32	14.0	143
2	8.11	14.1	139
3	7.19	13.4	123
4	7.06	10.8	123
5	6.37	11.9	143
6	6.15	11.1	185
7	6.03	12.3	135
8	5.72	10.5	176
9	4.92	10.7	150
10	4.90	10.6	129
11	4.78	11.8	161
12	4.67	9.9	120
13	4.64	9.2	122
14	4.19	10.5	137
15	3.06	11.1	154
16	2.73	8.2	153
17	2.33	8.3	126

If we choose $H_s' = 4.0$ m we find N = 14 storms exceeding this level over a period Y = 20 years, which gives $\nu = 14/20$. According to eq (7) α can be estimated to $\hat{\alpha} = 2.00$ m. It can now be tested if the data follow the assessed distribution, for example the exponential type given by eq (3). In this case a straight line with slope 1:1 should be obtained by plotting $\eta_i - H_s'$ against $-\hat{\alpha} \ln(1 - P(\tilde{\eta}_i))$, where $P(\tilde{\eta}_i) = 1 - \frac{i}{N+1}$, (Gumbel plotting positions). Figure 3 shows that the fit is reasonable.

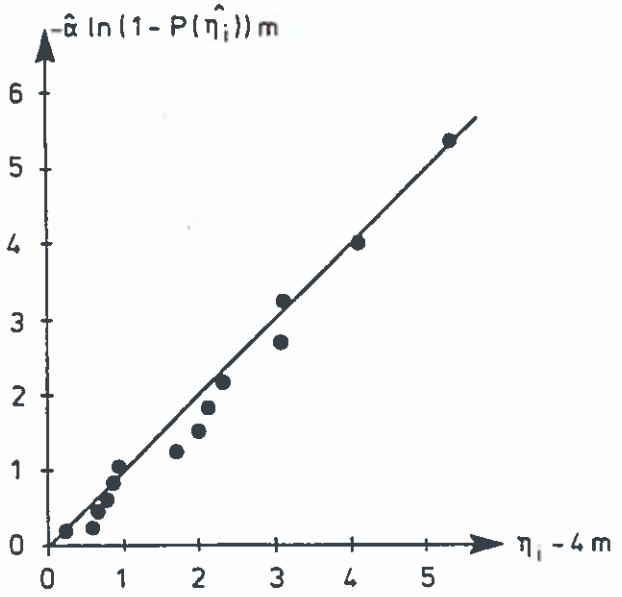

Figure 3. Test on exponential distribution of wave height exceedences.

Formulae (4) - (6) are then valid and the expectation values and the standard deviations can be calculated for various return periods, for instance

Return period R years	H_s metres	σ_s metres	σ_s'
50	11.11	1.97	0.18
100	12.50	2.33	0.19

Note that a change in the exceedence level H_s' for example to 3.50 m, which still gives N = 14, will change H_s and σ_s significantly since for R = 50 years H_s = 12.39 m, σ_s = 2.47 m, σ' = 0.20 and for R = 100 years H_s = 14.12 m, σ_s = 2.92 m, σ' = 0.21 m. This important problem is not discussed further here.

It is obvious that the 14 data points also fit a Weibull distribution.

If all the 17 data points given in Table 1 are considered, it corresponds to a exceedence level of $H_s' \cong 2.25$ m because the lowest value in the data set is H_s = 2.33 m. It turns out that in this case the data do not fit neither the exponential distribution, eq (13), nor the Weibull distribution, eq (8). However, if the exceedence level is not interpreted as the physically true cut-off level, but is regarded a fitting coefficient only, like α and γ, then the 17 data points follow the Weibull distribution very closely, as demonstrated in Figure 4. The coefficients are in this case H_s' = 0.73 m, α = 5.27 m and γ = 2.80, all estimated by the method of moments.

From eqs (9) - (11) we obtain the following corresponding values

Return period R years	H_s metres	σ_s metres	σ_s'
50	9.19	0.88	0.10
100	9.71	0.97	0.10

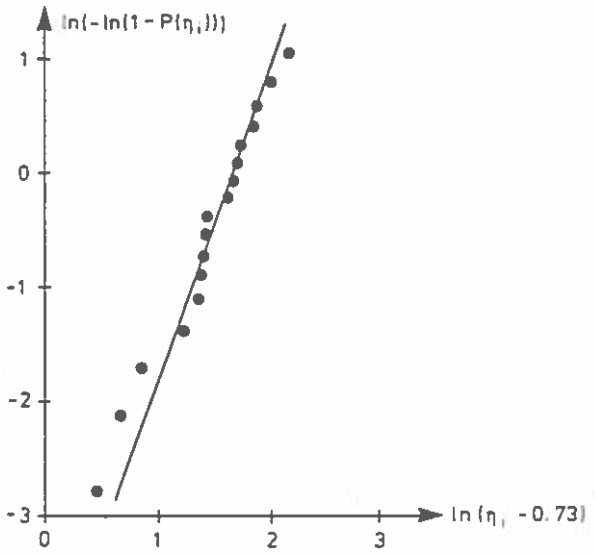

Figure 4. Data fit to the Weibull distribution. Gumbel plotting positions.

The Weibull distribution shown by the straight line in Figure 4 is a result of the chosen method of fitting. A least square fit or a visual fit will produce different lines and different estimates on the extreme events.

Thus it is concluded that also the choise of exceedence level and the method of fitting the data to a chosen distribution introduce uncertainty on the estimates of extremes.

As discussed previously the confidence limits for an extreme estimate can be determined under certain assumptions. Figure 5 illustrates this by showing an example of the variation of the 80% probability control curves corresponding to various return periods for the data in Table 1 of which the 14 largest storms follow the exponential probability distribution, eq (3), cf. Fig. 3.

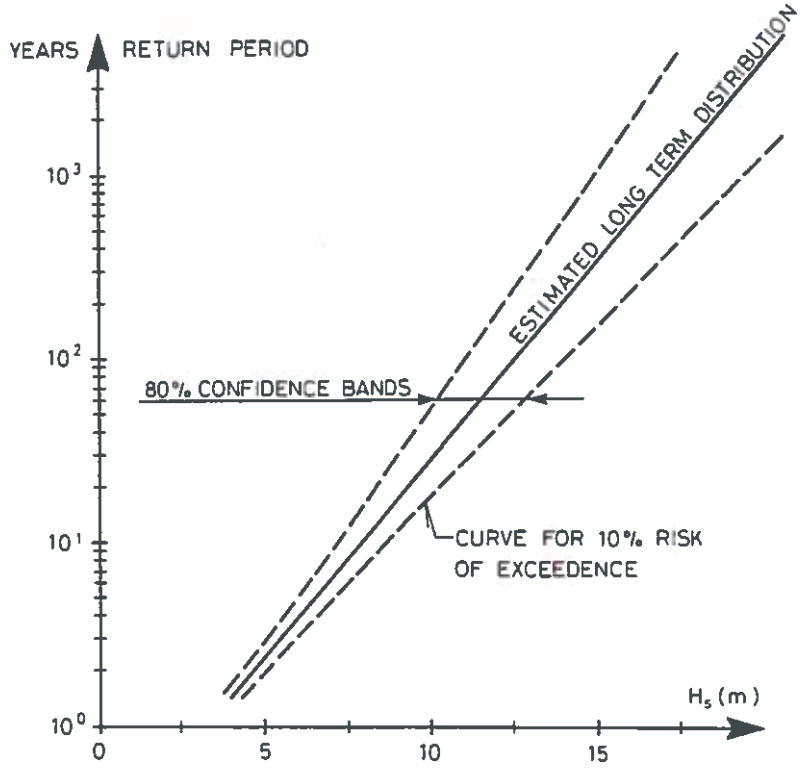

Figure 5. Example of 80% probability control curves for a data set of 14 storms in a 20 years' period.

The figure clearly shows the positive influence of a longer period of observation.

When evaluating the *R-year event* (the return period R), it is very important to notice that this event has a probability E of being equalled or exceeded (encounter probability) in the specific lifetime L of the structure.

The relationship is

$$E = 1 - (1 - \frac{1}{R})^{L} \tag{15}$$

which in the case of large R can be approximated

$$R = -\frac{L}{\ln(1 - E)}$$

The encounter probability is illustrated in Figure 6, which shows that for a specific long term storm wave history a structure with a 20 years' lifetime might experience very different wave loads dependent on the actual location in time.

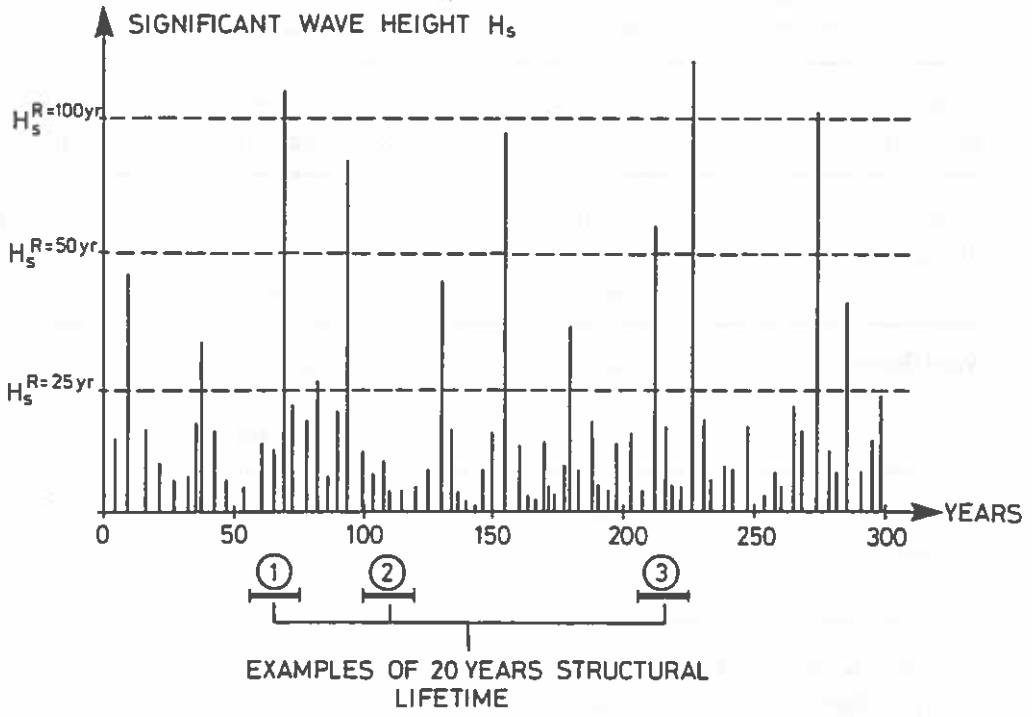

Figure 6. Illustration of encounter probability.

If for example the structural lifetime is 20 years and a 10% exceedence probability is acceptable the structure must be designed for the 190 years' event, R = 190 years. If the lifetime is increased to 50 years the design level rises correspondingly to R = 500 years.

Many offshore structures with an estimated lifetime of 20 years are designed for the 50 years' event which implies an exceedence probability as high as 33%. Using as an example from Figure 5 the upper bound 80% probability curves means a design H_s of 12.5 m. But if for the same structure an encounter probability of 10% corresponding to R = 190 years is applied then the design H_s increases to 15.4 m.

ad C. and D. Errors due to the lack of knowledge on the true long term distribution and due to plotting positions.

Several probability distributions are used to describe extreme wave height statistics. These include for example the log-normal distribution, the extremal type I or Gumbel or Fisher-Tippett I distribution, the extremal type II or Fretchet or Fisher-Tippett II distribution, the Ward-Borgman distribution and the extremal type III or Weibull distribution. Although each of these distributions has a theoretical base, they cannot be evaluated and related to the extreme waves on a physical base. As a consequence they are only fits to the available data. Most often the scales used for the plotting are such that the chosen distribution lies on a straight line, simply because of the more convenient visualization of the extrapolation. However, when extrapolating, one should always be aware of possible physical processes, such as for example wave breaking, which might interrupt the probability distribution at some probability level.

It follows from these comments that due to unknown extreme distribution errors can only be estimated by a sensitivity analysis in which various distributions are fitted. Table 2 shows such an analysis by the Delft Hydraulics Laboratory performed on the wave data given in Table 1.

Table 2. Example of influence of choise of extremal distribution and plotting position on low-probability wave heights. Data by Delft Hydraulics Laboratory.

Extremal distribution	Plotting position	Correlation coefficient	Return period H_s 50 year	100 year
Type I Gumbel	Gumbel	0.9875	11.0 m	12.2 m
	Gringorten	0.9852	10.3 m	11.3 m
Ward/Borgman	Gumbel	0.9872	9.8 m	10.5 m
	Gringorten	0.9920	9.4 m	10.1 m
Type III Weibull	Gumbel	0.9877	9.6 m	10.2 m
	Gringorten	0.9877	9.3 m	9.9 m

Although no accurate figures can be given it seems reasonable from this table and the above given example based on the distribution, eq (3), that due to unknown extreme distribution a normalized standard deviation σ'_D might be in the order of

$$\sigma'_D \cong 0.05 - 0.10.$$

for return periods of approximately 50 to 100 years, progressively increasing as the return period increases.

In order to plot the data a position formula must be adopted. Many different plotting positions, all based on some statistical considerations, exist, but it is not easy or possible to select a specific one as the most correct. For this reason it is reasonable to estimate the error due to plotting positions by sensitivity analyses involving a number of reasonable plotting rules.

Table 2 gives an example where only two plotting rules are used, namely

Gumbel/Weibull
$$P(\eta_i) = 1 - \frac{i}{N+1} \tag{16}$$

and

Gringorten
$$P(\eta_i) = 1 - \frac{i - 0.44}{N + 0.12} \tag{17}$$

It is seen that significant deviations in the estimated extreme wave height occur due to the plotting rules. It is believed that a realistic normalized standard deviation σ'_p on extreme events will be in the order of

$$\sigma'_p \cong 0.05$$

ad E. Errors due to climatological variations.

An additional source of uncertainty is the natural variation of the wave climate. Le Mehaute et al., 1984, considered this difficult problem under the assumption of the natural climatology being ergotic and stationary and governed by the statistical law of Weibull distribution. By setting Y = R in eq (2) they found that the normalized standard deviation of climatological variations in R years at a particular location is given by

$$\sigma'_C = \frac{1}{\gamma \ln(R\,\nu)} \tag{18}$$

If for instance we estimate $\gamma \cong 1.2$ as proposed by the authors we find for $\nu = 365$ and R = 50 or 100 years $\sigma'_C \cong 0.08$.

Combined errors.

The above mentioned sources of uncertainty can be assumed mutually independent except for an unknown but probably weak correlation between the climatological variation and the data samples.

The total normalized standard deviation might then be estimated by

$$\sigma' \cong (\sigma'^{\,2}_M + \sigma'^{\,2}_s + \sigma'^{\,2}_D + \sigma'^{\,2}_p + \sigma'^{\,2}_C)^{0.5} \tag{19}$$

With reference to the foregoing discussion one can establish the following two examples:

Examples.

Direct wave height measurement. $\nu = 365$ observations per year. Y = 5 years. R = 50 years.

$$\sigma' \cong (0.05^2 + 0.27^2 + 0.07^2 + 0.05^2 + 0.08^2)^{0.5} = 0.30$$

- Hindcasted wave heights. 14 data sets over Y = 20 years. R = 50 years.

$$\sigma' \cong (0.15^2 + 0.18^2 + 0.07^2 + 0.05^2 + 0.08^2)^{0.5} = 0.26$$

From this it is seen that, even with what is generally regarded reasonable lengths of data sample and observation period, the uncertainty related to the 50 years' event is significant and in the order of $\sigma' \cong 0.25 - 0.30$. If we assume normally distributed random variables it means a 16% probability of the wave height being bigger than 1.25 - 1.30 times the estimated height.

The uncertainty increases significantly when the lengths of data sample and the period of observation are reduced to figures below those given above. The uncertainty also increases with the design return period which might very well be well over 50 years, cf. the foregoing discussion on encounter probability.

CONCLUDING REMARKS

As said in the introduction a statistics suitable for the estimation of extreme environmental conditions can be established only with the knowledge of the joint distribution of the key parameters related to waves, current, sea level and wind. However, even when dealing with *one* key parameter, as for example the wave height, the usual shortage of data leads to large uncertainties on estimates of extremes as explained above. When dealing with joint data which are considerably more difficult to obtain, one might expect even larger uncertainties.

To-day it is normal practice to design offshore structures for the simultaneous effect of a certain extreme value of each environmental parameter, i.e. the 50 years' wave, the 50 years' current, the 50 years' wind . . . This of course means that the structure is designed for a total load which has a probability of occurrence less than once in 50 years. Very often this is interpreted as overdesign. However, this is not necessarily the case when one thinks of the large exceedence probability corresponding to a 50 years' return period and a 20 to 50 years' structural safety. How- it might well be that this "conservative" approach leads to a reasonable structural safety. However, the problem is that without knowing the joint distribution of the key parameter we cannot evaluate the safety level. In other words we have no idea about the design load exceedence probability.

Joint data on wind, waves, currents and sea level are difficult to obtain. The most promising approach is to apply numerical hindcast models. However, it should be mentioned that when dealing with multivariate analyses the concept of a return period value has no meaning as it cannot be given a relevant interpretation. Therefore a better way might be to calculate the overall forces in the structure or the stresses in the structure as a combined function of wind, waves, current and sea level and thus reduce the extreme analysis to a single parameter analysis for which the return period concept is applicable.

Two things should be mentioned in this connection. Firstly the fact that the calculation of forces and stresses introduces other sets of uncertainties on top of those related to the environmental parameters. Secondly the observation that the return period concept is not very expedient as it might give biased conceptions because of the strong non-linear relationship between the return period and the key parameter values.

REFERENCES

Battjes, J.A., 1984: A review of methods to establish the wave climate for breakwater design. Coastal engr., 8 (1984) pp 141 - 160.

Le Mehaute, B., Wang, S., 1984: Effects of measurement error on long-term statistics. Proc. 19th Coastal Eng. Conf., pp 347 - 361, Houston, 1984.

Nielsen, S.R.K., Burcharth, H.F., 1985: On the uncertainties related to estimates on Weibull distributed parameters. Note in Danish. Hydraulics & Coastal Engineering Laboratory, Department of Civil Engineering, University of Aalborg, Denmark.

Petrauskas, C., Aagaard, P.M., 1971: Extrapolation of historical storm data for estimating design wave heights. Journal of Society of Petroleum Engineers, Vol. 2, 1971, pp 25 - 35.

Rosbjerg, D., 1981: Estimation af ekstreme bølgefænomener. Lecture note (in Danish). ISVA. Technical University of Denmark.

Wang, S., Le Mehaute, D., 1983: Duration of measurements and long-term wave statistics. Journal of Waterway, Port, Coastal and Ocean Engineering, ASCE, Vol. 109, No. 2, 1983, pp 236 - 247.

UNCERTAINTIES RELATED TO THE ASSESSMENT OF DESIGN WIND, WAVE, AND CURRENT PARAMETERS.

BY

JØRGEN BO NIELSEN

DANISH HYDRAULIC INSTITUTE
DK 2970 HØRSHOLM
DENMARK

ABSTRACT

Since the mid-seventies DHI has been involved in the assessment of environmental design data for offshore constructions in almost all major offshore areas of the world. Most of these studies have been socalled hindcast studies, ie. studies in which numerical models have been used for determining wind, wave, current, and water level conditions during a number of historical storm events. This paper gives some recent examples of results from such studies, focussing mostly on the North Sea. It also gives some rough estimates of the uncertainties attached to design data obtained by these methods.

1. INTRODUCTION

In the early years of offshore exploration, design values of the various environmental parameters (wind, waves, currents, and water levels) often had to be derived from information which by todays standards can only be characterized as inadequate and unreliable. Ships observations covering a large inhomogeneous region or measurements from a single winter season (or sometimes even less than that) are typical examples of the sort of basic data available to the designers of the first offshore jackets. The fact that so far no major disasters can be attributed directly to erroneous design data is either because the engineers of these early construction were prudently conservative in their interpretation of the available data or because too low design values have been outbalanced by margins in other aspects of the desin. Most probably both reasons are involved in some designs.

With the offshore activities moving into deeper water and more harsh environmental conditions, the demand for more reliable design data quite naturally increased. This demand was further increased as the margins of safety on other design aspects were gradually decreased as a function of more fierce competition which led to the development of more advanced design methods.

A feasible way of meeting these increased demands has been through the application of numerical hindcast models. By means of such models it is possible to establish a data coverage back in time as far as reliable meteorological records are

available. Further more, these models give a coverage in space, ie. a spatial resolution which goes far beyond the resolution which can be obtained by any other method.

On the other hand, the numerical models do not completely replace field measurements. Measurements are still needed for the assessment of certain design parameters (eg. the wave crest height) and above all they are needed for calibration and validation of the models. Only through a critical comparison of the model results against high-quality measurements is it possible to give reliable estimates of the uncertainties (eg. in terms of standard deviations) associated with the design parameters resulting from a hindcast study. Accordingly a substantial part of every hindcast study consists of blind-testing the hindcast models against field data which is kept by the client until hindcast results from the same storms have been produced by the modeller. The comparisons shown in this paper are taken from this type of validation excercises.

2. TYPICAL CONTENTS OF A HINDCAST STUDY

A typical hindcast study, whether it aims at hindcasting waves, currents, or water levels or any combination of these parameters, consists of basically the same main tasks. Fig. 2.1 shows these main tasks and a brief description of the contents of some of the tasks is given in the following.

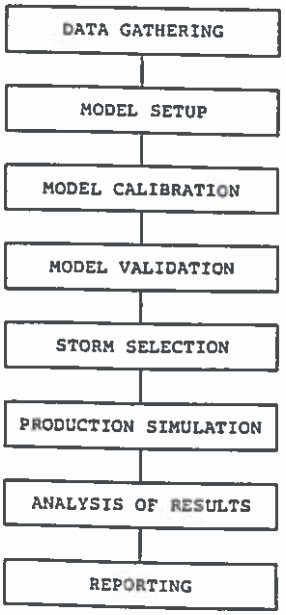

Fig. 2.1 Main Tasks of a Typical Hindcast Study.

Model Calibration

Hindcast models usually contain a number of tuning possibilities which are applied in order to obtain accurate results for the specific problem considered.

By comparing model results with measurements and using these tuning possibilities, the model can be calibrated accurately.

Some models require more calibration than others. In general, an advanced model (ie. a model which incorporates a detailed description of the relevant physical processes) requires less calibration than a more primitive model.

Of the modelling systems developed by DHI for hindcast studies the wave modelling system (SYSTEM 20) usually does not require any tuning at all, while the current/water level modelling system (SYSTEM 21) sometimes requires tuning of the bed resistance coefficient.

Model Validation

As mentioned in the introduction, the model validation is a very important part of any hindcast study. In most cases this validation is carried out as blind tests, ie. the measurements are released by the client after the simulations have been completed, in order to ensure a fully objective assessment of the model performance.

Examples of model validation results are given in the following chapter.

Storm Selection

The selection of storms to be included in the hindcast study is an important and non-trivial task. If some of the truly most severe storms are omitted from the simulations, this will be reflected as errors in the extreme value analysis.

Depending on the area of interest, various techniques can be applied in the ranking of historical storms. Wind recordings, pressure patterns, water level recordings from coastal stations can all be applied.

It should be realized, however, that a certain amount of failures will occur in any such selection procedure. These failures will emerge as hindcast results which are lower than indicated by the ranking procedure. Results from such misselected storms should of course be left out from the statistical analyses.

A method for selection of storms based upon pattern recognition methods has been developed by DHI. When used iteratively together with the hindcast models, the software is able to gradually improve its strategy for selection of storms in an intelligent manner. More details on this "learning system" have been published by Nielsen (1986).

Analysis of Results

The results from the production simulations are analysed statistically in order to arrive at extreme values corresponding to return periods which are usually beyond the time range of the hindcast storms. The statistical analysis is frequently based on a Peaks-Over-Threshold method (POT). This method includes the following main steps:

- Selection of candidate probability distribution(s)
- Estimation of parameters for the selected distribution(s)
- Evaluation of the validity of each candidate distribution by testing the goodness of fit
- Extrapolation to T-year events
- Assessment of standard error associated with T-year events

More details regarding the statistical methods can be found in Nielsen and Kej (1986).

3. EXAMPLES OF MODEL VALIDATION RESULTS.

Wave Model Validation

Fig. 3.1 shows four examples of results from blind tests of DHI's North Sea wave hindcast model. The examples are all taken from a recent study carried out for Phillips Petroleum Company, Norway, dealing with extreme wave conditions at Ekofisk in the central North Sea. Similar examples have been presented for other locations, see eg. Brink-Kjaer and Rodenhuis (1983) or Brink-Kjaer et al (1985).

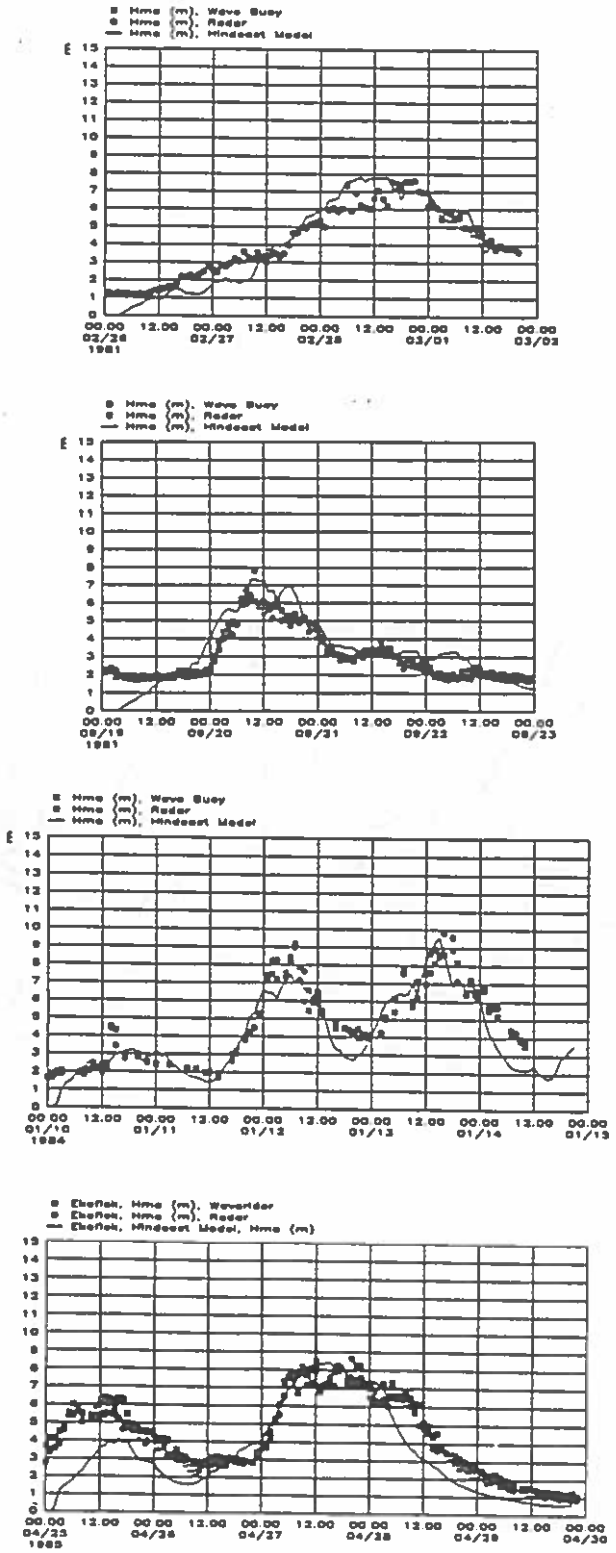

Fig. 3.1 Measured and Hindcast Time Series of Significant Wave Height (Hm0) at Ekofisk During Four Storms.

Depending on the subsequent application of the model results, the validation procedure may focus on different key numbers. For instance, it is common practice to compare peak sea-states for each storm when the assessment of extreme wave heights is the goal of the study.

Fig. 3.2 shows two such comparisons of peak sea-states for two very severe North Sea storms. For each of these two storms field data is availble from several locations covering a range of water depths from approximately 20 to 110 meters. The model results are seen to be in very good agreement with the measurements at all water depths.

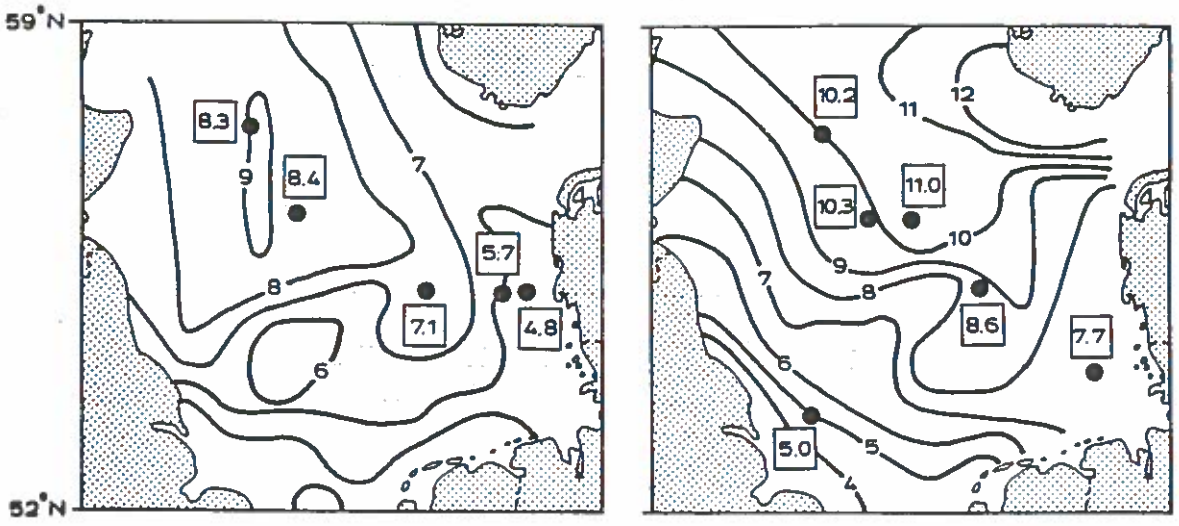

19-21 April 1980

23-25 November 1981

Fig. 3.2 Simulated (isolines) and Recorded (in boxes) Peak Sea-states During Two Severe North Sea Storms.

It should be mentioned that Fig. 3.2 also serves to illustrate the extreme severity of the storm of 23 - 25 November 1981. Peak sea-states (significant wave heights) above 12 meters, corresponding to something like a 100 year event, are hindcast in the deep waters in the Norwegian Trench. This indication of the severity of the storm of 23 - 25 November 1981 is supported by the water level measurements from Esbjerg, which reached the highest level ever recorded over the more than 100 years for which measurements exist.

Validation data for the North Sea Wave model is so far available from a total of 82 storm events, where one event is defined as a comparison at one location for one storm. The comparisons cover the 13 different locations shown in Fig. 3.3.

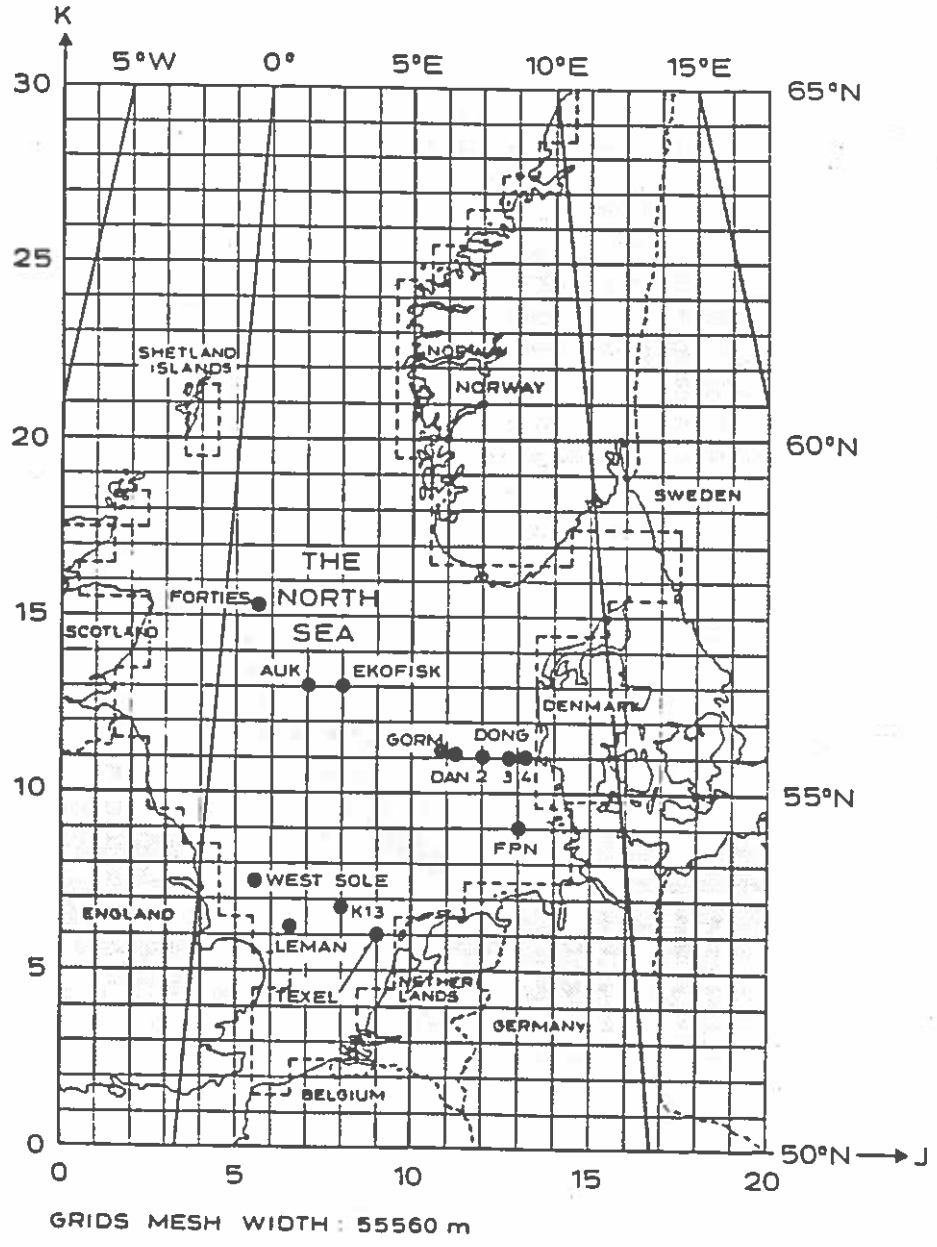

Fig. 3.3 North Sea Wave Model Validation Stations.

Fig. 3.4 shows the peak to peak comparisons for the 82 North Sea storm events. From Fig. 3.4 the model accuracy can be defined in terms of an RMS value:

$$RMS = \sqrt{\sum_{n} \frac{(H_{measured} - H_{model})^2}{n-1}}$$

Using this definition, the overall RMS error of the North Sea wave model is found to be 0.71 m.

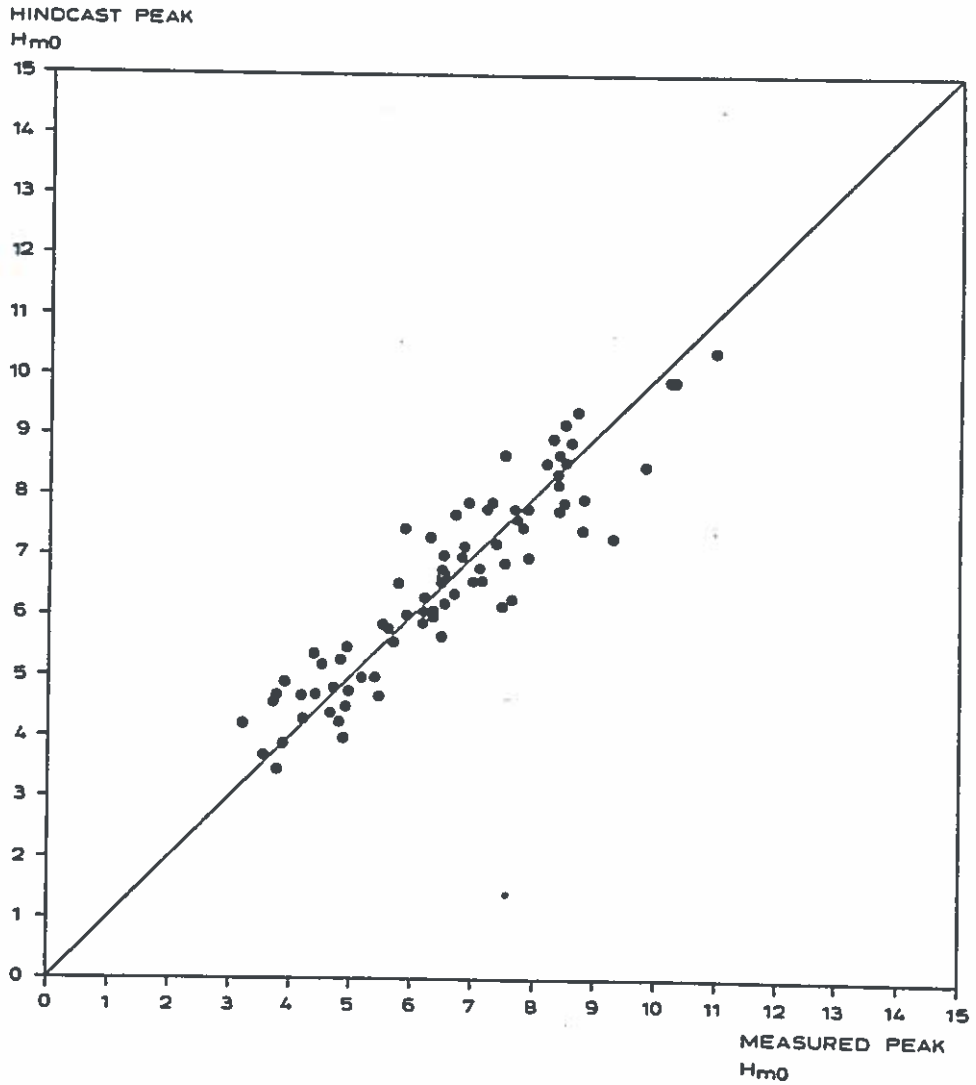

Fig. 3.4 Comparison of Measured and Hindcast Peak Significant Wave Heights for 82 North Sea Validation Storm Events.

For comparison, Fig. 3.5 shows a similar comparison of peak sea-states, only this time the comparison shows results from two different meters located approximately 2 km from each others at Ekofisk. The RMS value of this comparison is 0.80 m, ie. slightly higher than the similar value for the previous comparison. A similar result has been found at Forties in the U.K. sector in a recent study for BP International. The main conclusion which can be drawn from these results is that the errors associated with the use of a good wave hindcast model using good input winds is comparable to the errors associated with the use of measured data of the type which is traditionally recorded at most platform based data gathering systems. More details on the Ekofisk study can be found in Brink-Kjaer et al (1986) and Nielsen et al (1987), while the BP study is described in Nielsen et al (1986).

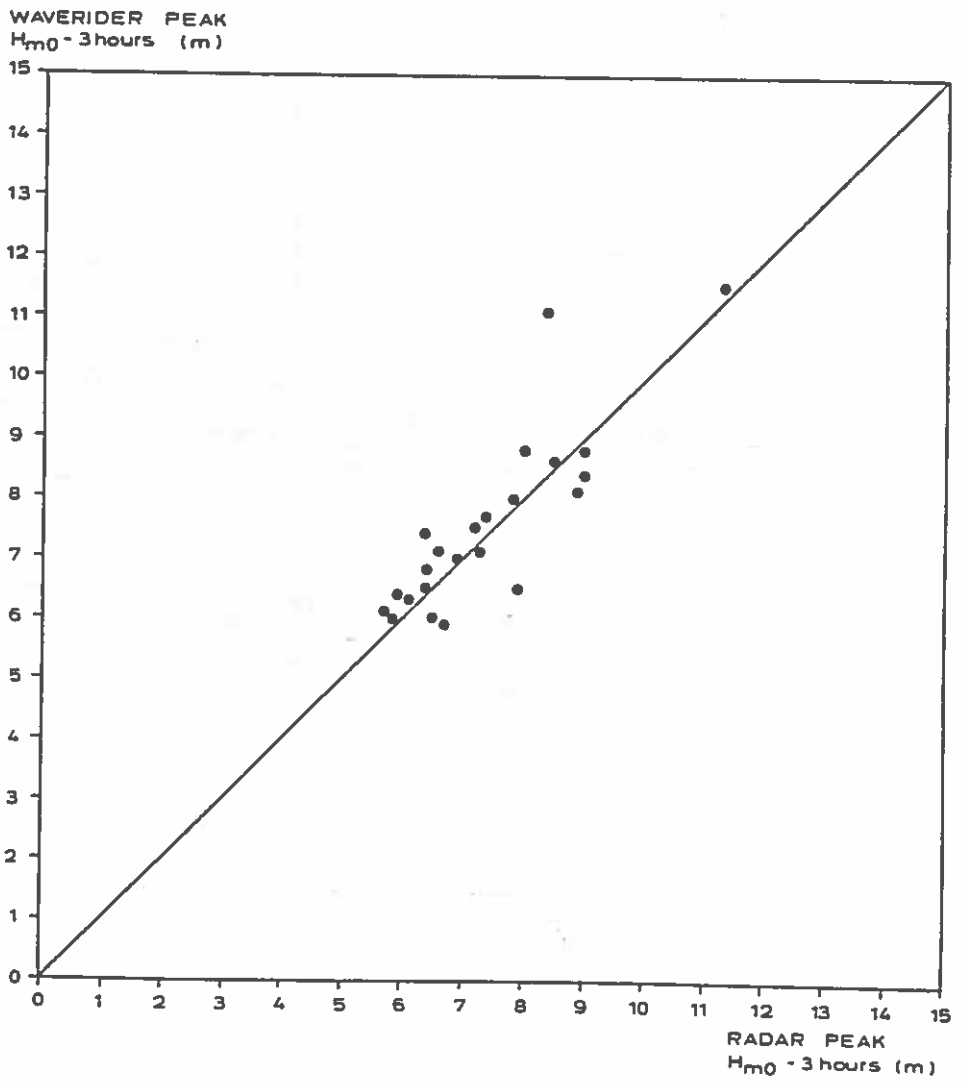

Fig. 3.5 Comparison of Peak Sea-states Measured By Two Different Recorders at Ekofisk During 23 Severe Storm Events.

Current/Water level Model Validation

DHI's North Sea current and water level model was originally established with the purpose of predicting storm surges along the coast of southern Jutland. Accordingly the models ability to simulate water level variations during severe storms was thoroughly validated. Fig. 3.6 shows the SYSTEM 21 model grid for the North Sea model and the locations of 13 stations used in the validation of the model.

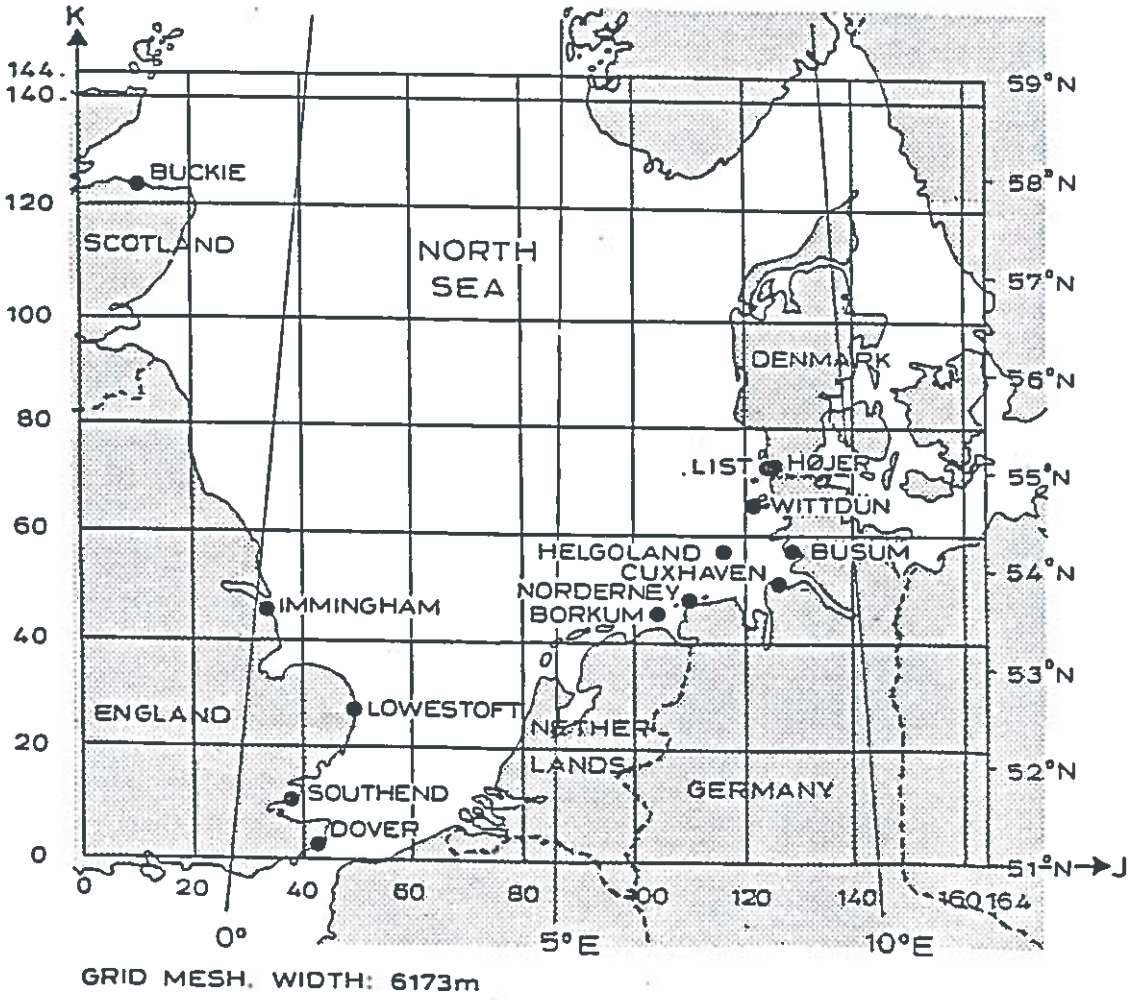

Fig. 3.6 North Sea Current/Water Level Model Grid and Validation Stations.

Fig. 3.7 shows comparisons between hindcast and recorded water levels at the 13 validation stations during a very severe storm surge in January 1976.

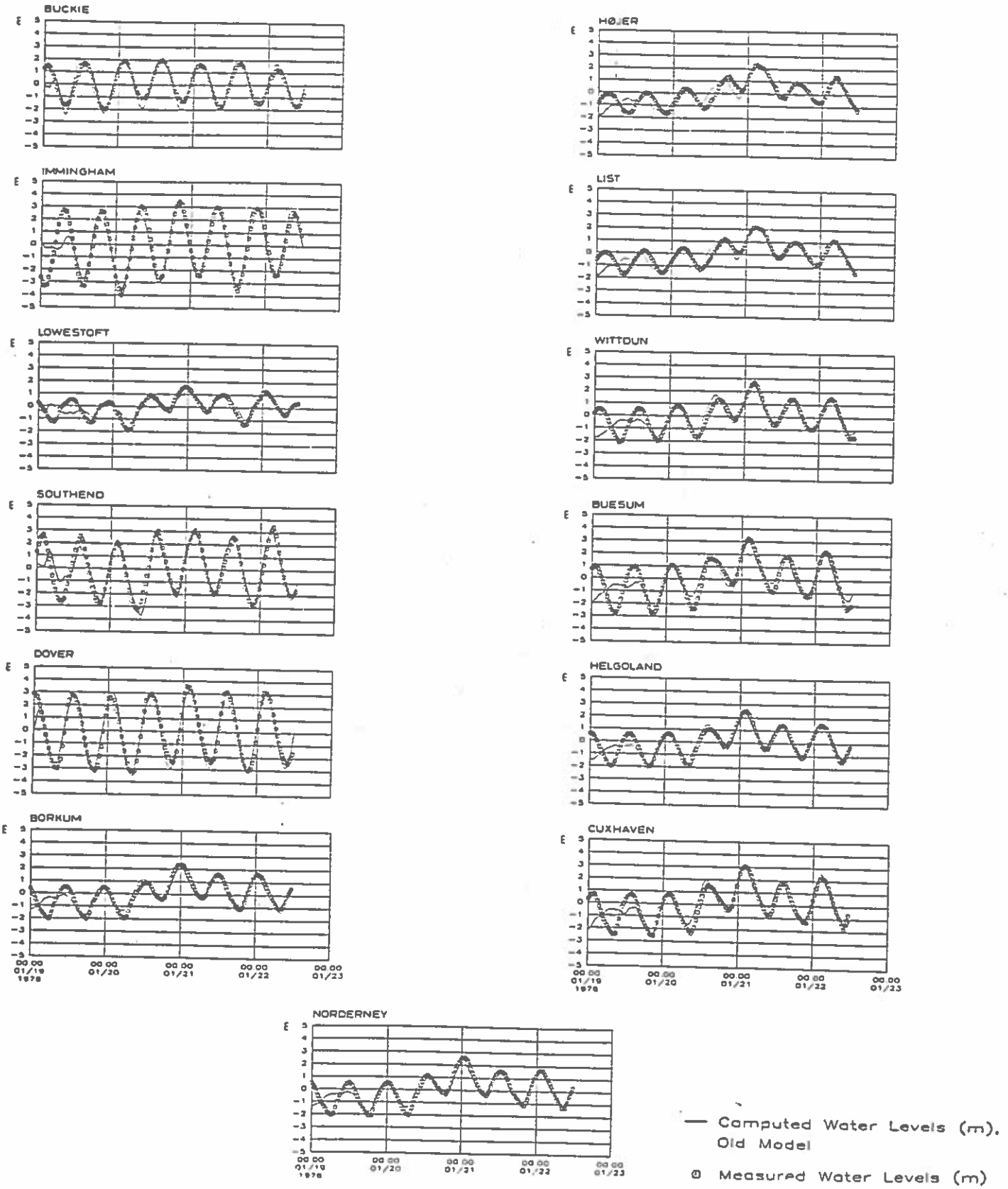

Fig. 3.7 Comparison Between Recorded and Hindcast Water Levels for a Storm Surge of 20 - 21 January 1976.

Offshore recordings of current velocities are not as abundant as wave recordings. However, one example from the Gorm platform in the central North Sea is given in Fig. 3.8.

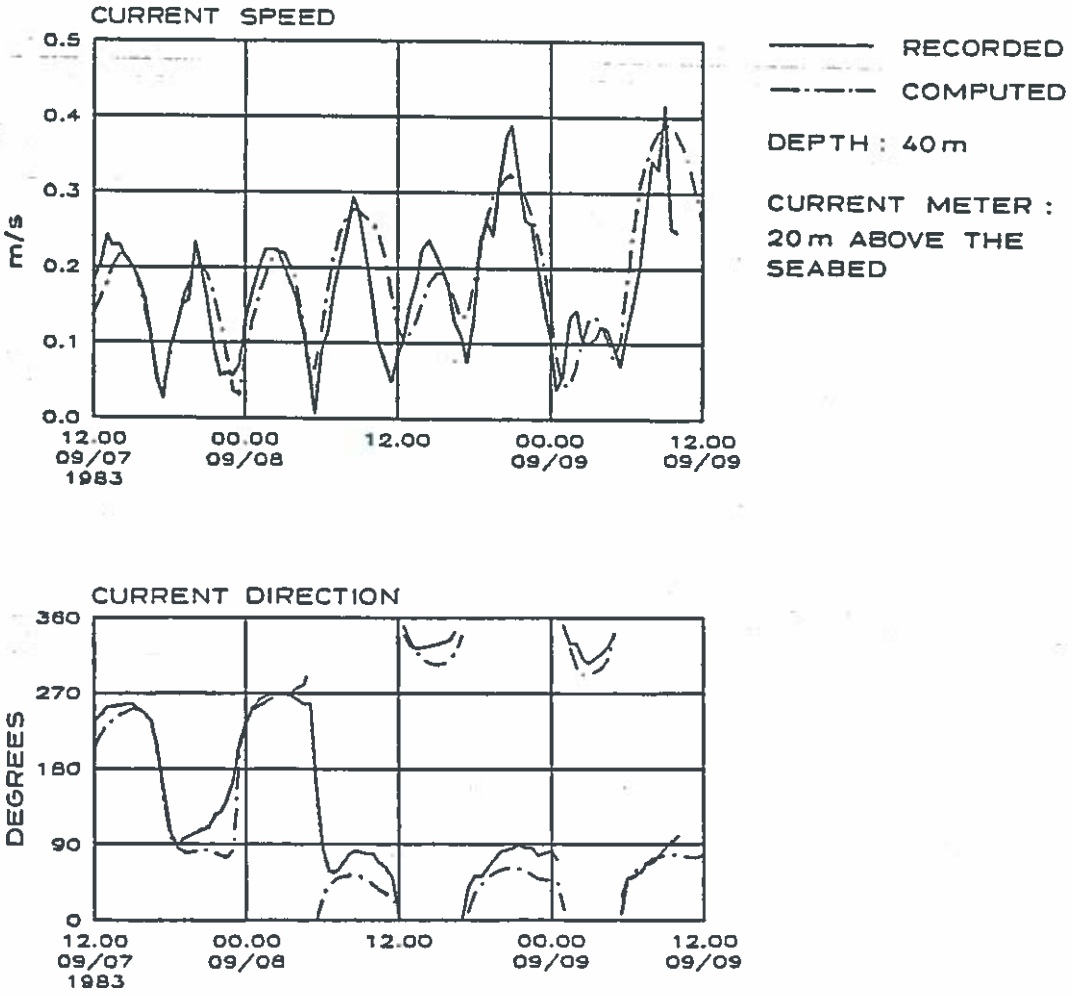

Fig. 3.8 Measured and Hindcast Current Speed and Direction at Gorm During a Minor North Sea Storm.

In a recent study for Shell U.K. SYSTEM 21 demonstrated its abilities to simulate very complex current patterns. This study also shows very clearly that numerical models constitute the only practical engineering tool for some problems.

The study delt with current conditions in Yell Sound in the Shetland Islands, see Fig. 3.9. One of the most important North Sea crude trunklines leads from the Brent oilfield to the Shetlands through the southern parts of Yell Sound. Yell Sound is notorious for its very complex tidal current regime with frequent occurrences of disturbed and very fast moving water masses. Current speeds of up to 7 knots have been reported for certain locations.

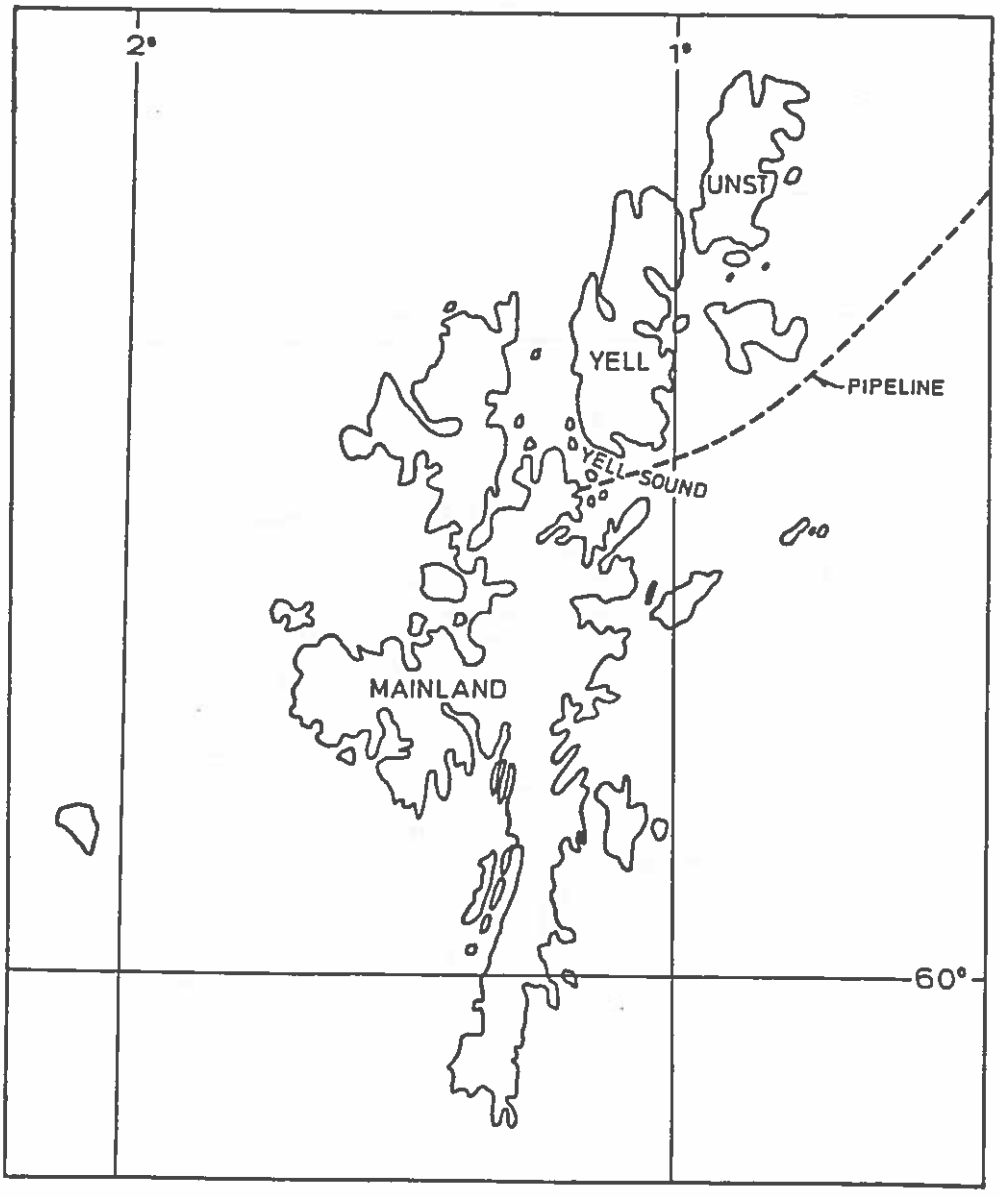

Fig. 3.9 Yell Sound Location Plan.

As part of a reassessment of Shell's design data for that pipeline a company called WIMPOL measured the current conditions at a number of locations in the area, see Fig. 3.10.

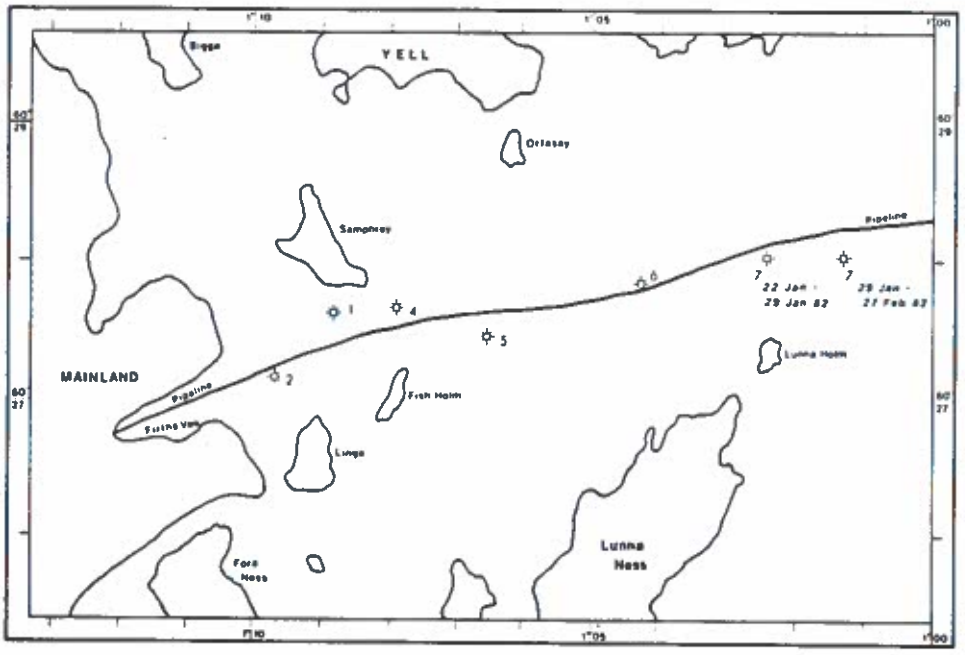

Fig. 3.10 WIMPOL Current Meter Locations.

Fig 3.11 shows 24 hours of recordings from location 1 immediately south of the island Samphrey. The current pattern is quite different from a typical undisturbed tidal flow. Very intense short periodic surges occur during the periods when strong eastgoing currents were expected. Most of the time these surges revert the current direction completely to give westgoing currents instead.

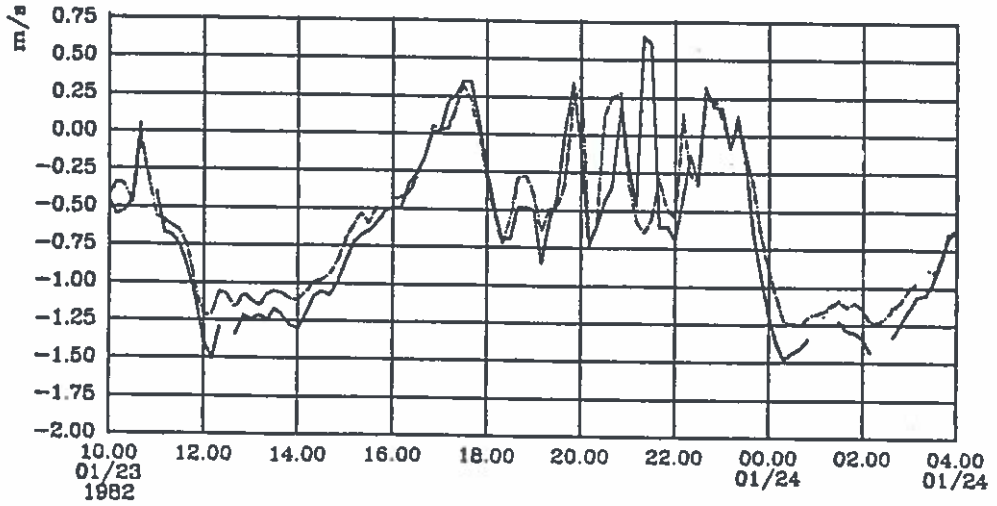

Fig. 3.11 Currents Recorded at Location 1 by WIMPOL.

WIMPOL did not find an explanation for these strange surges which were found (with differing intensities) at all the different locations. In an attempt to find such an explanation DHI was asked to establish a SYSTEM 21 model of the area.

Fig. 3.12 shows the simulated results corresponding to the measurements from Fig. 3.11. SYSTEM 21 reproduces the strange current pattern extremely well.

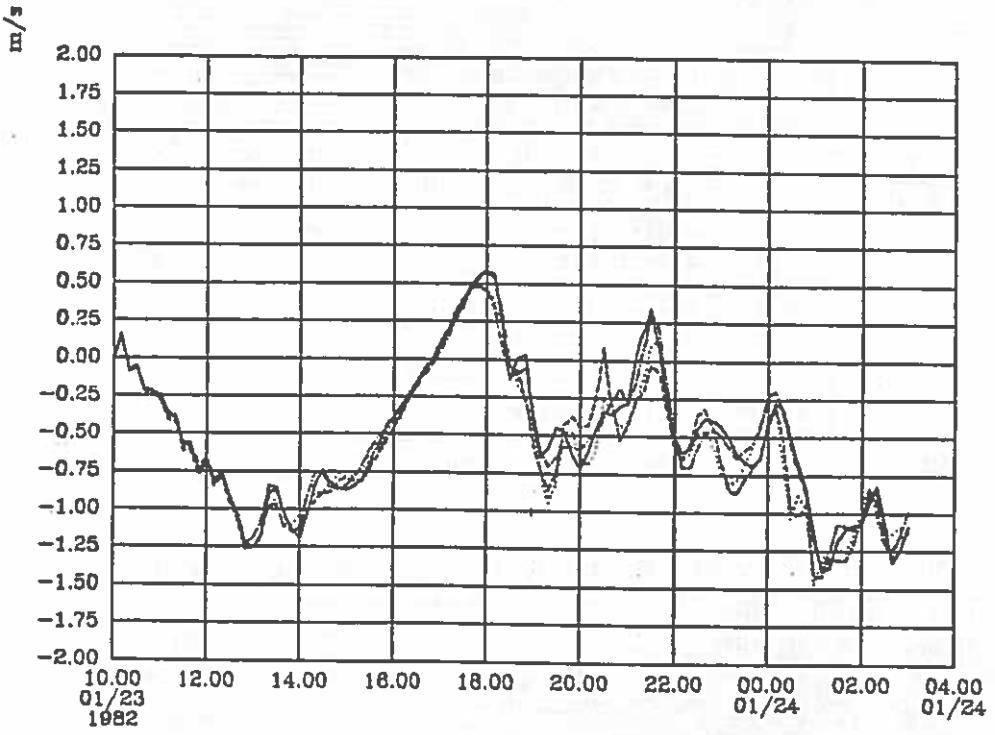

Fig. 3.12 Simulated Current Velocities at Location 1.

The only major difference is in the exact phases of the individual surges and that difference as well as the required explanation of the phenomena is found when looking at the complete current patterns produced by the model. Figs. 3.13 - 3.16 show four "snap-shots" of current patterns taken at 15 min intervals during a period of strong eastgoing currents.

The "snap-shots" show how gyres are generated in lee-zones behind the various islands and how the gyres are shedded into the main current while new gyres form in their place. In the area near location 1 these gyres are seen to lead to westgoing currents most of the time, exactly as found by WIMPOL.

As far as we know, this is the first published example of model simulations of tidal induced vortex shedding from islands. More details regarding this very interesting study can be found in Williams and Nielsen (1987).

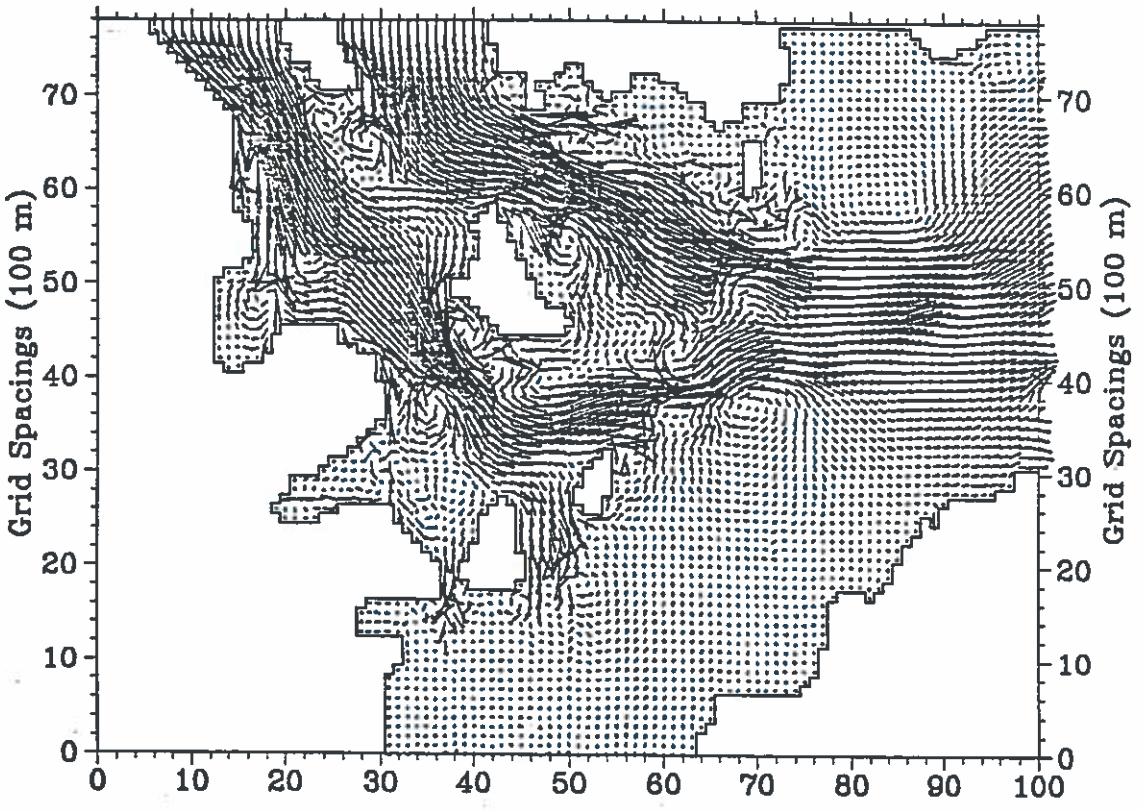

Fig. 3.13 Simulated Current Pattern in Yell Sound, 1930 hrs.

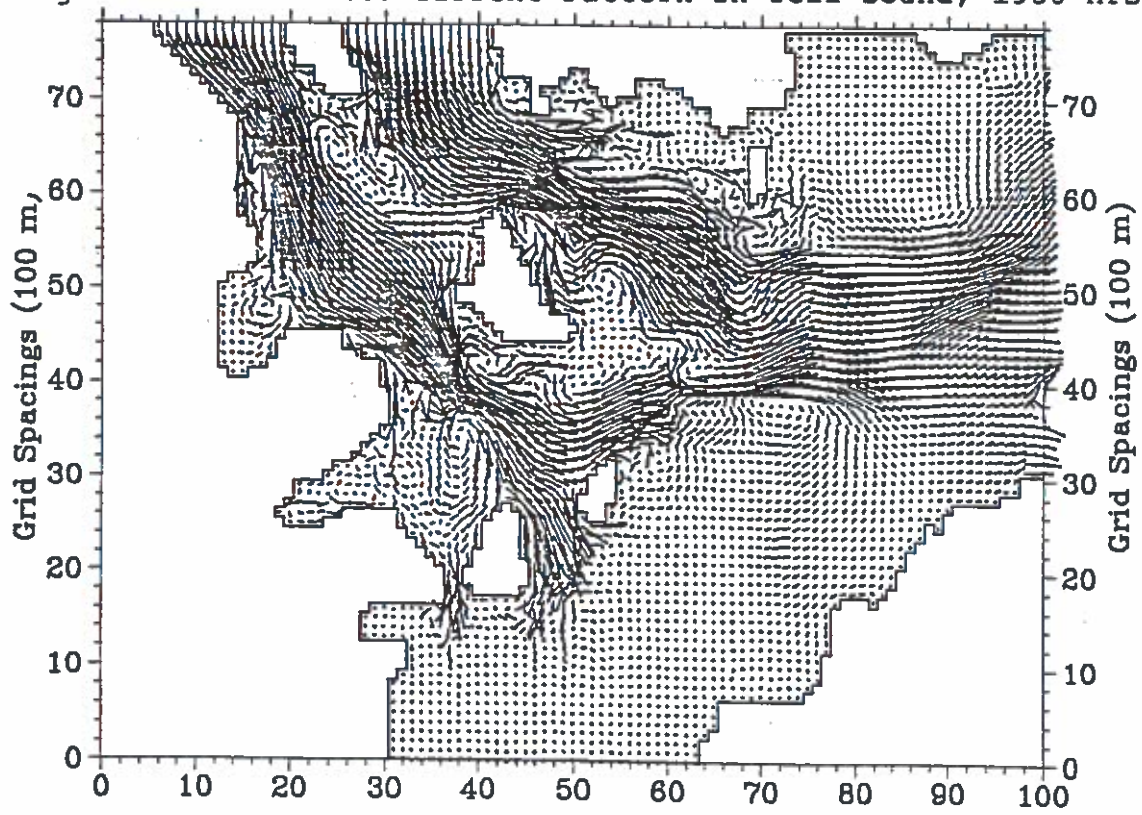

Fig. 3.14 Simulated Current Pattern in Yell Sound, 1945 hrs.

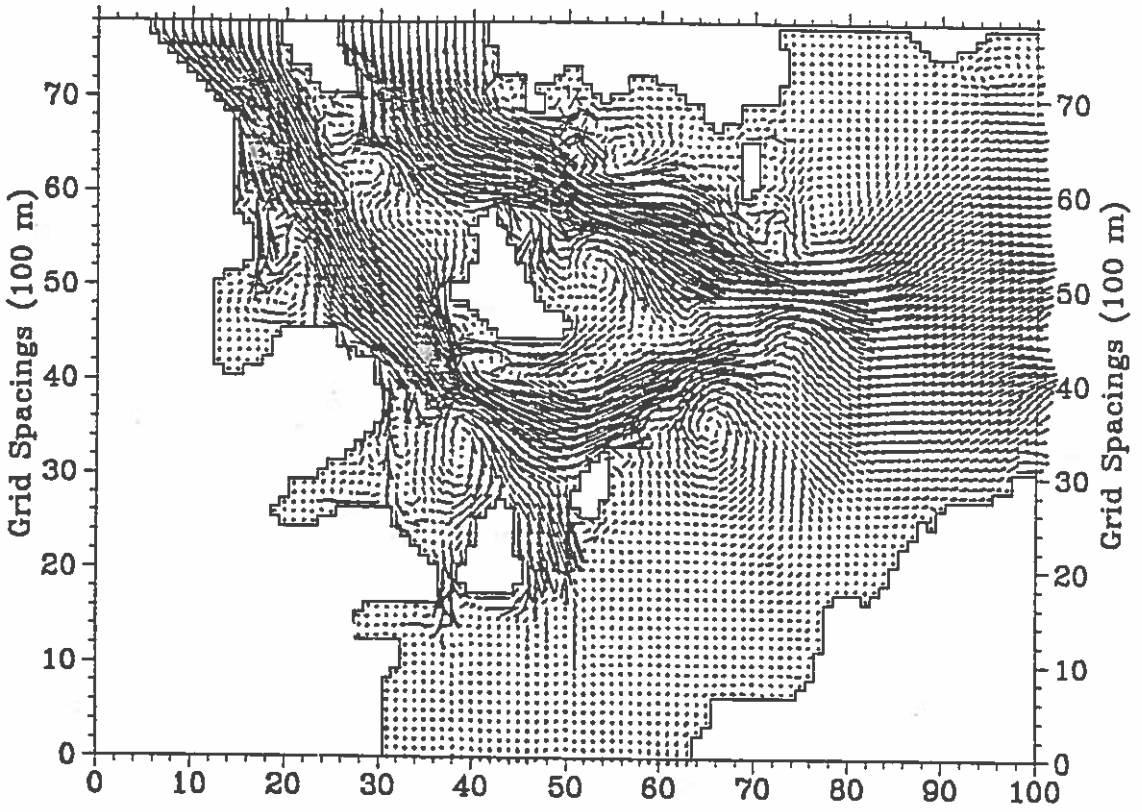

Fig 3.15 Simulated Current Pattern in Yell Sound, 2000 hrs.

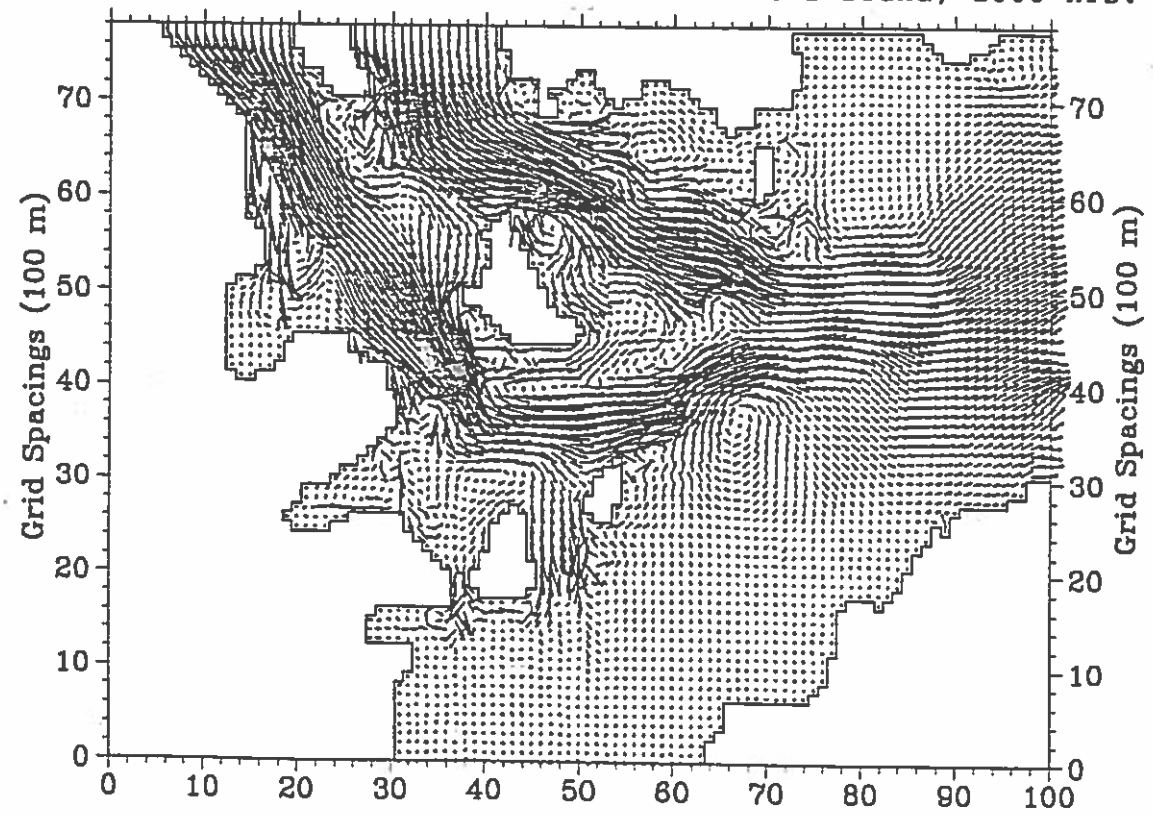

Fig. 3.16 Simulated Current Pattern in Yell Sound, 2015 hrs.

4. CONCLUSION

Based upon the experience accumulated through many design data studies it is possible to give some estimates of the uncertainty associated with the central estimates which are usually reported for the various environmental design parameters.

The uncertainties (here represented by one standard deviation) naturally depend on several factors. One very important factor is the amount and quality of available historical meteorological data for the given area of interest. Another factor is the resources put into the hindcast study in terms of the number of storms included, the time allocated for analysis of the meteorological data, etc. The numbers quoted below should be seen as an indication of the kind of accuracy which can be achieved by todays methods, provided that the data coverage and quality is good and sufficient resources are allocated. They also reflect rather well the kind of accuracy with which we believe that DHI hindcast results from the North Sea area can be given today.

WIND

Measurement	(single value)	:	approx. 10%
Measurement	(100 year value)	:	-- 10%

WAVES

Measurement	(single 18 min record)	:	approx. 5%
Measurement	(100 year value)	:	min. 20%
Hindcast	(single 3 hour mean value)	:	approx. 7%
Hindcast	(100 year value)	:	-- 10%

CURRENTS

Measurement	(single value)	:	approx. 10%
Measurement	(100 year value)	:	-- 30%
Hindcast	(single value)	:	approx. 15%
Hindcast	(100 year value)	:	-- 20%

WATER LEVELS

Measurement	(single value)	:	approx. 0%
Measurement	(100 year value)	:	-- 5%
Hindcast	(single value)	:	-- 20 cm
Hindcast	(100 year value)	:	-- 30 cm

At first glance it may appear strange that the numbers above show higher accuracy of the hindcast 100 year values of waves and currents than of the 100 year values based upon measurements, especially in view of the fact that the similar numbers for single values show the opposite tendency. However, the explanation to that is simply the much better data coverage (longer series in time) which can be obtained by using model data. It is much preferable to extrapolate to 100 year values from 20 - 30 years of data instead of making the extrapolation from only 1 - 5 years of slightly more accurate data.

Bearing in mind the advantage of the complete spatial coverage provided by a numerical model as opposed to a field programme, it becomes evident that numerical models will cotinue to gain in importance with respect to design data studies for offshore structures.

REFERENCES

Brink-Kjaer, O. and Rodenhuis, G.S.: Environmental Design Aspects of Marine Pipelines for the Danish Part of the North Sea. Proc. Workshop Meeting on the Application of Joint Probability of Metocean Phenomena in the Oil Industry's Structural Design Work. E&P Forum, London, U.K. 1983.

Brink-Kjaer, O., Lyngberg, B. and Nielsen, J.B.: Direct Assessment of Environmental Forces From Hindcast Time Series Of Environmental Parameters. Proc. Workshop Meeting on the Application of Joint Probability of Metocean Phenomena in the Oil Industry's Structural Design Work. E&P Forum, London, U.K. 1985.

Brink-Kjaer, O., Nielsen, J.B. and Watson, L.: The Establishment of a Severe Storms Data Base for the Prediction of Extreme Environmental Conditions from Hindcast Data. Proc. International Workshop on Wave Hindcasting and Forecasting. Halifax, Canada, 1986.

Nielsen, J.B.: A Learning System For The Identification And Ranking Of Severe Storms. Proc. 1st International Conference on Applications of Artificial Intelligence in Engineering Problems, Southampton, U.K. 1986.

Nielsen, J.B. and Kej, A.: Hindcast of Environmental Data for Design of Marine Structures and Pipelines. DHI, Denmark, 1986.

Nielsen, J.B., Grant, C.K., Webb, R.M. and Brink-Kjaer, O.B.: Investigation of the Importance of Joint Probability and Directionality of Environmental Data for Platform Design. Proc. Offshore Technology Conference, Houston, U.S.A. 1986.

Nielsen, J.B., Brink-Kjaer, O. and Watson, L.: Numerical Models for Hindcasts of Waves, Currents and Water Levels in the North Sea. Proc. International Conference on the Modelling of the Offshore Environment. London, U.K., 1987.

Williams, R.V. and Nielsen, J.B.: Modelling of Currents in Yell Sound. Proc. International Conference on the Modelling of the Offshore Environment. London, U.K., 1987.

10 December 1986
VJ/isc
4001/01-ON2

Note on Some Inaccuracies and Uncertainties Associated with Calculation of Hydrodynamic Forces on Cylinders.

Based on View Graphs presented at meeting in Danish Society of Hydraulic Engineering on May 22, 1986.

by

Vagner Jacobsen
Danish Hydraulic Institute

As illustrated by the sketch in Fig. 1 cylinders form the basic elements of offshore jacket structures. The cylinders may be horizontal, vertical, or inclined, and they may be closely spaced, e.g. in conductor arrays.

This note deals with the calculation of hydrodynamic forces on single cylinders exposed to wave and current flows. The total hydrodynamic force on a jacket including interference effects due to adjacent elements is discussed in a subsequent section. Furthermore, the present discussion is related to the in-line forces only. Fluctuating transverse forces induced by vortex shedding may be of great importance for some structural elements (e.g. risers, conductors) but they are of less significance for the forces on a total jacket structure as phase differences tend to cancel out the transverse forces.

In summary, the examples discussed in the following demonstrate that hydrodynamic force coefficients may be determined with great accuracy when all important parameters are well-known and controlled, and the flow is regular, as is the case in laboratory experiments. The widely applied and rather simple force formulation - the Morison equation - is found to yield peak forces with acceptable accuracy for these cases.

In the real offshore environment man is not in control of the flow field, and important parameters (e.g. the roughness of structural elements in the design situation) may not be well defined. Our way of modelling the complex real life situation may thus not always be adequate. The inaccuracies associated with model predictions of wave induced flows are clearly reflected in the scatter in force coefficient data from field measurements, and it is evident that classical 2-dimensional wave theories are inadequate for predicting water particle velocities induced by the natural (3-dimensional) waves in a confused sea state generated by a storm. Furthermore, it is also shown that even if we do have measurements of forces and of the fluid motion (velocities, accelerations), and the scatter in force coefficient data are reduced, then the traditional force expression may not accurately predict the force variation.

Present research therefore concentrates on establishing accurate descriptions of the flow field and its interaction with the structural elements of jacket structures with a view to further our understanding of the processes resulting in the hydrodynamic forces.

Detailed quantification of the inaccuracies and uncertainties in the hydrodynamic force calculation has not been included as such values highly depend on the problem in question (e.g. wave characteristics, size and layout of structure). For overall assessment of uncertainties reference is given to the subsequent section.

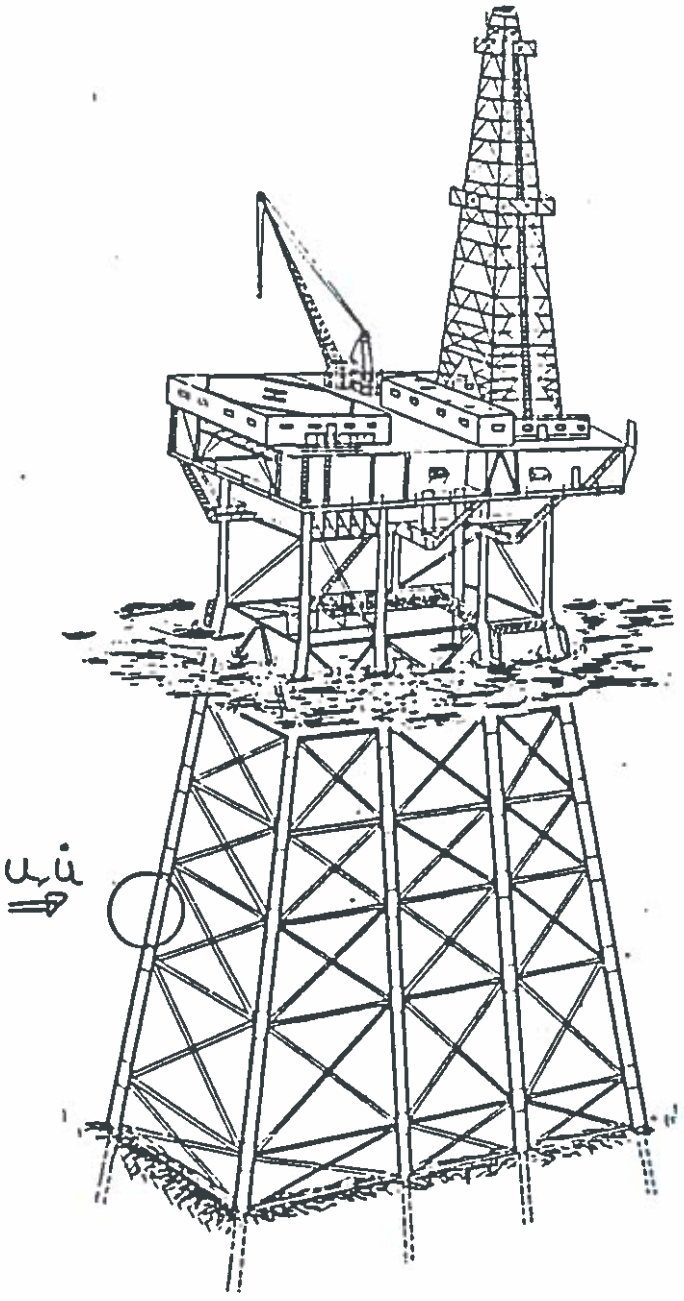

Fig. 1 Sketch of a jacket structure

Hydrodynamic forces on a single cylindre:

U_c, U_w, $\dot{U}_w$ =>  $\longrightarrow F(t) = F_D(t) + F_M(t)$

The in-line force is traditionally calculated by use of the Morison equation, i.e. by linear superposition of the drag and the inertia force:

$$F = F_D + F_M$$

$$= \frac{1}{2} \rho D C_D U(t) |U(t)| + \frac{\pi}{4} \rho D C_M \dot{U}(t)$$

where

$U(t) = U_c + U_w(t)$ (current + wave velocity)

$\dot{U}(t) = \dot{U}_w(t)$ (acceleration)

C_D, $C_m = f$ (KC, Re, k/D, t/T)

$KC = U_w \cdot T/D$ (Keulegan-Carpenter number)

$Re = U_w \cdot D/\nu$ (Reynolds number)

k = pipe surface roughness

D = pipe diameter

This poses the following problems:

- Determination of C_D, $C_M = f$ (KC, Re, k/D)
- Assessment of the accuracy of the force description based on Morison's equation.
- Determination of U(t) and $\dot{U}_w(t)$. (Water velocity and acceleration).

-

C_D and C_M from laboratory Experiments

2-dimensional regular oscillatory flow (Sarpkaya).

Fig. 2 shows examples of C_D and C_M values for KC = 20 and KC = 100. The data exhibit little scatter, but it is seen that large variation in the coefficient values may appear for different values of the governing parameters. Especially the roughness ratio is seen to affect the C_D-values, whereas the force coefficients are independent of the Reynolds number when this exceeds a certain value close to 10^5.

As an illustration it can be noted that a 20 m high wave with a period of 14 sec in 40 m of water will yield velocities in the order of 5 m/s. A cylinder with a diameter of 1 m will thus have a KC number of $5 \cdot 14/1 = 70$ and a Re-number of $5 \cdot 1/10^{-6} = 5 \cdot 10^6$.

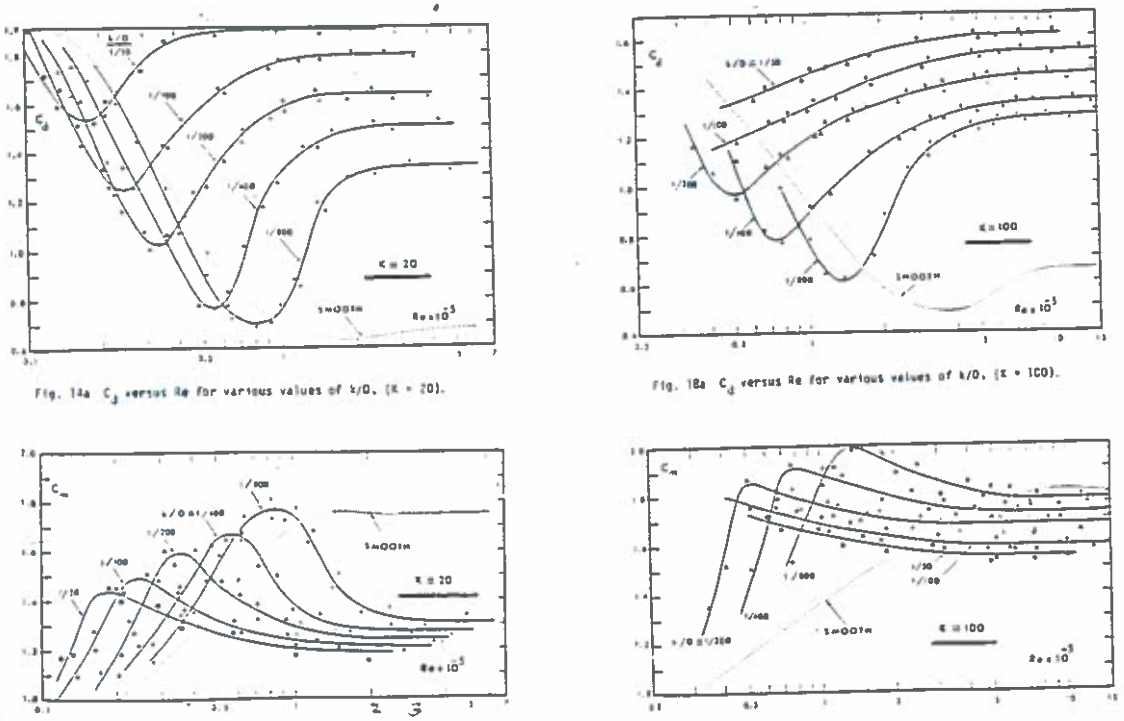

Fig. 2 C_D and C_M-values for KC = 20 and KC = 100
Data from Sarpkaya. (Note KC = K in figures)

Effect of Inclination

As shown in Fig. 1 most of the structural elements have a certain inclination.

Fig. 3 below shows C_D-values for different inclinations or yaw-angles. The recorded data have been analysed using the flow components normal to the cylinder. It is seen that the inclination only affects the C_D-values at low KC-numbers where the force is dominated by the inertial component. Generally, the cylindrical elements of a jacket will have dimensions that relate to large KC-number in a design situation, meaning that the design force will be drag dominated.

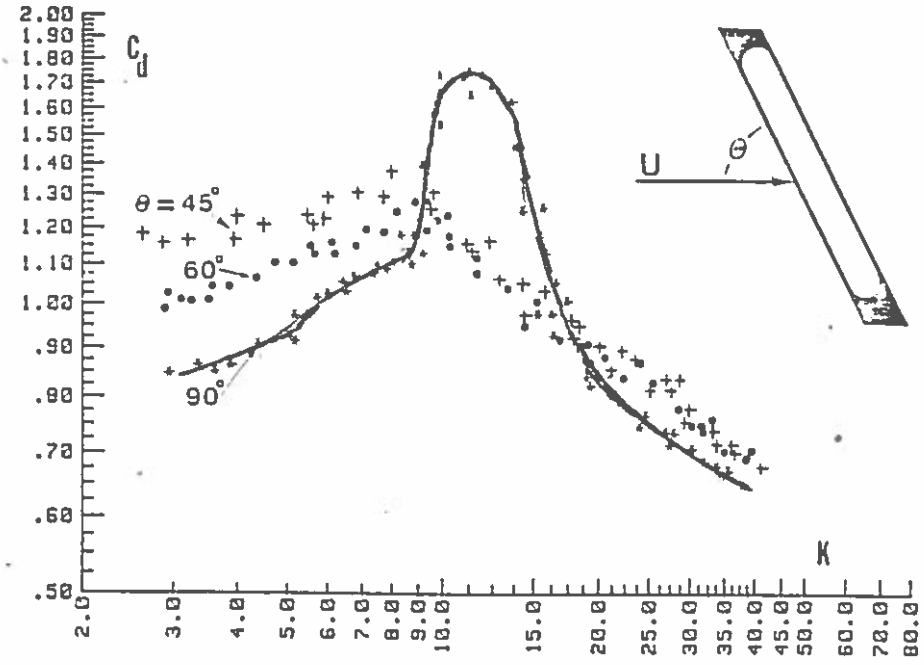

Fig. 3 — Drag coefficient versus Keulegan-Carpenter number (yawed smooth cylinder)

Effect of Combined Wave-Current Action

Data for C_D and C_M for oscillatory flow with a superimposed steady current are shown in Fig. 4. The total velocity has been applied in the analysis, and the resulting force coefficients are slightly smaller than those for pure oscillatory motion. This points to a small relative reduction in the forces compared to the pure wave case.

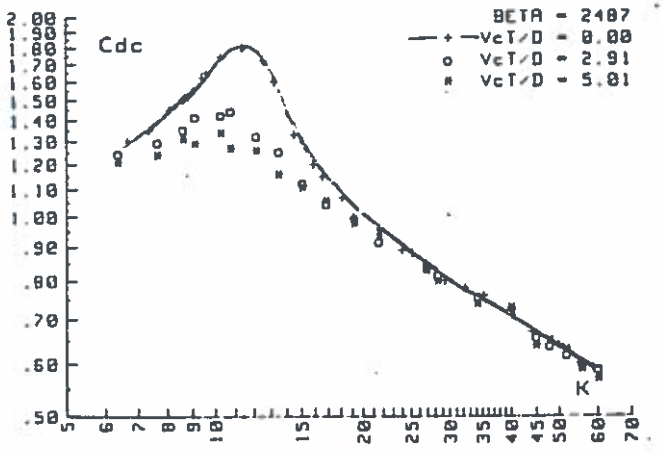

Fig. 2—C_{dc} vs K for a smooth cylinder for beta = 2,487 and various values of VK

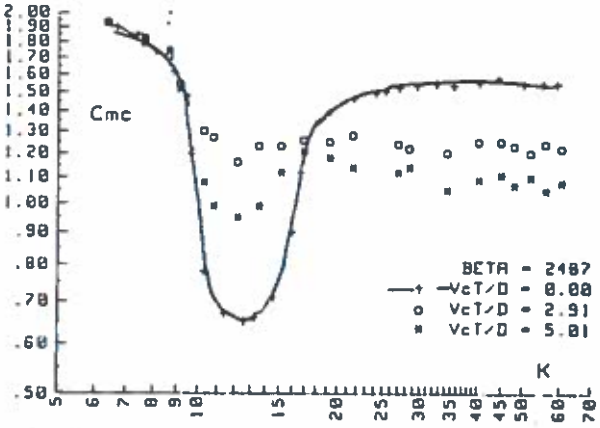

Fig. 4—C_{mc} vs K for a smooth cylinder for beta = 2,487 and various values of VK

Fig. 4 Force coefficients for combined wave-current action

V_C = steady current velocity

T = wave period

β = Re/KC

Effect of Orbital Motions

All the data presented in the previous figures relate to 2-dimensional, rectilinear flow. According to simple 1st order wave theory, the water particles move in elliptic paths. Tests simulating this flow condition have been carried out, and Fig. 5 shows the force coefficients for a vertical cylinder and for a horizontal cylinder. Flow components normal to the cylinder have been used in the analysis. It is seen that C_D decreases slightly and C_M increases for orbital flow conditions.

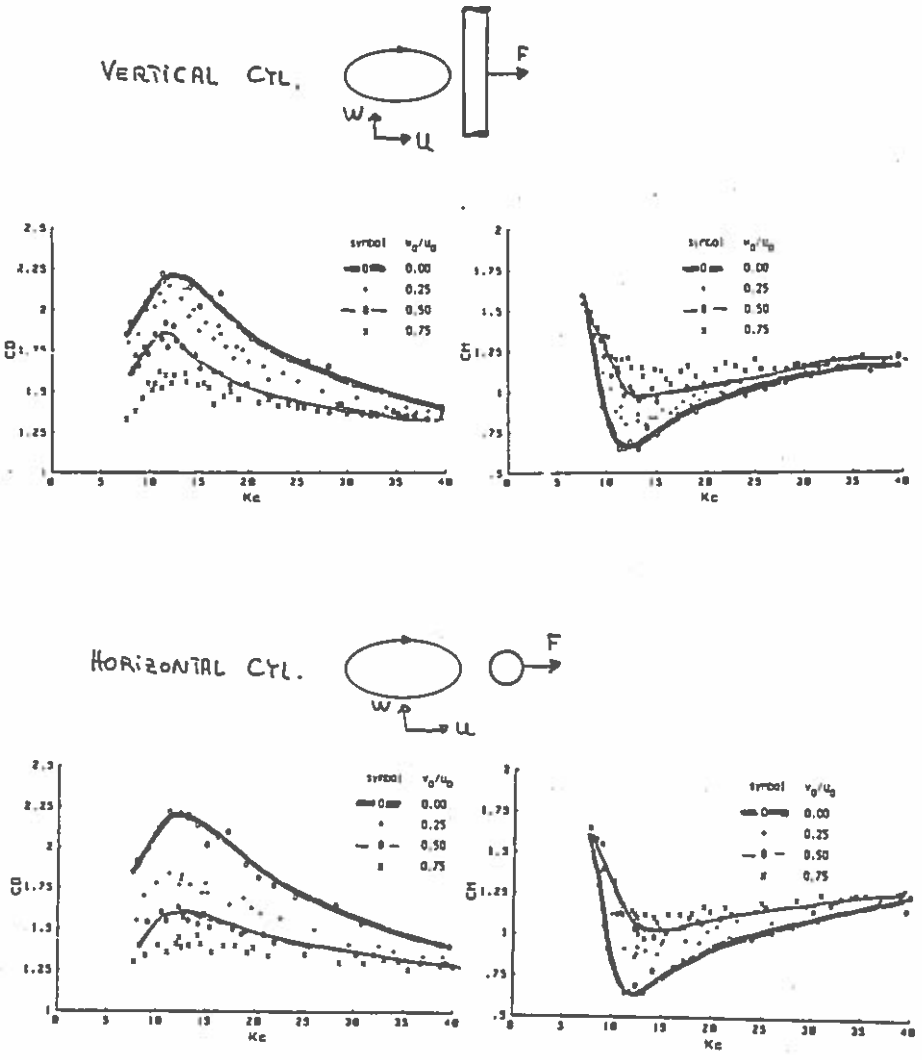

Fig. 5 Force coefficients for orbital flow.
Vertical and horizontal cylinder.

Prediction of In-Line Forces

By using the Morison equation and the force coefficients determined from the laboratory tests, time series of predicted forces may be produced. Fig. 6 below shows two examples of predicted and measured in-line forces.

The measured force is in general well reproduced, the differences being caused by the shedding of vortices and by changes in the local flow field in the vicinity of the cylinder.

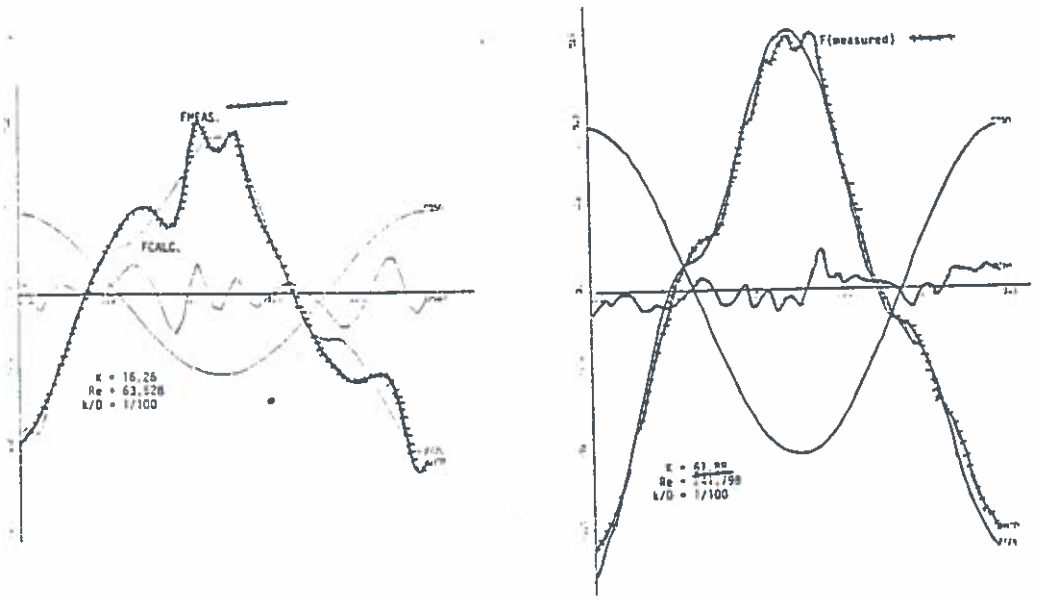

Fig. 6 Measured and calculated forces.

All the laboratory data presented have been taken from tests carried out by Sarpkaya et al in a vertical U-shaped water tunnel. Many other data sources are available, but the use of data from one facility leads to a more consistent evaluation of the effects of different parameters.

From the laboratory data it may be concluded that:

- Only little scatter appears in the force coefficients when all basic parameters are well controlled and well-known.

- Pipe surface roughness yields larger forces.

- Inclination leads to slightly decreasing forces.

- Orbital motion decreases the forces.

- The superposition of a steady current on the oscillatory flow leads to a relative decrease in the forces.

- The measured force time series are reasonably well predicted by the Morison equation in case of regular oscillatory flow.

All the aspects investigated individually in the laboratory may well be present simultaneously in the real life offshore environment: Inclined cylinders - roughened due to marine growth - being exposed to the combined action of current and waves. In this situation the roughness is not well defined and neither is the flow field.

Field test programs monitoring environmental conditions and forces have been conducted at various locations. Fig. 7 shows an example of C_D-values determined from measurements on the Ocean Test Structure. The scatter in the data is quite significant, which illustrates some of the uncertainties arising in the real life situation, and points towards the third problem mentioned in connection with force calculation by the Morison equation: The uncertainties associated with the determination of the water velocity and acceleration.

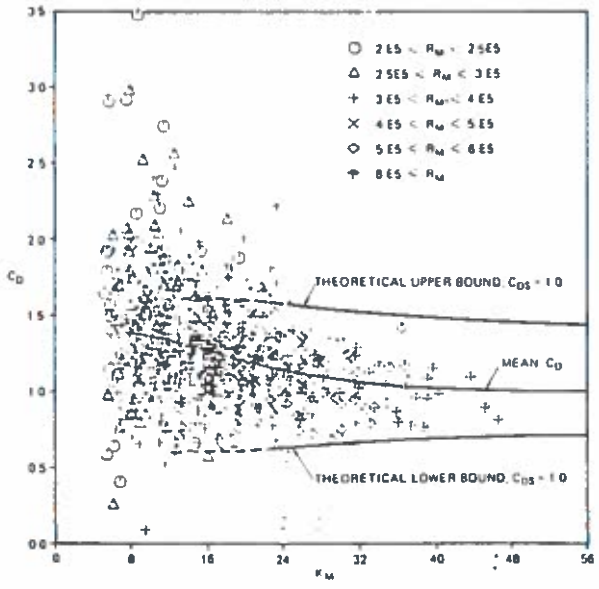

Fig. 2. C_D versus K_M for ranges of R_M, from Method I, at the SW WFT on 3/04/77, for half wave cycles producing at least 30 pounds force on the WFT

Fig. 7 C_D-values from the Ocean Test Structure.

Wave Theories

A number of wave theories are available which may be used to calculate the wave induced velocities and accelerations. Fig. 8 shows the ranges within which various wave theories appear to be most appropriate. Fig. 9 below illustrates how various wave theories may yield quite different values of the horizontal water velocity. It is stressed that Fig. 9 is not intended to illustrate the relative accuracy of any of the theories shown, as some of the wave theories a priori are known not to apply well for the specific case. However, the differences in results one could obtain depending on the wave theory applied are clearly illustrated.

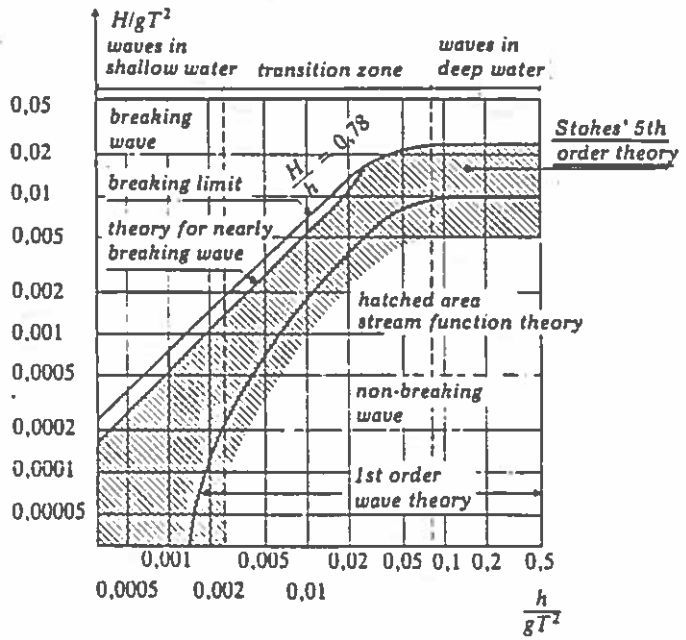

Fig. 8 Ranges for applicability of different wave theories.

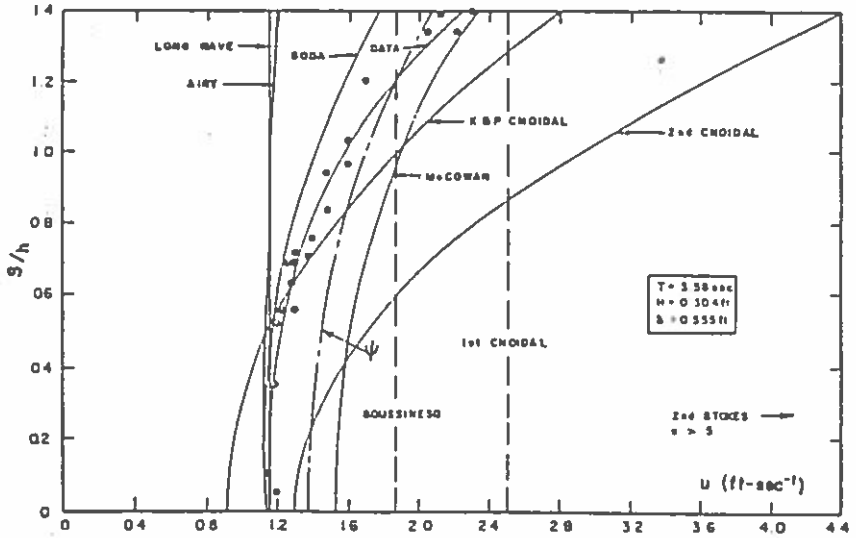

Fig. 9 Predicted horizontal velocities from various wave theories.

Two of the most widely applied wave theories are the linear (1st order) wave theory and Stokes 5th order theory. The former is based on very small amplitude waves, whereas the latter applies to large amplitude waves, having higher crests and smaller troughs.

Fig. 10 shows comparison between these two theories and measurements in 2-dimensional laboratory waves. It is concluded that both theories yield velocities that differ from the measured ones, and that the maximum horizontal velocities under the crest are overpredicted.

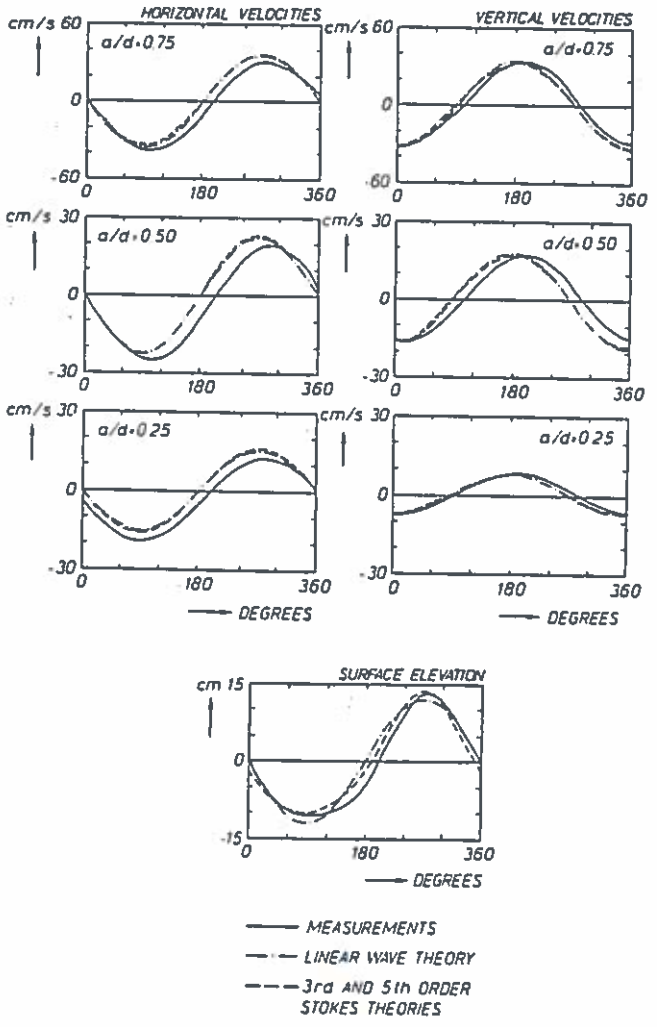

Fig. 10 Comparison of measured and predicted velocities in 2-dimensional waves.

Fig. 11 shows an example of measured horizontal velocities together with velocities predicted with three wave theories. The recording is from the largest wave recorded during the hurricane Delia. The figure illustrates the difficulties or inaccuracies associated with predicting the velocities created by real, 3-dimensional waves, using 2-dimensional wave theories. The velocities under the crest are largely overpredicted, by factors of up to approximately 2.

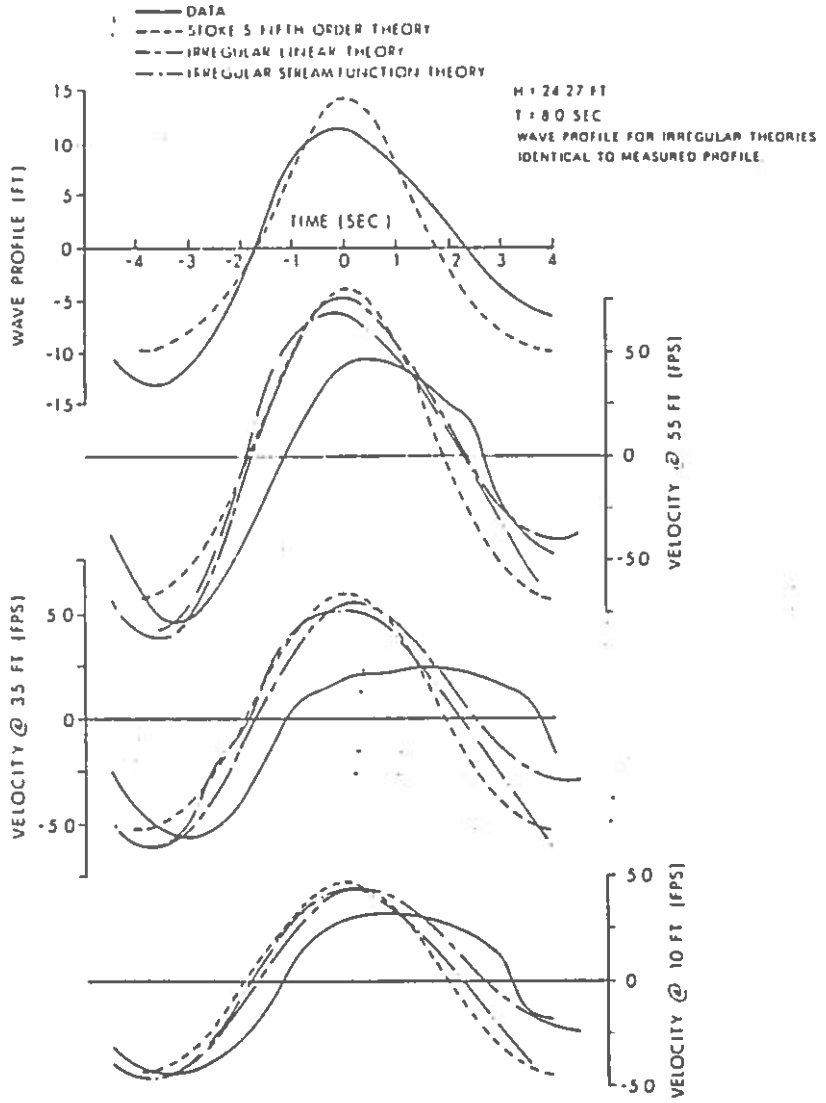

Fig. 11 Measured and predicted horizontal velocity during the largest wave of hurricane Delia.

The overpredictions by Stokes 5th order theory of the wave induced velocities under the wave crests are elucidated in the figure below for the largest waves associated with Delia.

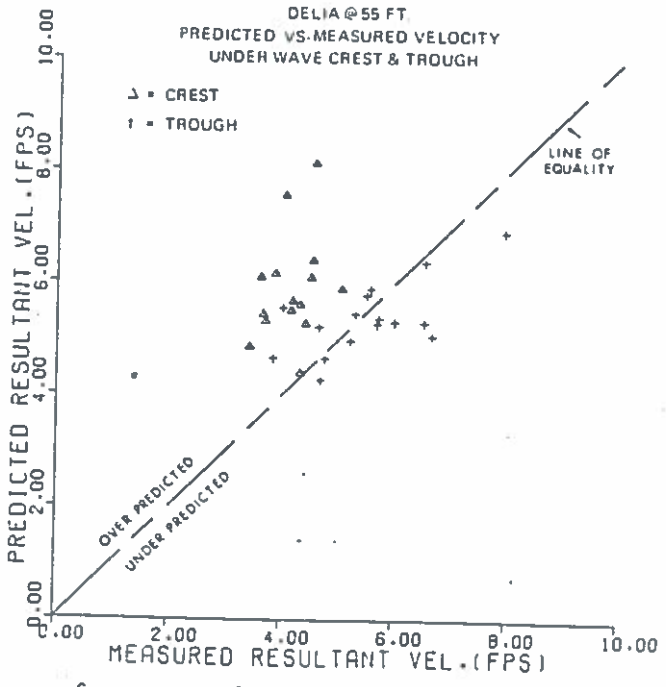

Fig. 12 - Comparison of Stokes fifth-order to measured maximum velocities during the largest waves at the top current meter.

The 3-dimensionality of sea waves is further illustrated in Fig. 13, showing recordings of the horizontal velocity from the same wave as in Fig. 11.

The scatter in C_D-values shown in Fig. 7 may partly be attributed to uncertainties in the velocity calculations.

It is concluded that the velocity variation associated with 3-dimensional sea waves is not accurately predicted by the traditional 2-dimensional wave theories. 3-D wave theories are needed for this purpose.

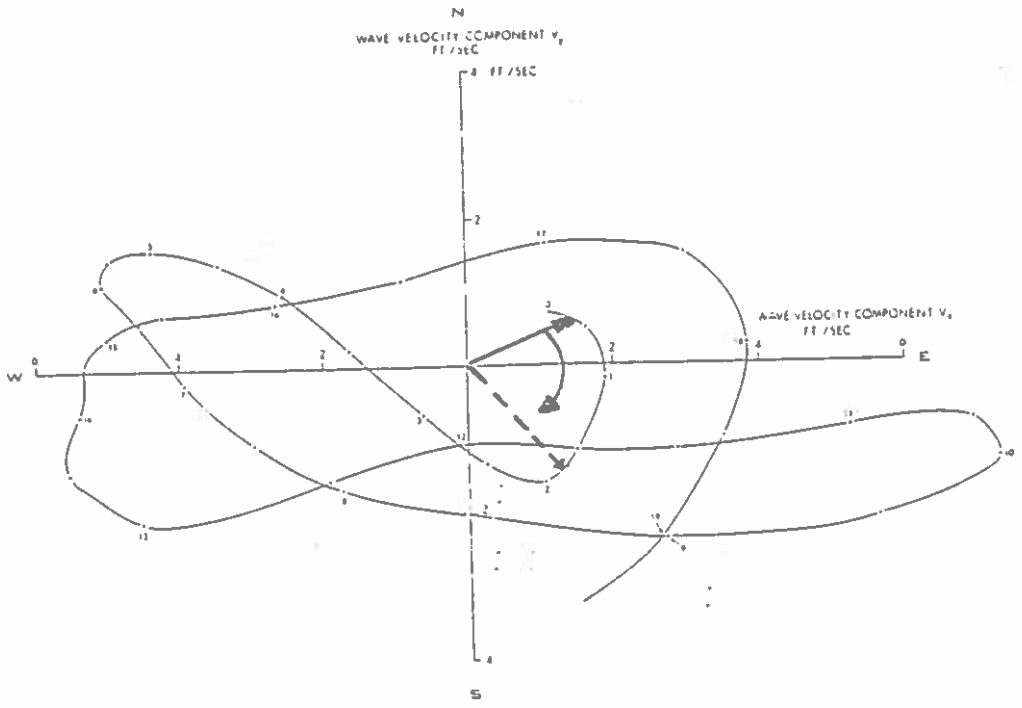

Fig. 13 Horizontal velocity variation associated with the wave in Fig. 11.

When measured velocities are used in the analysis, as has been done for the Christchurch Bag Tower Tests, the scatter in the force coefficients may be reduced and a clear trend with the KC number is found, as shown in Fig. 14 below.

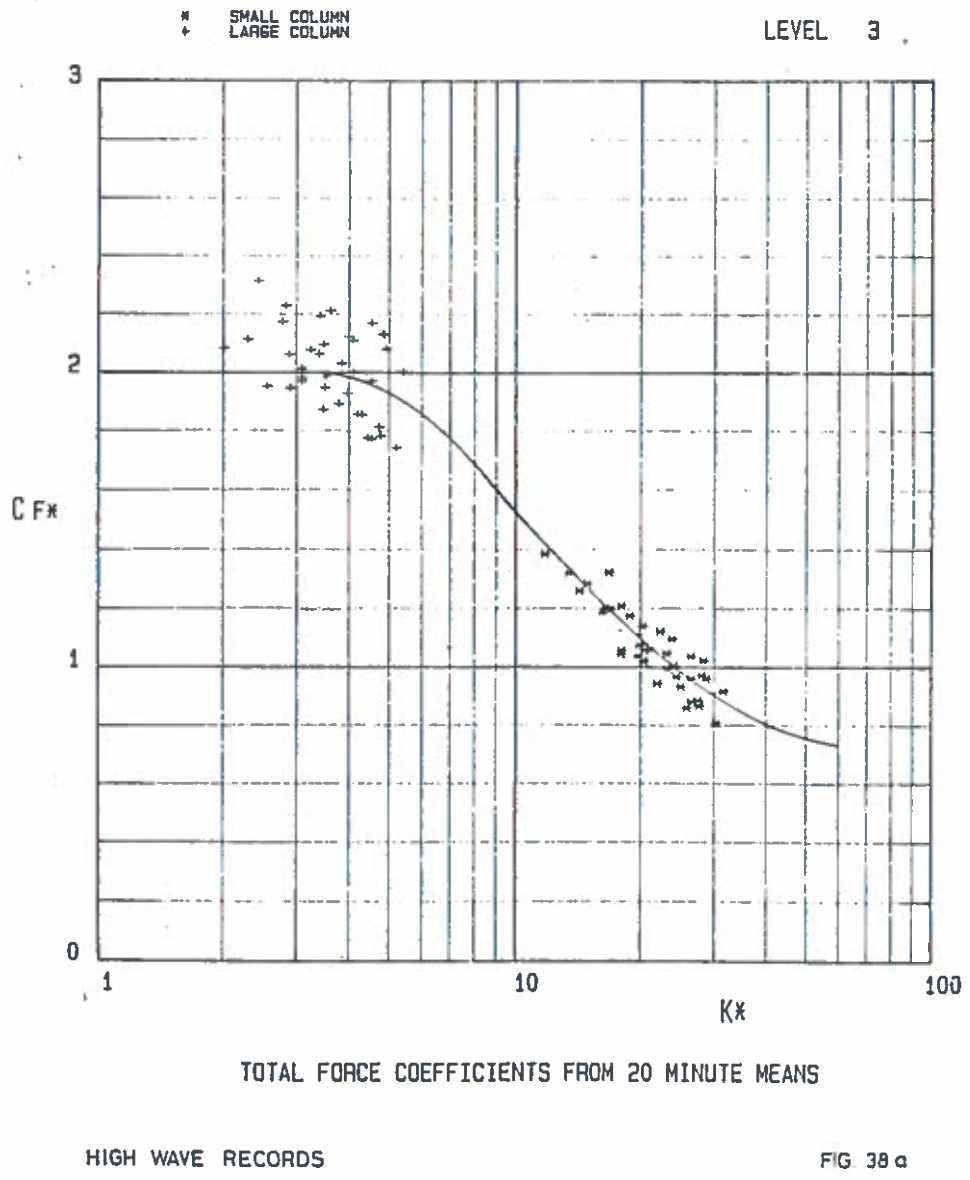

Fig. 14 Force coefficients from the Christchurch project.

The reduced scatter in force coefficients does not directly imply that the measured forces are always accurately described by the Morison equation.

Figs. 15 and 16 below show two recordings of horizontal velocities and associated forces for two succeeding waves. Despite the similarities in velocity recordings the forces are very different, and even if the actual measured velocity was applied in the force calculations the correlation with the measured force would be quite different in the two cases.

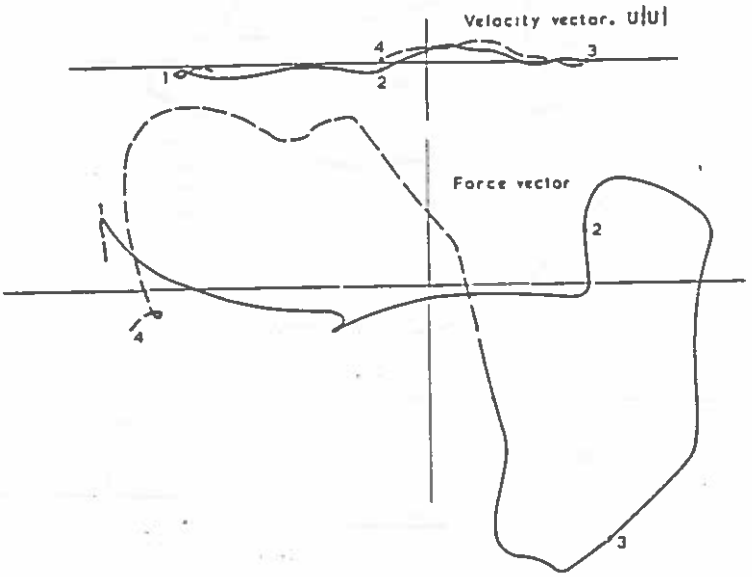

Fig. 15 Measured horizontal velocity and force.

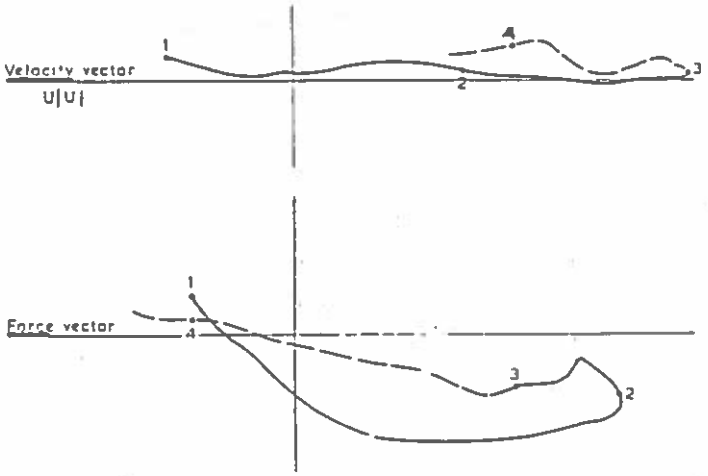

Fig. 13 Measured horizontal velocity and force in wave preceding that of Fig. 13.

The difference that may appear between measured and calculated forces is illustrated below for a horizontal cylinder, where the measured velocity vector has been used to predict the hydrodynamic force.

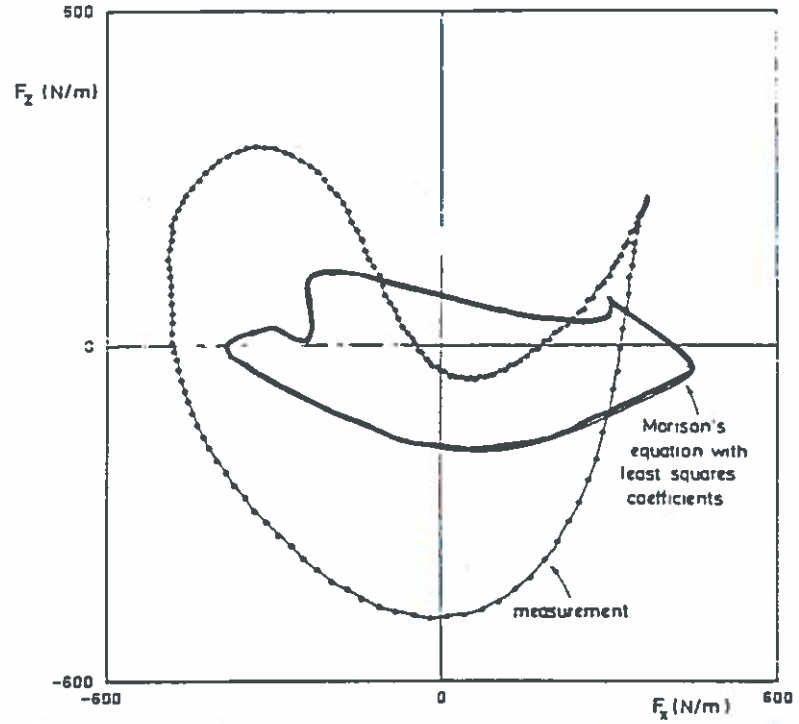

Fig.10 Horizontal cylinder: polar representation of the total force vector, averaged over about 30 waves of run OCH32; comparison with the least-squares Morison's equation.

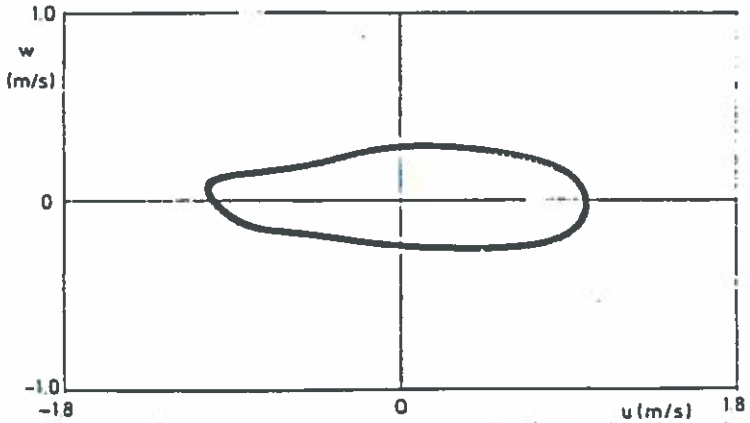

Horizontal cylinder: polar representation of the velocity vector for run OCH32

Fig. 17 Measured and predicted force on a horizontal cylinder.

Although a measured velocity was applied in the previous figure, this velocity was measured at some distance from the pipe. The use of the Morison equation may not be ruled out based on such observations. In fact, research projects carried out by DHI have shown that very accurate predictions of forces on pipelines can be obtained by the Morison equation, when a velocity very close to the pipe is applied in the analysis as illustrated in the two examples below.

This points to the fact that more detailed knowledge of the flow field near cylinders, i.e. the flow field affected by the presence of the cylinder, is needed for accurate force calculations.

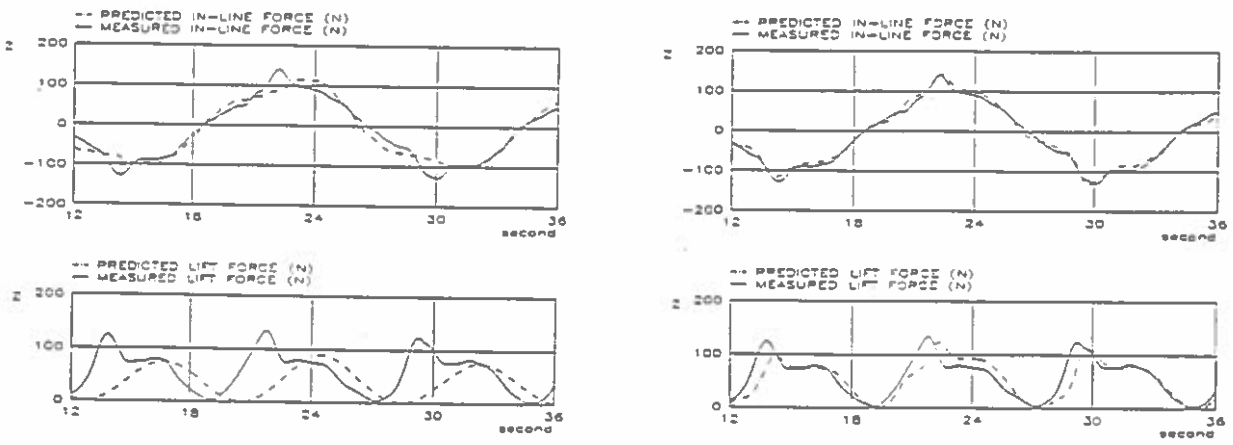

Fig. 18 Measured and predicted forces on a pipeline (DHI)
a) Freestream velocity b) Near pipe velocity

Based on the examples discussed it may be concluded that calculations of the hydrodynamic forces on single cylinders exposed to real, 3-dimensional sea waves combined with steady currents are associated with inaccuracies and uncertainties, which arise from various sources, for instance:

- o Inaccuracies in the determination of the flow field (i.e. wave induced velocities and accelerations), see Fig. 11.

- o Inaccuracies in the transformation of flow kinematics into hydrodynamic forces, see Figs. 7 and 15-18.

To improve the accuracy of hydrodynamic force calculations we need, on a short term basis:

More, reliable and correlated data for

- Waves (3-D)
- Wave kinematics (over the entire water column)
- Forces (local and global)

Special emphasis is needed on data and theories for wave and current velocities above the mean water level, i.e. in the wave crest, because the velocities are large in this area, and the contribution to the total force and especially to the overturning moment is substantial for the part of the jacket above mean sea level.

On long term basis improved force calculations will need:

- improved models for transferring 3-D wave data to wave velocities and accelerations over the entire water column

- improved understanding of the physics involved in the fluid-structure interaction

- on basis of this, development of detailed numerical models for calculating the hydrodynamic forces.

A joint effort on theoretical/analytical developments, experiments (laboratory, at sea) and numerical work is thus needed to further the accuracy and reliability of the force calculations.

UNCERTAINTIES IN THE DETERMINATION OF STRUCTURAL LOADS FROM WAVES AND CURRENT

BY

NIELS-ERIK OTTESEN HANSEN

INTRODUCTION

This note summarizes the current knowledge on the uncertainties which are present in connection with the determination of loads from waves and current in offshore jacket structures. It has been compiled for a seminar held 22 May 1986 by the Danish Society of Hydraulic Engineering.

One major problem in the topic considered is the uncertainty in the definition of uncertainty. The usual definition would be to define an uncertainty interval of two or three standard deviations around a mean value. This definition can be used for some phenomena in relation to loadings on a platform. On the other hand, in connection with the determination of wave kinematics the theoretical predictions may be conservative such that the uncertainty interval should be asymmetric. As an example the relative uncertainty will be smaller on the determination of a large velocity than on a small velocity.

Consequently it is necessary to make use of different definitions depending on the nature of the phenomenon. In the following, the definitions used are indicated for each case.

CALCULATION PROCEDURE

Loadings on jacket structures can normally be considered quasi-static except for platforms in very deep water.

The typical procedure for the determination of the loads is as follows:

1. Wave and current kinematics are determined for the design wave and current situations.

2. The forces on the individual members, F, are determined from the wave kinematics by use of the Morison equation

$$F = \frac{1}{2} \rho C_D D \vec{u}\cdot\vec{e} \, |\vec{u}\cdot\vec{e}| + \rho C_M A \dot{\vec{u}}\cdot\vec{e}$$

in which u is the instantaneous water particle velocity, $\dot{u}$ the instantaneous water particle acceleration, ρ the density of sea water, D the diameter of the member, A the cross sectional area, and $\vec{e}$ the unit perpendicular on the member axis.

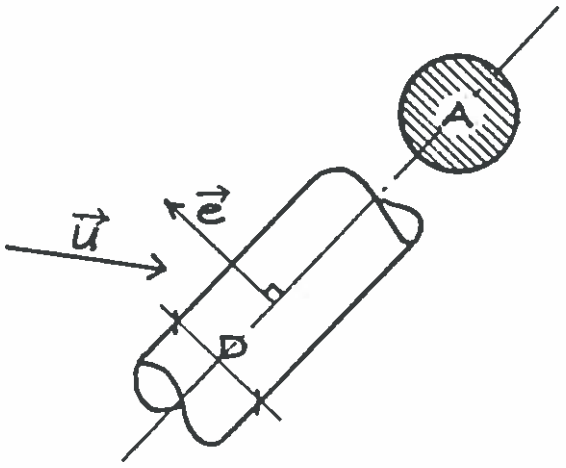

The force F acts perpendicular to the member axis. C_D and C_M are the drag and inertia coefficients respectively, and they are functions of the shape of the cross section, Reynolds number, surface roughness, and the ratio between the particle amplitude and the diameter (this ratio is commonly described by the Keulegan-Carpenter number KC = $U_{max}T/D$). Due to this, the coefficients may also be frequency dependent.

3. In case of dynamic loads from e.g. vortex shedding locking-on or deep water jackets susceptible to dynamic amplification specialized calculation procudures are applied to determine the structural response. In this case, the loads may be functions of the response itself.

RUN DOWN OF PHENOMENA AND UNCERTAINTY

In the following a number of different phenomena with the related uncertainties are presented. The basis for this review is mainly field data from the instrumented jacket platforms

- EXXON OTS (Offshore Test Structure).
- CONOCO CAGC Eugen Island 266 F. Platform.
- Mærsk GORM-D Platform.
- GRIP: Gulf Riser Instrumentation Project.

PHENOMENON	DESCRIPTION	COMMENTS
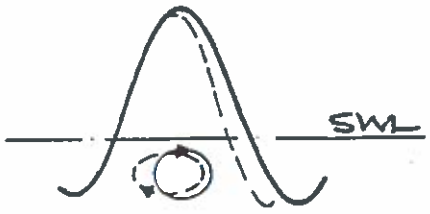	Probability distribution for orbital velocity and acceleration.	Usually Rayleigh or Rice distribution are on the unsafe side. Error in deep water small. In shallower waters: Up to 20% below SWL Up to 40% above SWL.
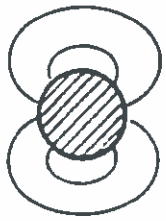	Mass coefficient C_M	Uncertainty in practice for simple cross section 10%
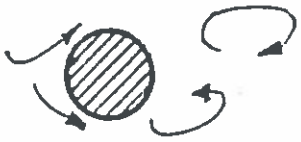	Drag Coefficient C_D	Uncertainty in practice for simple cross section 20%
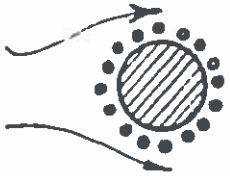	Drag coefficient C_D as a function of roughness.	Uncertainty in practice for simple cross section 20%
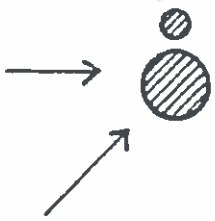	Drag coefficient C_D for a composite structure.	Uncertainty 20-30%

PHENOMENA	DESCRIPTION	COMMENTS
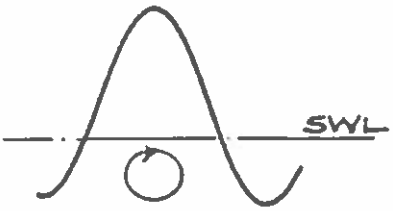	Orbital velocity and acceleration below SWL for known wave height	Uncertainty severely influenced by 3-dimensionality Uncertainty, horizontal vel. and acc.: 50-60% Uncertainty, vertical vel. and acc.: 20-30% Uncertainty, direction: ± 10° (Usually conservative method is applied).
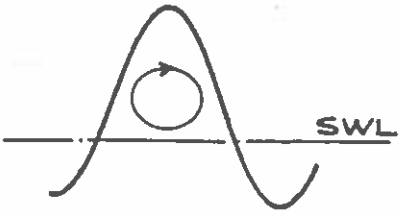	Orbital velocity and acceleration above SWL for known wave height	Uncertainty severely influenced by 3-dimensionality and steepness of crest. Uncertainty, horizontal vel. and acc.: 60% Uncertainty, vertical vel. and acc.: 30% Uncertainty, direction: ± 20° (Usually conservative method is applied).

PHENOMENA	DESCRIPTION	COMMENTS
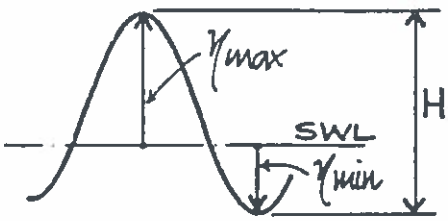	Determination of design wave height and design crest and trough from known significant wave height.	Distribution dependent on water depth. Large water depth: Rayleigh-distribution or Rice-distribution Water depths where bottom influences waves: Distribution function steeper than Rayleigh or Rice distribution. Uncertainty on determination of largest wave: Water depth 80m: 10% Water depth 40m: 40%
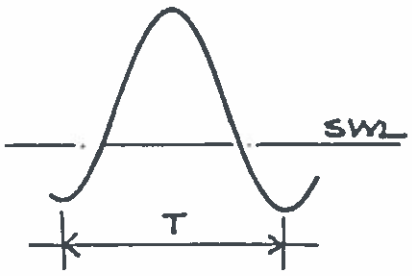	Determination of design wave period from largest wave height.	Uncertainty: 15% The uncertainty on the load depends on the lay-out of the structure. Dense structure in the waterline = large uncertainty on loads.

PHENOMENA	DESCRIPTION	COMMENTS
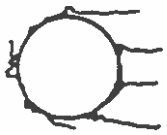	Marine growth, Soft Growth, Seaweed.	Uncertainty on drag coefficient is large. C_D is increased under certain circumstances and decreased under different. Uncertainty: ± 30%
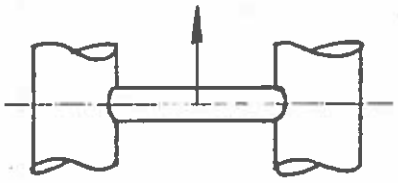	Force on horizontal or vertical member	In case of a short member the force is poorly described by the Morison equation. At small KC-numbers there is no uncertainty on C_D and C_M, but uncertainty on the total force. Uncertainty: 40% In case of a long member, L/D > 10, the Morison equation can be used in practice.

PHENOMENA	DESCRIPTION	COMMENTS
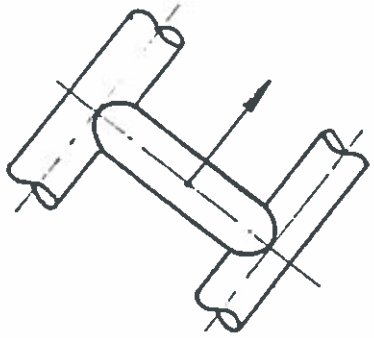	Force on a short member.	For small KC-numbers the uncertainty on C_D and C_M is larger than for higher KC-numbers (KC > 10). Uncertainty: 50%
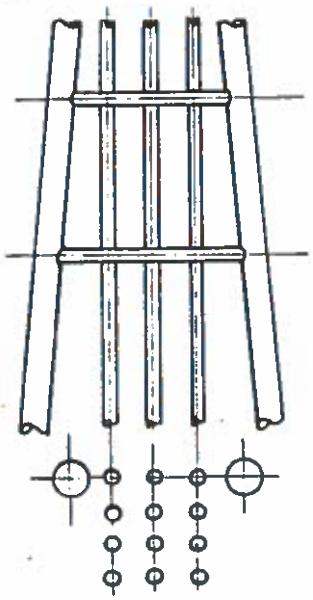	Force on pipe arrays (conductors) with small spacing	If a newly developed calculation procedure (Property of oilcompanies) is used the uncertainty is that of the Morison Equation. In case of old-fashioned practice: Uncertainty on one pipe: 80 Uncertainty on total force: 30%.
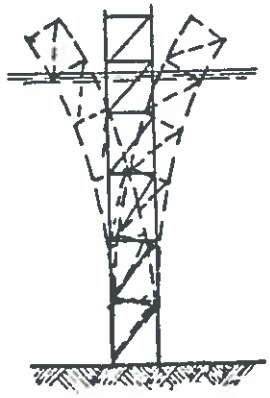	Dynamically amplified platform (resonance)	Damping (Drag and wave damping) Uncertainty: 30% (mainly drag).

PHENOMENA	DESCRIPTION	COMMENTS
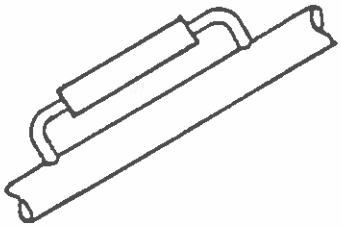	Anodes are accounted for by increased coefficients.	Uncertainty: 20%
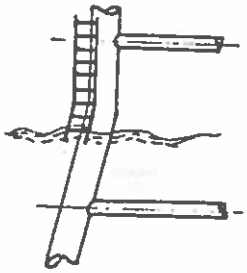	Appurtenances	Uncertainty: 20%
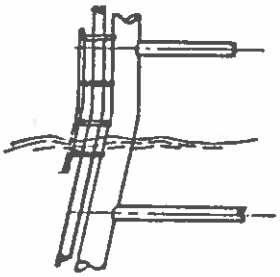	Risers + Riser guides.	Uncertainty on total force: 30% Uncertainty on one pipe (riser) 60%
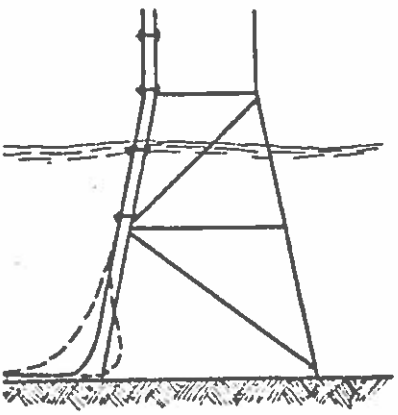	Dynamic problems in connection with risers. Vortex shedding.	Threshold for onset of locking-on (resonance). Uncertainty: 10% Uncertainty on response (using proper analysis): 30%

PHENOMENA	DESCRIPTION	COMMENTS
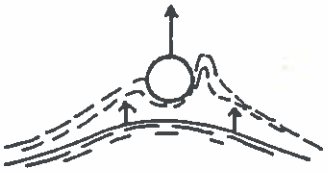	Impact loads from waves.	Uncertainty: 100% (large) (Analysis should be conservative).

When all uncertainties are added, and we compare field measured forces with forces calculated from the sea state, the general uncertainty in calculations is

30%

SEMINAR OM USIKKERHEDER I FORBINDELSE MED DESIGN OG UDFØRELSE AF OFFSHORE JACKET KONSTRUKTIONER

22. maj 1986.

Bidrag fra: Civilingeniør, lic.techn. Svend Ole Hansen,
Skibsteknisk Laboratorium.

USIKKERHEDER PÅ BESTEMMELSE AF VINDLAST

INDHOLDSFORTEGNELSE Side:

1. VINDLASTKÆDEN

Vindlastproblemer kan systematiseres ved opdelingen vist på figur 1. De enkelte elementer er vist som led i en kæde. Derved illustreres dels, at analysen ikke er bedre end svarende til det svageste led, og dels, at leddene i nogen grad griber ind over hinanden.

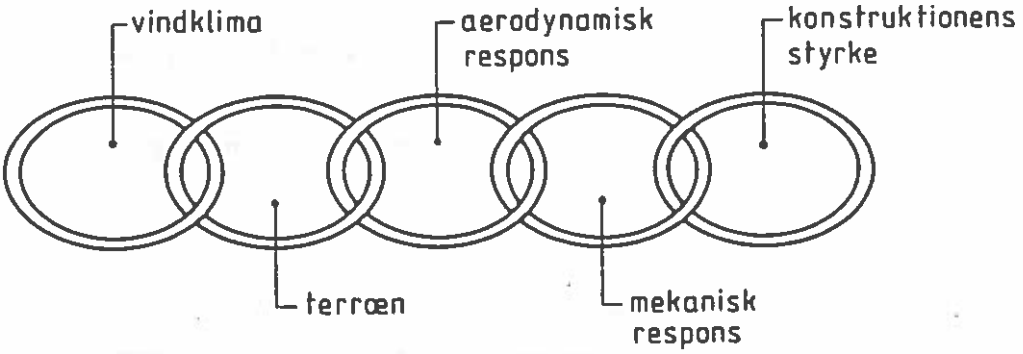

Figur 1. Vindlastkæden.

1.1 Vindklima

Vindklimaet refererer til den overordnede beskrivelse af vindforhold på forskellige geografiske lokaliteter. Det er i denne forbindelse vigtigt at tage hensyn til vindhastighedernes retningsfordeling.

Nedenstående tabel, der gælder for danske forhold (onshore), illustrerer vindens 50-års hastighedstryk q, som funktion af vindretningen, jfr. Ref. /1/:

Vindretning	q/q (WNW)
NNE	0.63
ENE	0.55
ESE	0.65
SSE	0.58
SSW	0.67
WSW	0.83
WNW	1.00
NNW	0.84

Tabel 1. Vindens 50-års hastighedstryk q, som funktion af vindretningen.
$q = \frac{1}{2} \rho U^2$, hvor ρ er luftens massefylde og U vindhastigheden.

1.2 Terrænforhold

Overfladens uregelmæssige form karakteriseret ved eksempelvis bølgehøjden bevirker, at strømningsforholdene i det nederste af atmosfæren er komplicerede og urolige. Gnidningsmodstanden bevirker, at vindhastigheden vokser med højden over terræn, og at der dannes hvirvler. Luftbevægelserne er derfor turbulente i grænselaget.

1.3 Aerodynamisk respons

Når vinden rammer en forhindring, vil luftstrømmens retning ændres. Dette medfører, at der på nogle dele af overfladen opstår et overtryk, på andre dele et undertryk.

Turbulensen bevirker, at vindhastigheden varierer i tiden og dermed også vindlasten. Principielt må vindlast derfor opfattes som en dynamisk last.

Lasten, W i vindretningen på en konstruktion kan udtrykkes ved:

$$W = A \cdot q \cdot C_D \cdot C_F$$

A = Konstruktionens projicerede areal vinkelret på vindretningen.

q = Vindens hastighedstryk. $q = \frac{1}{2} \rho U^2$, hvor ρ er luftens massefylde og U vindhastigheden.

C_D = Formfaktor for middellasten.

C_F = Lastfaktor, der tager hensyn til kraftens variationer i tiden.

1.4 Mekanisk respons

Det led i vindlastkæden refererer til beregningen af konstruktionens respons forårsaget af vindlasten.

1.5 Konstruktionens styrke

Konstruktionens respons sammenholdes med den pågældende konstruktions styrke.

I det følgende vil usikkerhederne i forbindelse med terrænforholdene og det aerodynamiske respons blive belyst nærmere.

Der gennemgås i kapitel 2 metoder til reduktion af usikkerhederne, og i kapitel 3 søges usikkerhederne kvantificeret.

2. REDUKTION AF USIKKERHEDER

Det er ikke muligt i dag at beregne egenskaberne af den turbulente strømning omkring - og dermed vindlasten på - en given konstruktion. Det er ofte kun muligt at bestemme vindlasten med rimelig præcision ved forsøg. Til dette formål anvendes normalt en grænselagsvindtunnel, hvor realistiske eksperimenter kan udføres under kontrollerede betingelser.

Skibsteknisk Laboratoriums grænselagsvindtunnel er vist på figur 2. Den er beskrevet nærmere i Ref. /2/.

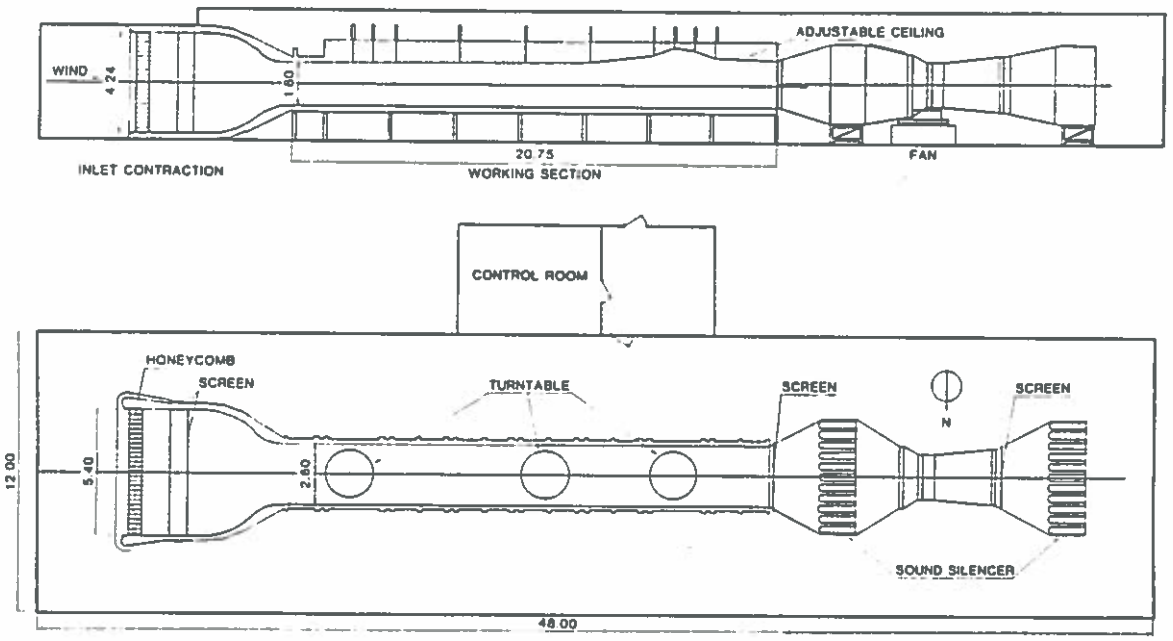

Figur 2. Grænselagsvindtunnelen på Skibsteknisk Laboratorium.

2.1 Terrænforhold

Strømningsforholdene i et komplekst terræn er blevet simuleret i grænselagsvindtunnelen for Norwegian Contractors. En model af Yrkefjord og Vatsfjord området, se figur 3, nord for Stavanger i Norge blev undersøgt i vindtunnelen i skala 1:5000, se figur 4.

Området anvendes af Norwegian Contractors i forbindelse med opførelsen af beton platforme. Sikkerheden er en vigtig faktor, hvilket gjorde modelforsøgene nødvendige.

Det kan nævnes, at resultaterne har medført væsentlige besparelser under konstruktionsfasen.

Figur 3. Det komplekse terræn omkring Yrkefjorden og Vatsfjorden.

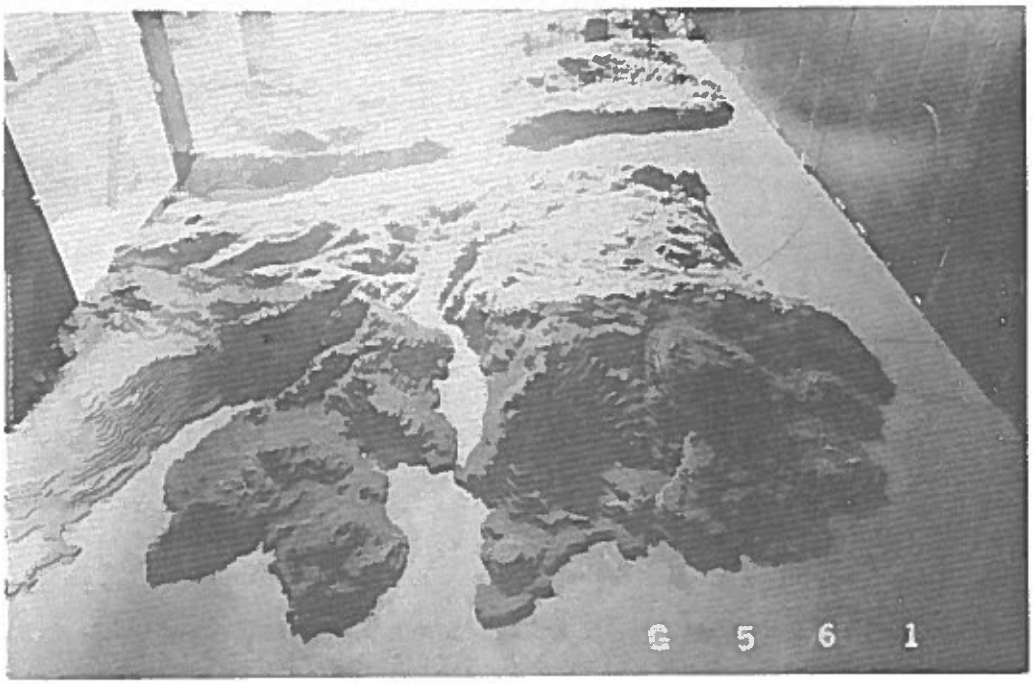

Figur 4. Det komplekse terræn i vindtunnelen i skala 1:5000. Området på figur 3 ses i baggrunden af figuren.

2.2 Aerodynamisk respons

Vindlasten på en konstruktion kan bestemmes med stor nøjagtighed i grænselagsvindtunnelen. Der anvendes typisk modeller af konstruktionen i en skala mellem 1:100 og 1:500. Vindlasten bestemmes for vindretninger hele kompasset rundt.

Nedenfor vises 3 eksempler på modeller af platforme placeret i grænselagstunnelen.

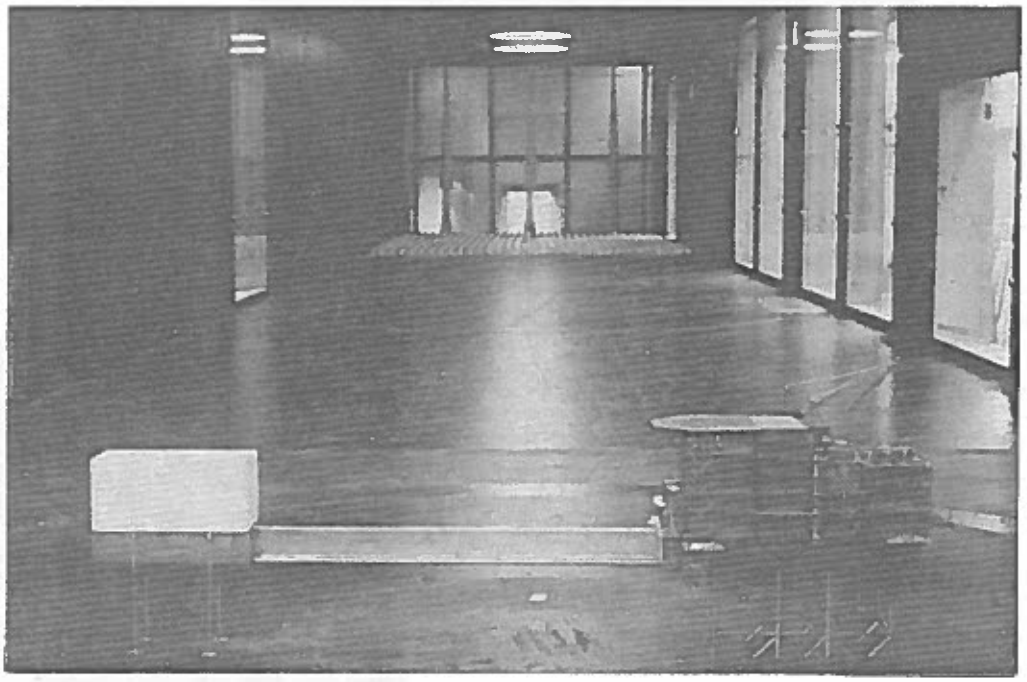

Figur 5. Jacket konstruktion (ikke vindlastmålinger).
Klient: Mærsk Olie og Gas.

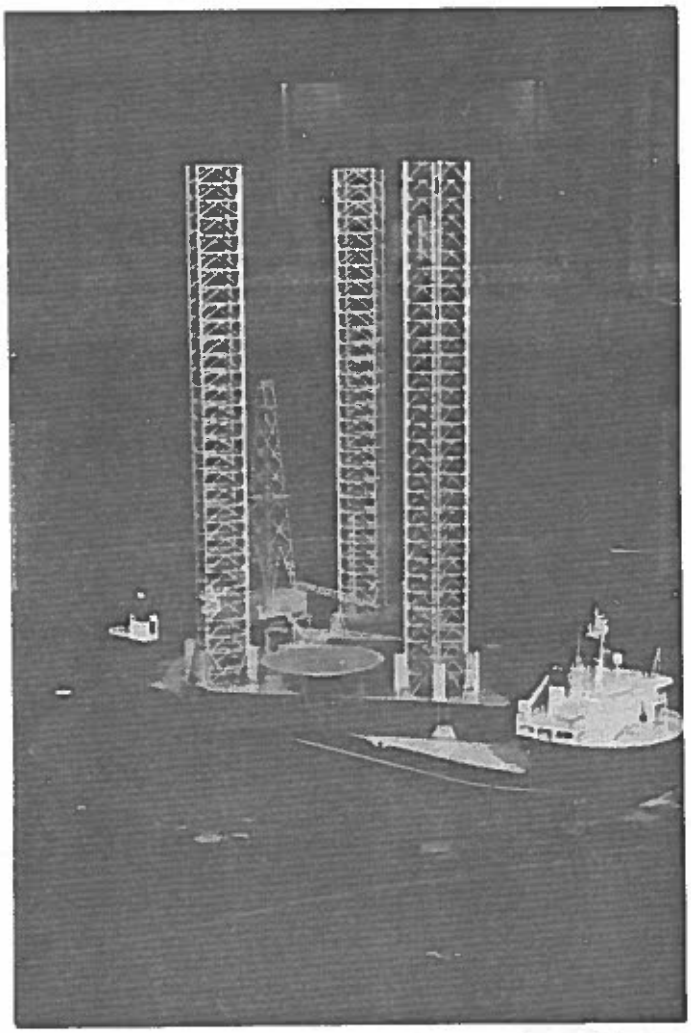

Figur 6. Jack-up.
Klient: J. Lauritzen.

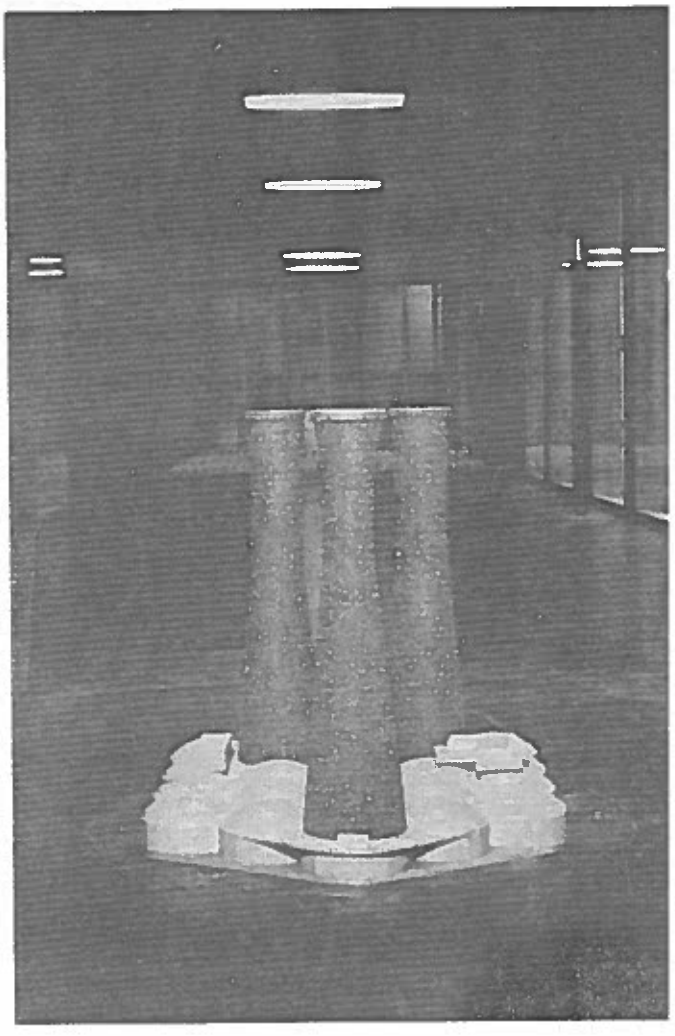

Figur 7. Condeep under tow-out.
Klient: Norwegian Contractors.

3. USIKKERHEDER PÅ VINDLASTEN

Usikkerheden på bestemmelse af vindlasten, W er illustreret i nedenstående figur. Der ses bort fra usikkerheder i forbindelse med konstruktionens geometri.

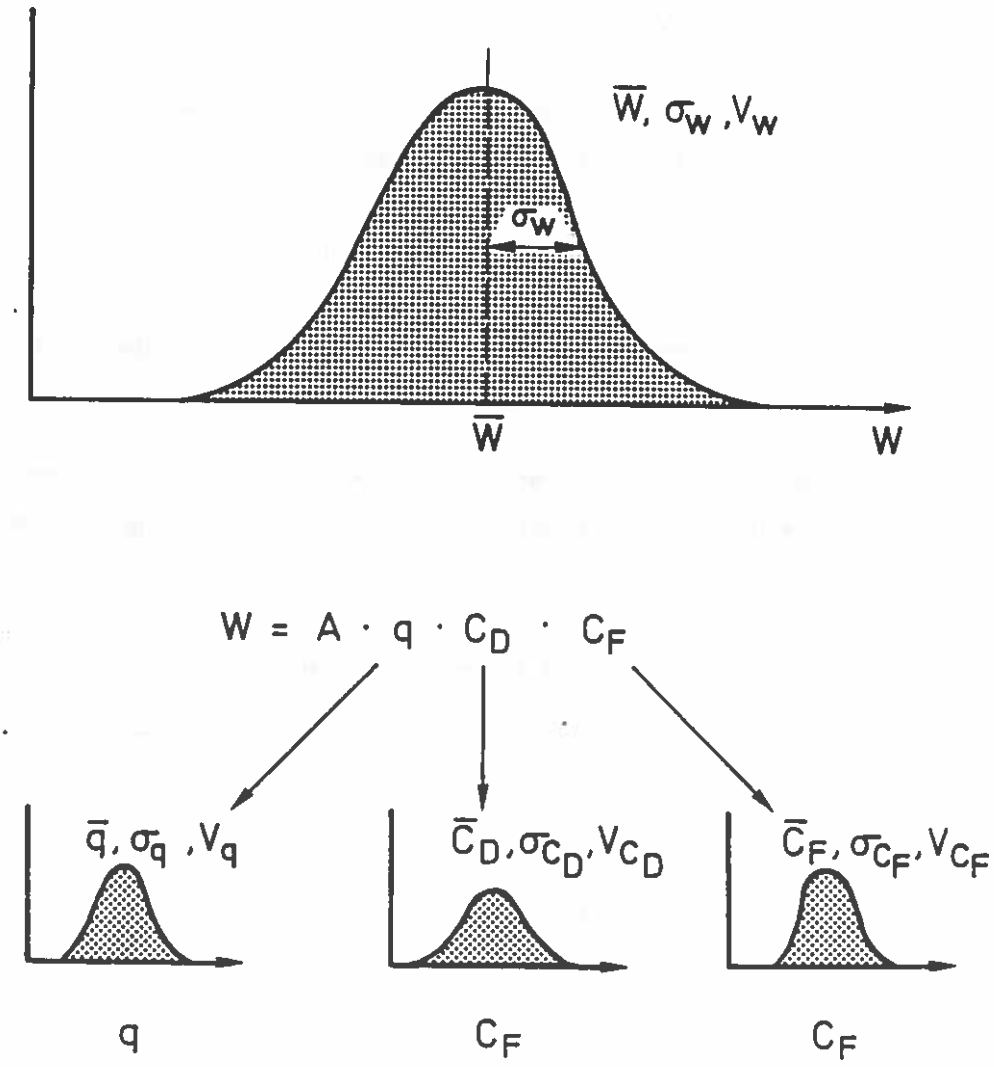

Figur 8. Statistiske faktorer ved bestemmelse af vindlasten W.

- A Konstruktionens projicerede areal vinkelret på vindretningen.
- q Vindens hastighedstryk.
- C_D Formfaktor for middellasten.
- C_F Hastighedsfaktor, der tager hensyn til kraftens variationer i tiden.

Hastighedstrykket q og lastfaktorerne C_D og C_F vist i figur 8 kan sædvanligvis med god tilnærmelse regnes uafhængige af hinanden. Middellasten $\bar{W}$ og variationskoefficienten V_W (spredningen/middelværdien) kan således bestemmes af udtrykkene:

$$\bar{W} = A \cdot \bar{q} \cdot \bar{C}_D \cdot \bar{C}_F$$

$$(1+V_W^2) = (1+V_q^2) \cdot (1+V_{C_D}^2) \cdot (1+V_{C_F}^2)$$

Som vist i Ref. /3/ og /4/ kan forholdet mellem designlasten og middellasten findes med rimelig tilnærmelse af udtrykket:

$$W_{design} / \bar{W} = \exp(0.55 \cdot \beta \cdot V_W),$$

hvor sikkerhedsindekset β er af størrelsesordenen 3 svarende til en overskridelsessandsynlighed på ca. 10^{-3}.

I nedenstående tabel er usikkerhederne skønnet svarende til dels anvendelsen af en standard norm og dels ved brug af mere præcise metoder.

	Standard norm	Meteorologiske målinger og vindtunnelstudier
V_q	0.30	0.15
V_{C_D}	0.15	0.05
V_{C_F}	0.15	0.05
V_W	0.37	0.17
$W_{design} / \bar{W}$	1.85	1.32

Tabel 2. Skønnede usikkerheder på bestemmelse af vindlasten.

4. KONKLUSION

Der kan konkluderes:

- Den væsentligste usikkerhedskomponent ved bestemmelse af vindlasten hidrører fra hastighedstrykket q.

- Anvendelse af meteorologiske målinger og vindtunnelstudier medfører en mere præcis fastlæggelse af lasten og reducerer samtidig usikkerheden på bestemmelsen.

Det foreslås, at fremtidige normer muliggør en rationel fastsættelse af partialkoefficienter under hensyntagen til den usikkerhed, der indgår i lastbestemmelsen. Anvendelse af modelforsøg i et konkret tilfælde kunne således - udover en mere præcis last - retfærdiggøre en lavere sat partialkoefficient.

5. REFERENCER

/1/ Christensen, O.: "Stormskaderisiko".

Temadag om stormskader. Vindteknisk Udvalg, Skibsteknisk Laboratorium. November 1982.

/2/ Hansen, S.O. and E.G. Sørensen: "A New Boundary-Layer Wind Tunnel at the Danish Maritime Institute".

Journal of Wind Engineering and Industrial Aerodynamics, Vol. 18, 1985, pp. 213-224.

/3/ Davenport, A.G.: "The Interaction of Wind and Structures".

Kapitel 12 af bogen: "Engineering Meteorology. Elsevier Scientific Publishing Company, 1982.

/4/ Davenport A.G.: "On the Assessment of the Reliability of Wind Loading on Low Buildings".

Proceedings of the 5th Colloquium on Industrial Aerodynamics, Aachen, June 14-16, 1982.

NGI

UNCERTAINTIES IN PILE DESIGN

Notes presented at a seminar on
UNCERTAINTIES RELATED TO JACKET DESIGN
Danmark Tekniske Højskole
22. May 1986
by
Per Magne Aas
Norwegian Geotechnical Institute

1. GENERAL

This presentation concentrates on uncertainties in pile design. There are several factors affecting the pile design. Fig. 1 lists some of them: wall friction, tip bearing capacity, axial and lateral stiffnesses of the pile-soil system and soil resistance during driving of the pile. The type of cyclic loading that is experienced by offshore piles is emphasized: one-way or two-way cyclic loading. Pile load tests conducted by NGI show that with current design practice the safety level depend on the type of loading. The presentation will concentrate on wall friction in both sand and clay, tip bearing capacity in sand and axial and lateral stiffnesses as these factors are considered to be of highest priority. Tip bearing capacity in clay is omitted, since it is often a minor (and thereby less important) contribution to the total bearing capacity of the piles.

2. WALL FRICTION IN CLAY

To estimate the wall friction empirical calculation methods are commonly used. Two of these are shown on Fig. 2, and in both methods the undrained shear strength, S_u, of the clay is the key parameter. There are, however, many ways to determine the undrained shear strength, as seen on Fig. 3. Consolidated, undrained direct simple shear tests (DSS) are not commonly used, but through recent pile test programs run at NGI, Ref. (1) and (2), it is shown that these tests are suitable to explain the behaviour of the soil adjacent to the pile during loading. This will be discussed later.

In the way the empirical formula are derived, the undrained shear strength relates to field vane, unconfined compression tests or uncon-

solidated, undrained triaxial tests. This should be noted when applying these formulas, as there can be a considerable discrepancy between undrained shear strength, measured in different ways, see Fig. 4 as an example.

Fig. 5, which is taken from the extensive study of pile load tests in Ref. (3), shows the ratio between calculated pile capacity and measured pile capacity for different sites, different measurements of S_u and evaluated soil sample quality. Fig. 6 indicates the proposed correction for S_u when applied to empirical formulas.

On Fig. 7 is shown typical range of calculated wall friction capacity, when seven different methods, Ref. (3) - (9), are applied to a pile in mainly normally consolidated clay. NGI's judgement of the capacity is indicated for an intended pile penetration of 80 m. The estimate is mainly based on the recommendations in Ref. (3).

Field model pile tests in an overconsolidated clay

NGI has recently carried out a series of static and cyclic pile load tests in order to measure the behaviour of the soil adjacent to the pile during the installation, consolidation and the subsequent loading phase. Fig. 8 shows extract from the pile instrumentation.

Fig. 9 shows the measured wall friction, as compared to predictions made by means of the empirical α - and λ - methods. It is seen that actually mobilized wall friction is totally different from the predicted mobilized wall friction. Thus, it can be concluded that the empirical methods do not necessarily model the real soil behaviour, even if the methods give reasonable estimates of total capacity.

Simultaneous with the pile testing direct, simple shear tests (DSS) were run in the laboratory on remoulded, reconsolidated clay specimens. Through the testing program it is shown that these laboratory tests can explain wall friction mobilization, preshearing effects and failure development as a function of cyclic loading.

Fig. 10 shows measured wall friction and computed wall friction based on DSS-tests on remoulded and reconsolidated clay. The laboratory test results are seen to fit reasonably well to the measured pile-soil friction.

The pile load tests also show another important phenomenon. There is a considerable difference between the first static loading, and the next static loading after intermediate cyclic loading and reconsolidation of the soil. This is shown on Fig. 11. The same effect (preshearing) can easily be seen in the laboratory test results.

Fig. 12 shows a summary of the cyclic pile load test results and results from cyclic DSS laboratory tests. The diagram shows the relationship between the average pile load Q_{ave} (average shear stress in the DSS tests), the cyclic pile load amplitude (cyclic shear stress in the DSS tests) and the number of cycles to failure (N_f). Again it can be seen that laboratory tests on remoulded and reconsolidated clay (RR clay) show a behaviour very similar to the measured behaviour of the soil adjacent to the piles. Failure of the piles is associated with rapid increase in the average displacement, cyclic displacement or both, dependant on the combination of average and cyclic loads, as seen on Fig. 13.

At NGI design of piles in clay is now performed on the basis of ordinary empirical formulas of pile wall friction capacity in addition to the concept of cyclic pile wall friction capacity. The latter is derived from the observed pile behaviour during static and cyclic load tests and the close correlation with DSS laboratory tests on remoulded

and reconsolidated clay specimens. The cyclic capacity concept includes the following features:

- DSS tests, giving the relationship between average and cyclic shear stresses and number of cycles to failure.

- Failure criterion, giving the stiffness and strength degradation for those soil elements along the pile that have reached a critical average and cyclic shear stress combination.

- Assumed storm build-up period with the maximum loading at the end.

- Iterative computation, adjusting the stress distribution along the pile according to stiffness and strength degradation until equilibrium or failure (excessive displacements).

A proper understanding of the pile behaviour during cyclic loading is necessary as the safety level is different for different type of loading. Failure is governed by excessive displacement, either cyclic, accumulation of average displacement or both.

Attractive economical solutions or the feasibility of new concepts (tension-leg platforms, simple mono-tower structures, deep water jackets) may depend on proper modelling of the pile-soil behaviour. More traditional jacket structures in shallower water can be optimized.

3. WALL FRICTION IN SAND

Design codes usually apply the formula

$$f = K_o \, p_o' \tan \delta$$

to calculate the wall friction in sand. K_o = earth pressure coefficient, p_o' = effective overburden stress, δ = pile/soil friction angle. A simple calculation shows that at a depth of 40 m the formula gives a wall friction of the order of 200-280 kPa, as shown on Fig. 14. However, design codes, Ref. (4), usually set an upper limit of wall friction to 120-150 kPa. This major discrepancy represents perhaps a significant hidden margin on the design of piles in sand. The limitation set on the wall friction may be due to

- Length effect
- Reduced soil friction angle with increasing effective stress
- It is an apparent effect: if friction fatigue takes place during driving there is less wall friction capacity along the upper part of the pile and higher wall friction capacity further down
- Residual stresses after driving. Fig. 15 shows measured wall friction along a pile installed in a sand deposit at Drammen, Norway. Unless the residual stresses in the unloaded state is taken into account, the mobilized wall friction along the lower part of the pile is underestimated.

Characteristic soil strength data are usually obtained from cone penetration test result, as shown on Fig. 16. The relative density is determined from the relationship between the cone tip resistance and

the overburden pressure. Triaxial tests carried out on reconstituted samples of various densitives give a measure of the friction angle as a function of the relative density. However, as shown by the sample calculation above the discrepancy between the theoretically calculated wall friction and the commonly applied upper limits represent a major shortcomming in the understanding of mobilization of wall friction in sand.

4. TIP RESISTANCE IN SAND

The bearing capacity of the pile tip is usually computed as

$$q = N_q \cdot \sigma_{vo}'$$

where N_q = bearing capacity factor

σ_{vo}' = effective overburden stress

Fig. 17 presents values for the bearing capacity factor N_q as a function of the friction angle. As seen from this figure there is considerable uncertainty when assessing this factor. The figure also includes the recommended N_q in the API-code, Ref (4). This is seen to lie reasonably low in the expected range of variation. However, as for wall friction, current practice of pile design sets limitation on the end bearing, as indicated in Fig. 18.

5. PILE-SOIL STIFFNESSES, AXIAL LOADING

The accuracy of the assumptions usually made with respect to axial stiffnesses (so-called t-z curves for the soil) is not of major importance in design of traditional jackets in relatively shallow water, where the dynamic behaviour of the structure is not decisive. Assumptions can therefore be made on the conservative side (low estimates) without major consequences for the design. This may not be the case in deeper waters, where the natural periods of the structure approach the wave periods such that considerable dynamic amplification can take place. Higher foundation stiffnesses will improve the design basis, so it is highly important to document higher stiffnesses than usually assumed in the design. Recent pile load tests, come to NGI's knowledge, may in fact indicate higher pile stiffnesses. It therefore remains to describe by analytical methods pile behaviour in accordance with such observations in order to be implemented in future designs.

6. PILE-SOIL STIFFNESSES, LATERAL LOADING

Lateral pile-soil stiffnesses are usually generated on the basis of the API-codes, Ref. (4). The soil is modelled as Winkler springs, where the spring stiffnesses are expressed as so-called p-y curves. API recommends p-y curves for static as well as cyclic loading for different soils.

It is NGI's experience that the recommended curves for static loading in general prescribe stiffnesses on the safe side (low stiffnesses). Cyclic p-y curves, however, are necessarily not on the low side.

The assumptions made with regard to p-y curves for traditional jacket structures are not of major significance for the computation of the pile reaction in the ultimate limit state load condition. On the other hand, for special platform concepts and for fatigue analyses the possibility of a considerably higher stiffness of the soil response (low strain modules of the soil) than presented by the commonly used p-y curves may be a question of major importance.

7. PARAMETRIC STUDY OF A PILED JACKET STRUCTURE

In order to investigate the effect of change of soil parameters on the analysis of a real jacket-pile configuration, a parametric study was carried out, Ref. (10). In the computation model, the piles were interconnected by the elastic jacket structure (elastic stiffness matrix). The structure is shown in Fig. 19. Jacket members marked on the figure and the piles were investigated.

The change in steel stresses for the different jacket members and the piles, for the different cases investigated, was assumed to require a corresponding change in member wall thicknesses and thereby a corresponding change in steel weight. Fig. 20 shows the results of the parametric study for the piles. Wall friction was not included as a parameter as it would determine the necessary pile penetrations (in fact this is the parameter of greatest interest, however, as soon as the wall friction is decided upon and thereby the required pile penetrations, it would not affect the results of jacket-pile interaction analyses).

In the basic case 2 m of scour was assumed. The change of scour depth to 4 m, which was considered to be an extreme value, turned out to be the parameter of greatest influence. This is, however, a parameter

that can be controlled, as measures can be taken to counteract the effect of scour. Besides, assumptions made with respect to computation of pile group load-displacement behaviour (group effects) were among the most sensitive assumptions. This is in fact, a question of soil modulus (soil stiffness) to be put into the analyses.

In the basic case a friction angle of 35° for the top sand was applied. In case 3 the friction angle was increased to 40° and the p-y curves were corrected accordingly. This change of the friction angle was considered to cover a reasonable scatter and uncertainty.

In case 4 the soil modulus governing the mobilization of wall friction was reduced by a factor of two, which was assumed to represent a reasonable variation.

Finally, a relevant calculation result requires modelling of the jacket elasticity. Otherwise the pile stresses are highly overestimated.

NGI

8. REFERENCES

1. Karlsrud, K. and T. Haugen (1985)
Behaviour of piles in clay under cyclic loading - results of field model tests.
International Conference on Behaviour of Offshore Structures, 4. BOSS'85. Delft 1985.
Proceedings, pp. 589-600.

2. Karlsrud, K., F. Nadim and T. Haugen (1986)
Piles in clay under cyclic axial loading. Field tests and computational modelling.
International Conference on Numerical Methods in Offshore Piling, 3. Nantes, 1986, pp. 165-190.

3. Dennis, Jr., N.D. and R.E. Olson (1983)
Axial capacity of steel pipe piles in clay.
Conference on Geotechical Practice in Offshore Engineering, Austin, Texas 1983.
Proceedings, N.Y. American Society of Civil Engineers, pp. 370-388.

4. American Petroleum Institute, Dallas (1982)
Planning, designing and constructing fixed offshore platforms.
API. Recommended practice, RP 2A. 13th edition.

5. Semple, R.M. and W.J. Rigden (1984)
Shaft capacity of driven piles in clay.
Analysis and Design of Pile Foundations. San Francisco, Cal. 1984
Proceedings of a symposium publ. by American Society of Civil Engineers , pp. 59-79.

6. Flaate, K. and Selnes, P. (1977)
Side friction of piles in clay.
International Conference on Soil Mechanics and Foundation Engineering, 9. Tokyo 1977.
Proceeding, Vol. 1, pp. 517-522.
Also publ. in: Norwegian Geotechnical Institute, Oslo. Publication, 118.

7. Vijayvergiya, V.N. and J.A. Focht Jr. (1972)
A new way to predict capacity of piles in clay.
Offshore Technology Conference, 4. Dallas, Texas 1972.
Preprints Vol. 2, pp. 865-871.

8. Kraft, L.M., J.A. Focht and S.F. Amerasinghe (1981)
Friction capacity of piles driven into clay.
American Society of Civil Engineers.
Proceedings, Vol. 107, No. GT11, pp. 1521-1541.

9. Janbu, N. (1976)
Static bearing capacity of friction piles.
European Conference on Soil Mechanics and Foundation Engineering.
6. Vienna 1976.
Proceedings, Vol. 1.2, pp. 479-488.

10. Clausen, C.J.F., P.M. Aas and I.B. Almeland (1982)
Analysis of the pile foundation system for a North Sea drilling platform.
International Conference on the Behaviour of Offshore Structures,
3. BOSS'82. Cambridge, Mass. 1982.
Proceedings, Vol. 2, pp. 95-104.

UNCERTAINTIES IN PILE DESIGN

WALL FRICTION, clay and sand

Type of loading - one-way - two-way

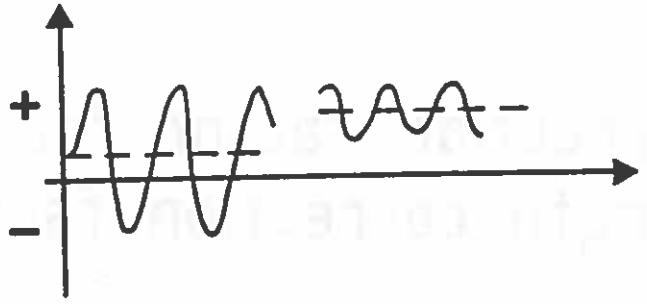

END BEARING, sand
AXIAL STIFFNESS

LATERAL STIFFNESS
END BEARING, clay
DRIVING RESISTANCE

Fig. 1

WALL FRICTION, clay

<u>α-method:</u> $f = \alpha \cdot F_C \cdot F_L \cdot s_u$

- F_C = Correction factor for s_u
- F_L = Length correction factor
- $\alpha \leqq 1.0$

<u>λ-method:</u> $f = \lambda(\bar{\sigma}_{vo}' + 2\bar{s}_u)$

- $\bar{\sigma}_{v'o}$ = mean vertical effective stress
- $\bar{s}_u$ = mean s_u over the pile length

s_u = undrained shear strength

Fig. 2

DETERMINATION OF s_u

fall cone
torvane
penetrometer
} index tests

field vane
cone penetration
} in-situ tests

Unconfined compr. test (UCT) 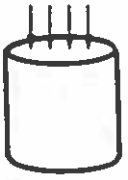

Unconsolidated, undrained triaxial (UU) 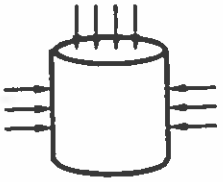

Consolidated, undrained triaxial (CiU) 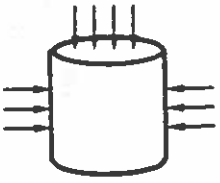

Consolidated, undrained direct simple shear (DSS) 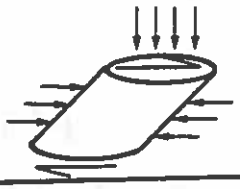

Fig. 3

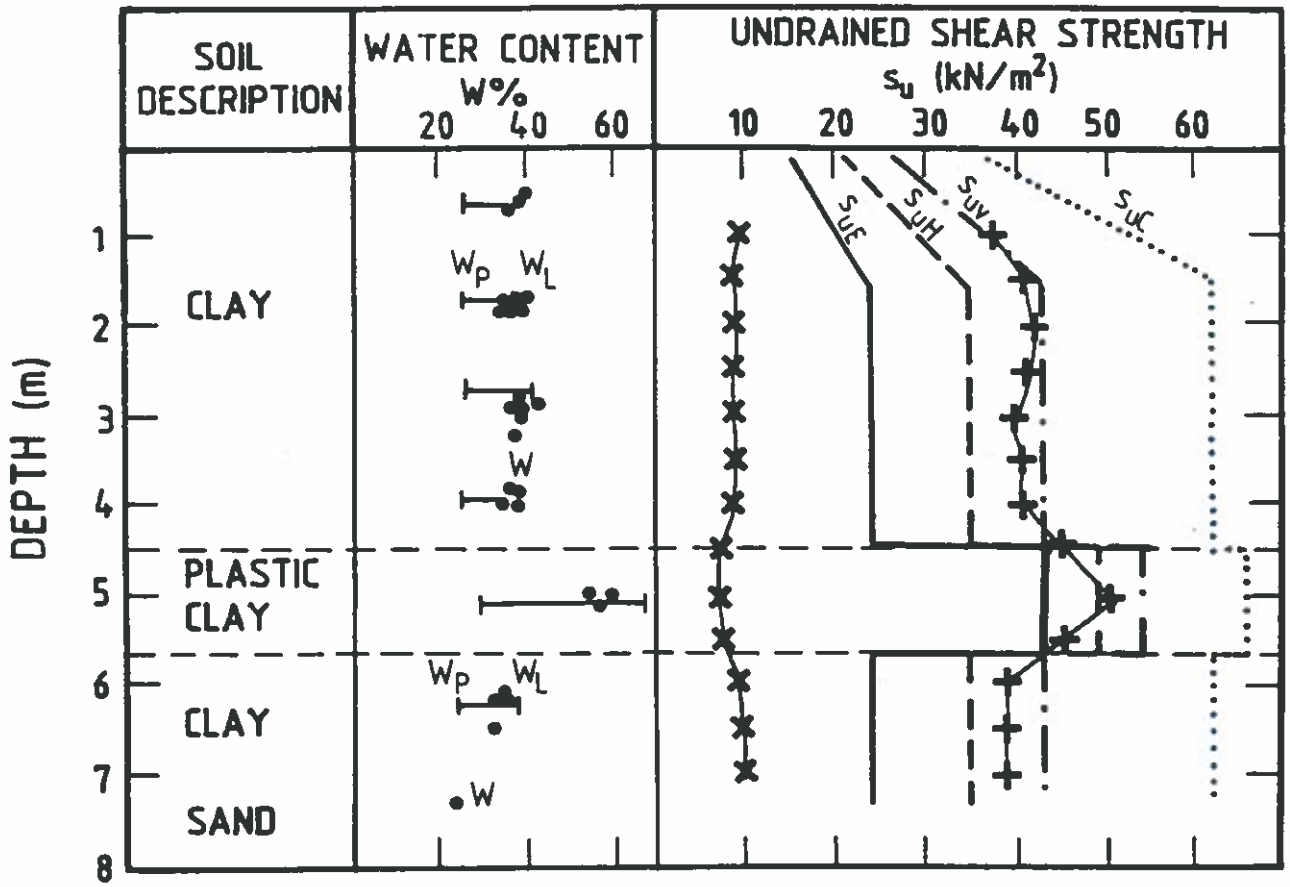

General soil profile and in-situ undrained shear strengths

Fig. 4

SITE	SQF	$Q_{calculated}/Q_{measured}$ for s_u (UC)	s_u(UU)	s_u(index)	s_u (FV)
San Francisco	4	1.06			2.38
	3	0.80	0.79		
		0.67	0.67		
		0.88	0.88		
		0.86	0.86		
Empire	2	0.88	0.84		1.11
		0.73	0.70		0.92
		0.66	0.88	0.78	1.27
		0.74	0.97	0.86	1.41
		0.61	0.42	0.68	
		0.82	0.55	0.92	
		0.54	0.63	0.81	
		0.76	0.89	1.15	
Houston	4	1.01	1.04	1.04	
		0.81	0.84	0.84	
		1.16	1.19	1.19	
		0.91	0.94	0.94	
		1.10	1.13	1.13	
		1.00	1.03	1.03	
		0.72	0.74	0.77	
		0.70	0.72	0.75	
Hamilton	4	1.04		1.24	
		1.56		1.85	
		1.66		1.98	
		1.18		1.41	
		1.28		1.52	
		1.91		2.27	
		1.82		2.16	
		1.35		1.60	

LEGEND

SQF — sample quality factor, ranges from 0 to 5

s_u(UC) — indicates use of unconfined compression shearing strength.

s_u(UU) — denotes use of unconsolidated-undrained triaxial compression test strength.

s_u(index) — used to denote use of miscellaneous index test shearing data (mainly laboratory vane and torvane).

s_u(FV) — use of field vane shearing strength.

SITE — details of site conditions are described in Olson (1984).

Fig. 5

Soil testing techniques	F_C
Unconfined compression tests on high quality samples	1.1
Unconfined compression tests on samples taken with typical driven samplers	1.8
In situ vane shear tests	0.7

$$F_C = \frac{S_u\ (UU)}{S_u\ (UCT,\ FV)}$$

Fig. 6

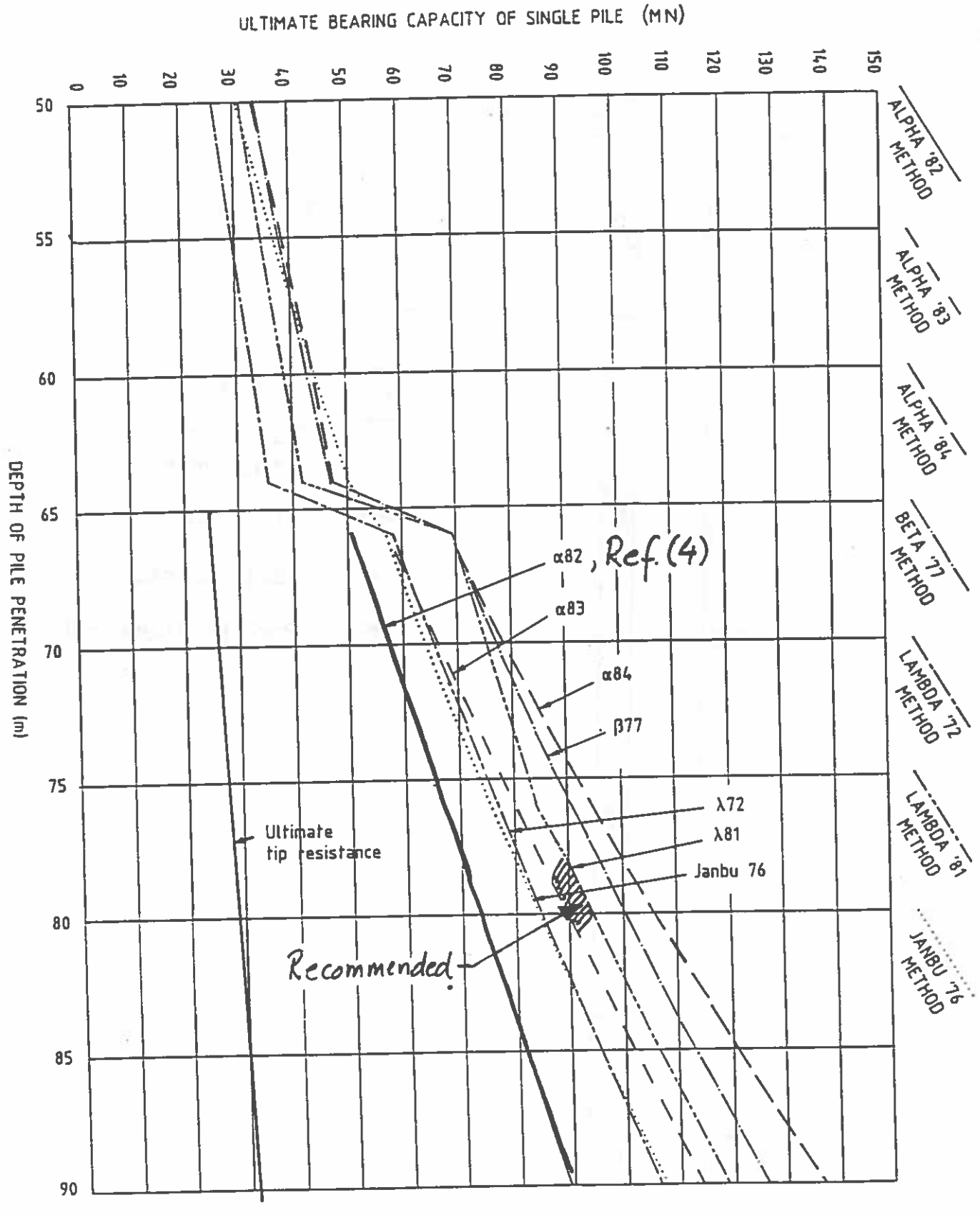
ULTIMATE BEARING CAPACITY OF SINGLE PILE (MN)
0
10
20
30
40
50
60
70
80
90
100
110
120
130
140
150
DEPTH OF PILE PENETRATION (m)
50
55
60
65
70
75
80
85
90
ALPHA '82 METHOD
ALPHA '83 METHOD
ALPHA '84 METHOD
BETA '77 METHOD
LAMBDA '72 METHOD
LAMBDA '81 METHOD
JANBU '76 METHOD
α82 , Ref. (4)
α83
α84
β77
λ72
λ81
Janbu 76
Ultimate tip resistance
Recommended

Fig. 7

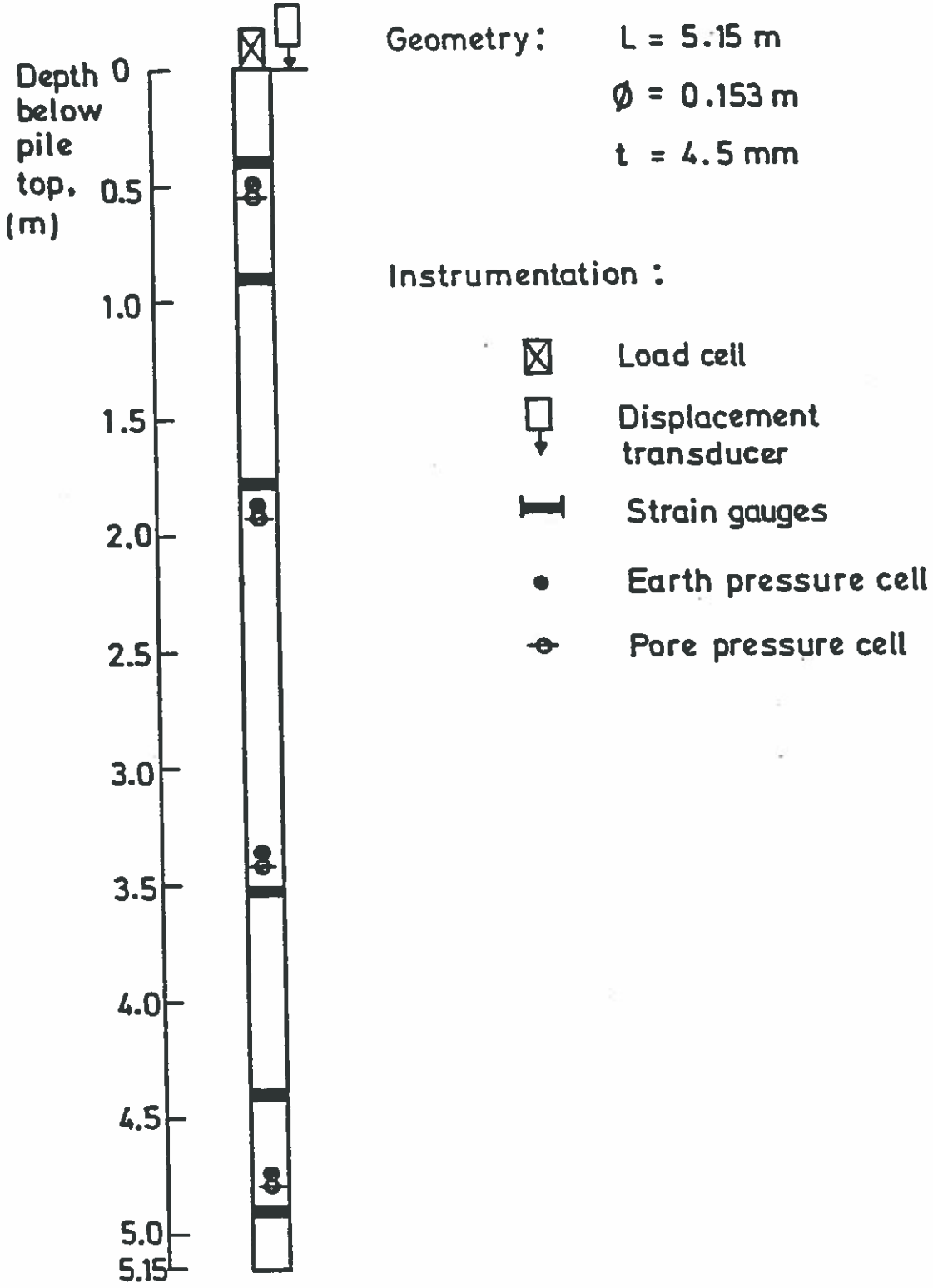

Model pile, HAGA

Fig. 8

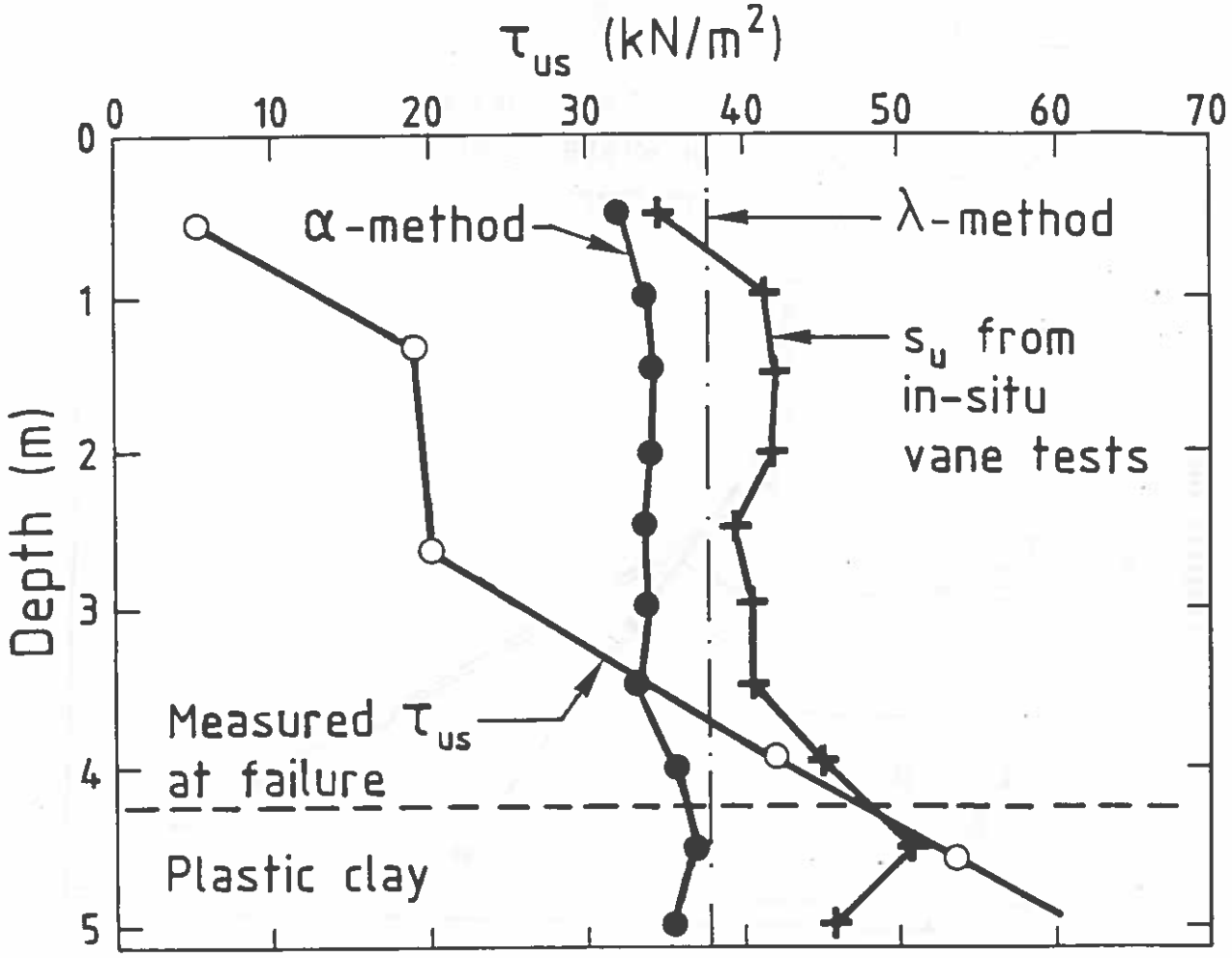

Measured and predicted limit skin friction, initial static tests

Fig. 9

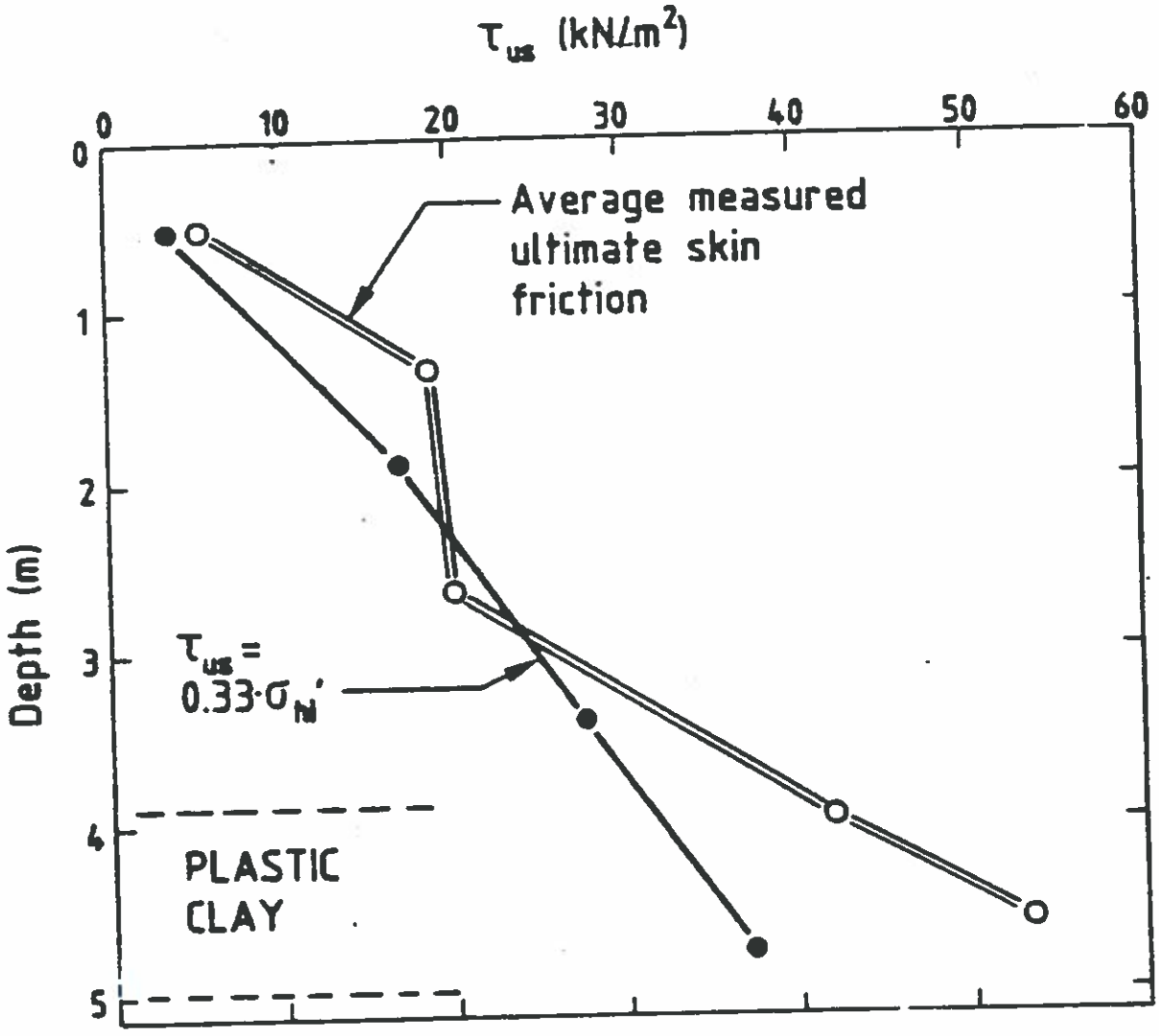

Measured ultimate skin friction and computed skin friction based on laboratory tests on remoulded, reco solidated clay

Fig. 10

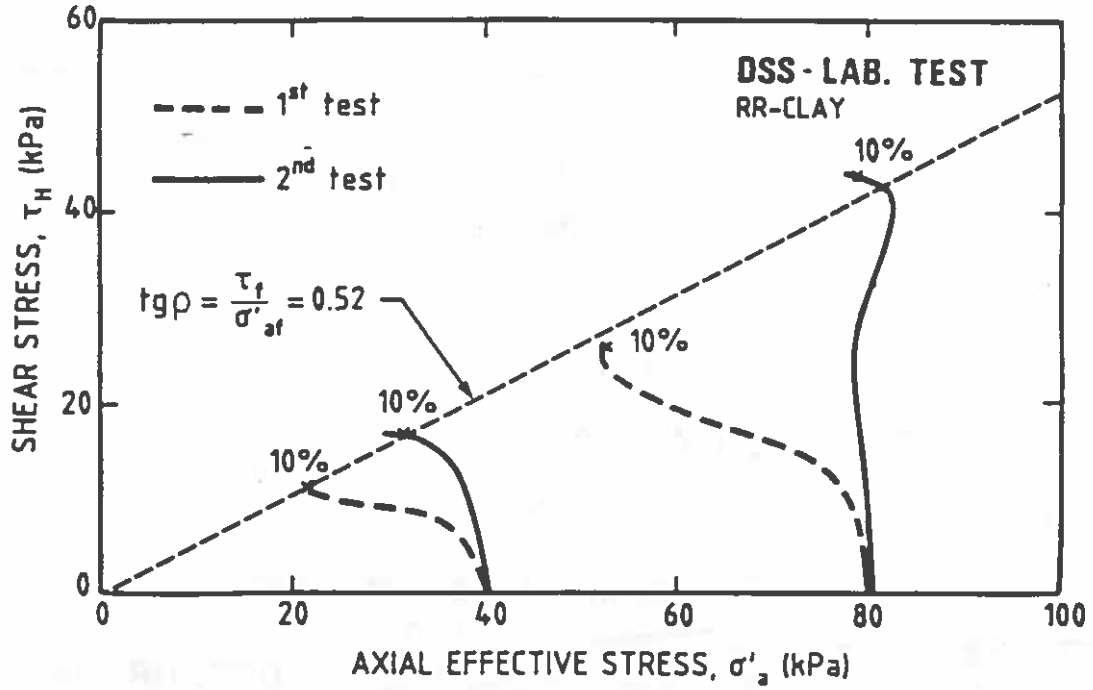
DSS - LAB. TEST
RR-CLAY
1st test
2nd test
$tg\rho = \frac{\tau_f}{\sigma'_{af}} = 0.52$
10%
10%
10%
10%
SHEAR STRESS, τ_H (kPa)
AXIAL EFFECTIVE STRESS, σ'_a (kPa)
0
20
40
60
80
100

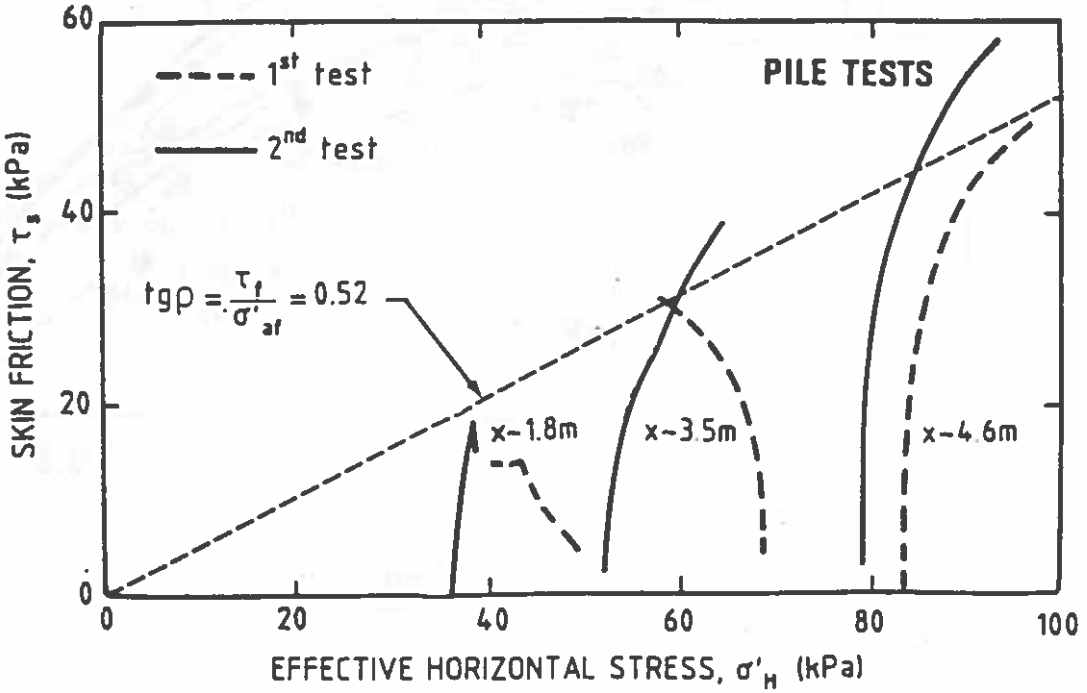
PILE TESTS
1st test
2nd test
$tg\rho = \frac{\tau_f}{\sigma'_{af}} = 0.52$
x-1.8m
x-3.5m
x-4.6m
SKIN FRICTION, τ_s (kPa)
EFFECTIVE HORIZONTAL STRESS, σ'_H (kPa)
0
20
40
60
80
100

Fig. 11

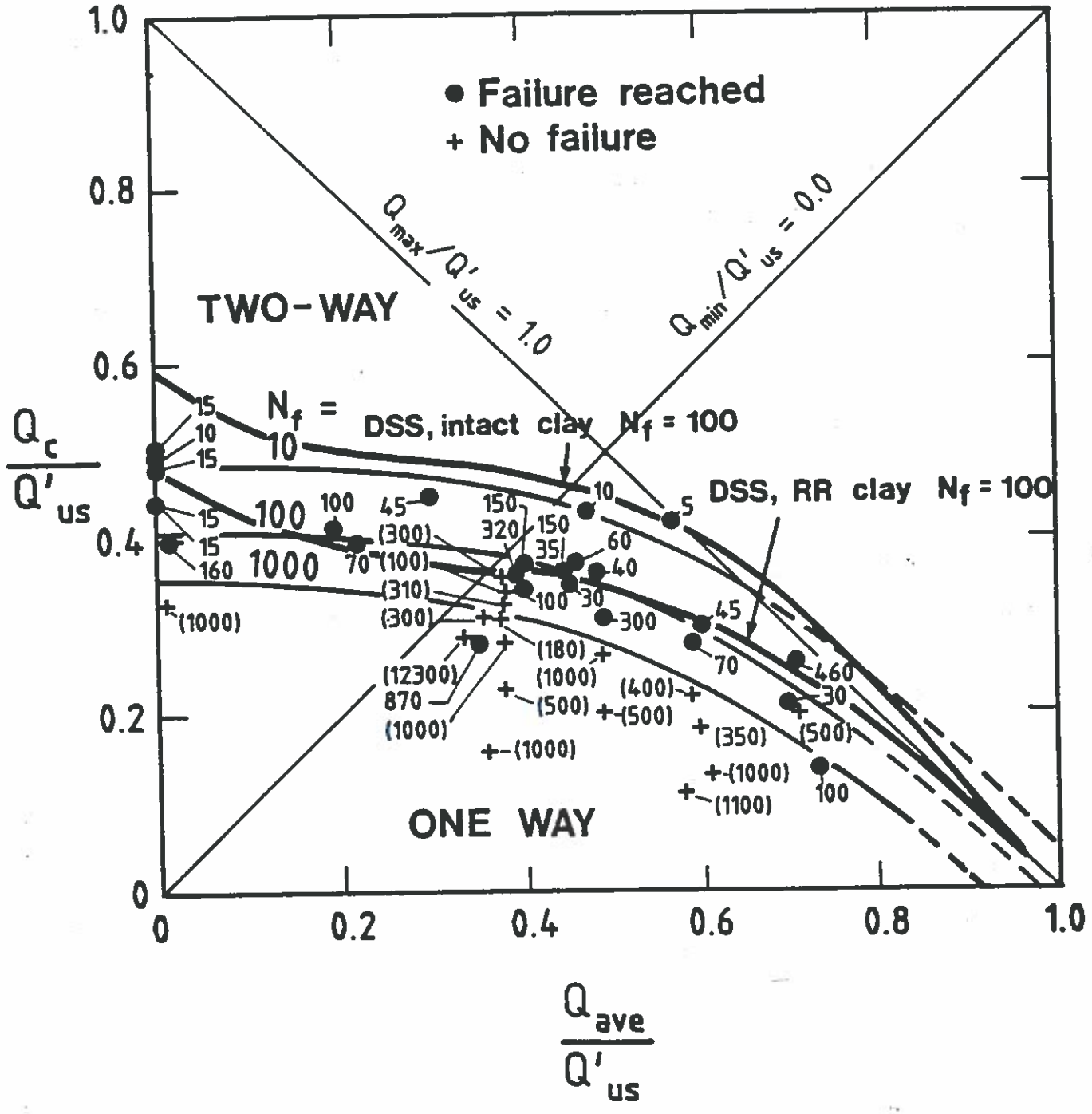
1.0
0.8
0.6
0.4
0.2
0
0
0.2
0.4
0.6
0.8
1.0
● Failure reached
+ No failure
$Q_{max}/Q'_{us} = 1.0$
$Q_{min}/Q'_{us} = 0.0$
TWO-WAY
ONE WAY
N_f =
DSS, intact clay N_f = 100
DSS, RR clay N_f = 100
$\frac{Q_c}{Q'_{us}}$
$\frac{Q_{ave}}{Q'_{us}}$

Fig. 12

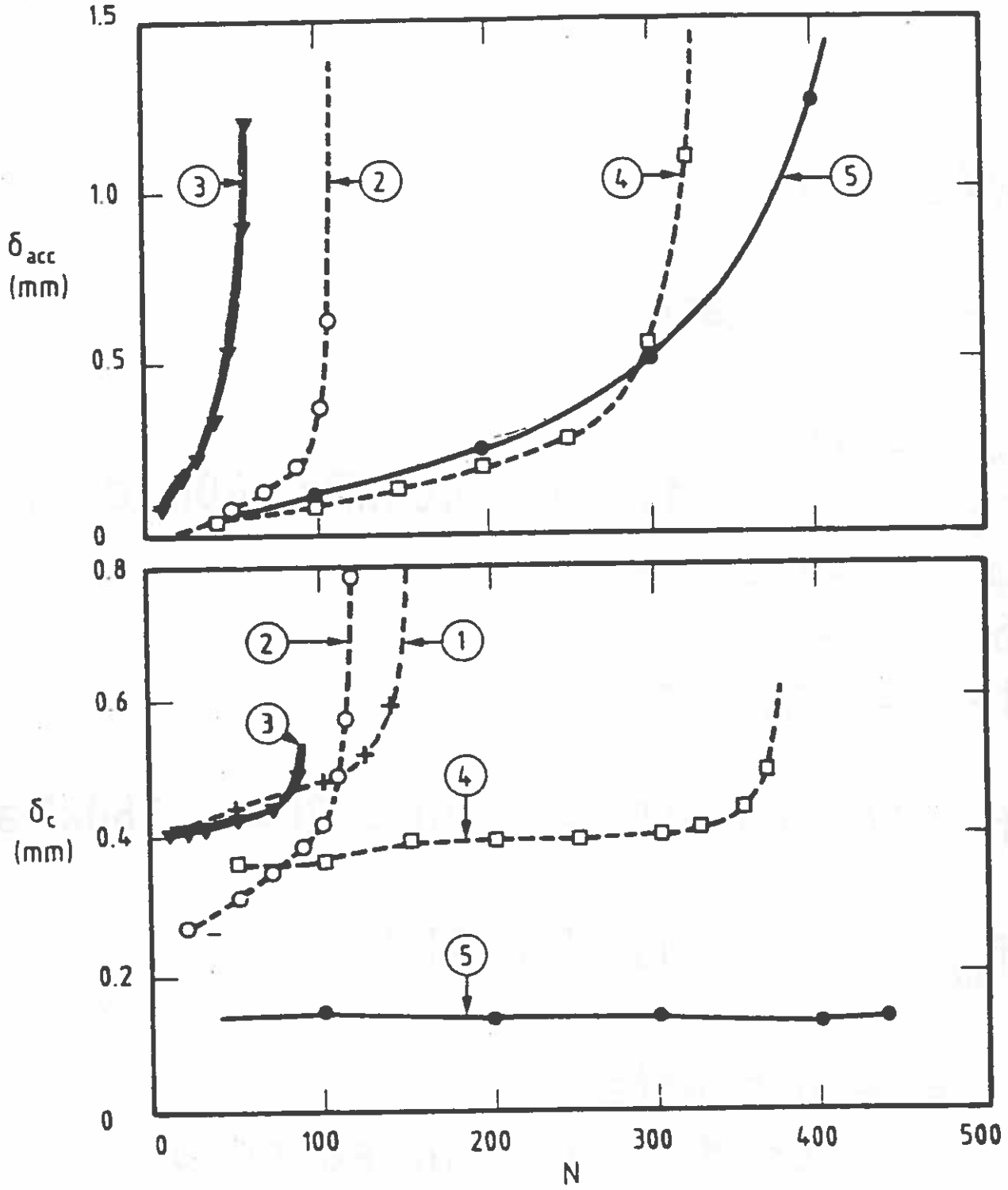

TEST	$\frac{Q_{max}}{Q_{us}}$	$\frac{Q_{ave}}{Q_{us}}$	$\frac{Q_c}{Q_{us}}$	N_f
1	0 40	0.00	0.40	160
2	0.39	0 10	0.29	100
3	0.83	0.46	0.37	60
4	0.75	0.39	0.36	320
5	0.97	0.26	0.71	460

Examples of evolution of accumulated average displacement, δ_{acc}, and displacement amplitude, δ_c, during some cyclic tests

Fig. 13

WALL FRICTION, sand

$$f = K_o \cdot p'_0 \cdot \tan\delta$$

K_o = 1.0
p'_0 = $\gamma' \cdot z$ = 10 · 40 = 400kPa (40m depth)
φ = 32 - 40°
δ = φ - 5°
$\tan\delta$ = 0.51 - 0.70

f = 1.0 · 400 · (0.51 - 0.70) = 204 - 280kPa

f_{max} = 120 - 150kPa (API)

- length effect
- reduced φ with increased σ'
- friction fatigue:
  Less friction towards the top,
  more friction further down.
- residual stresses

Fig. 14

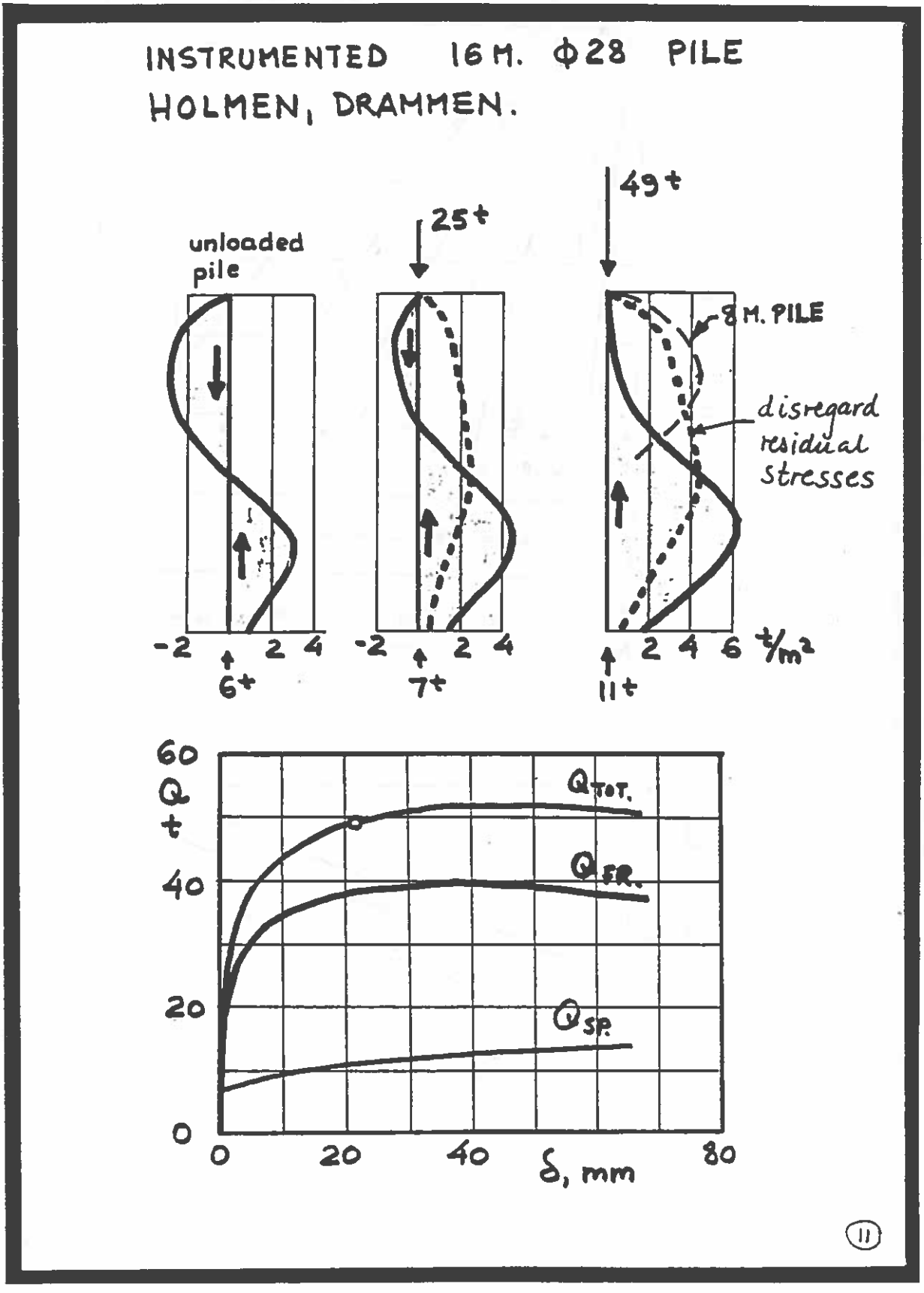
INSTRUMENTED 16 M. Φ28 PILE
HOLMEN, DRAMMEN.
unloaded pile
25t
49t
8 M. PILE
disregard residual stresses
-2
2
4
6
t/m²
6t
7t
11t
60
Q t
40
20
0
$Q_{TOT.}$
$Q_{FR.}$
$Q_{SP.}$
0
20
40
δ, mm
80
11

Fig. 15

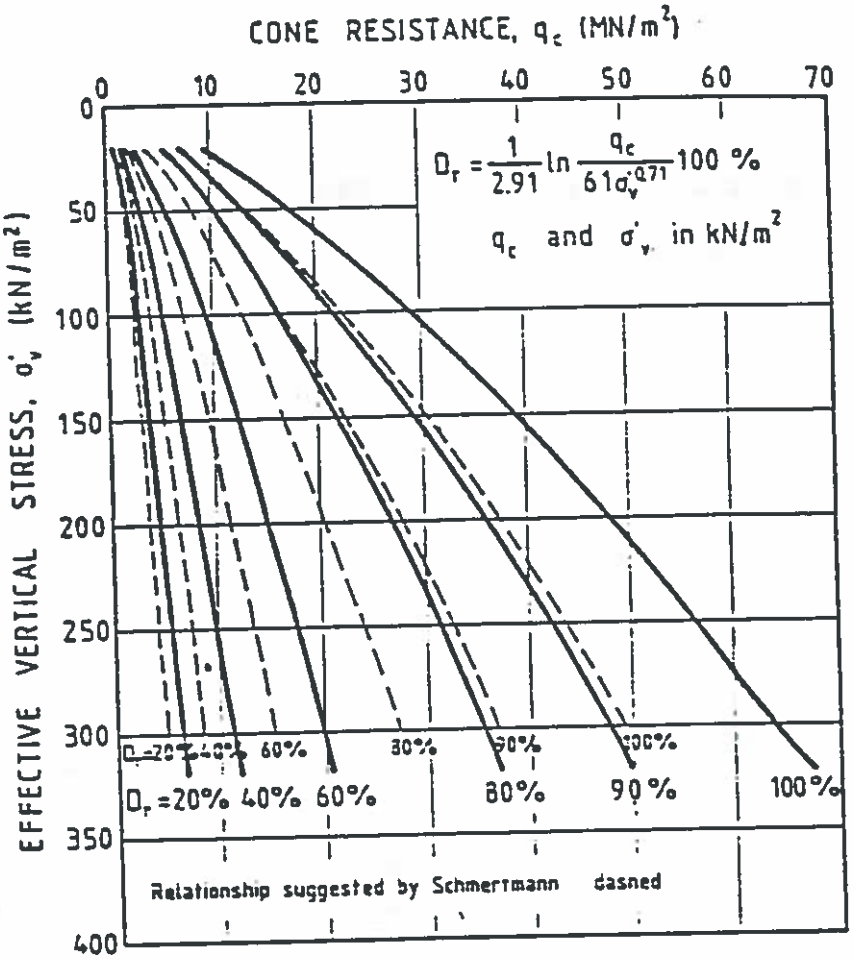

Recommended relationship among σ'_v, q_c and D_r for NC fine-medium quartz sand.

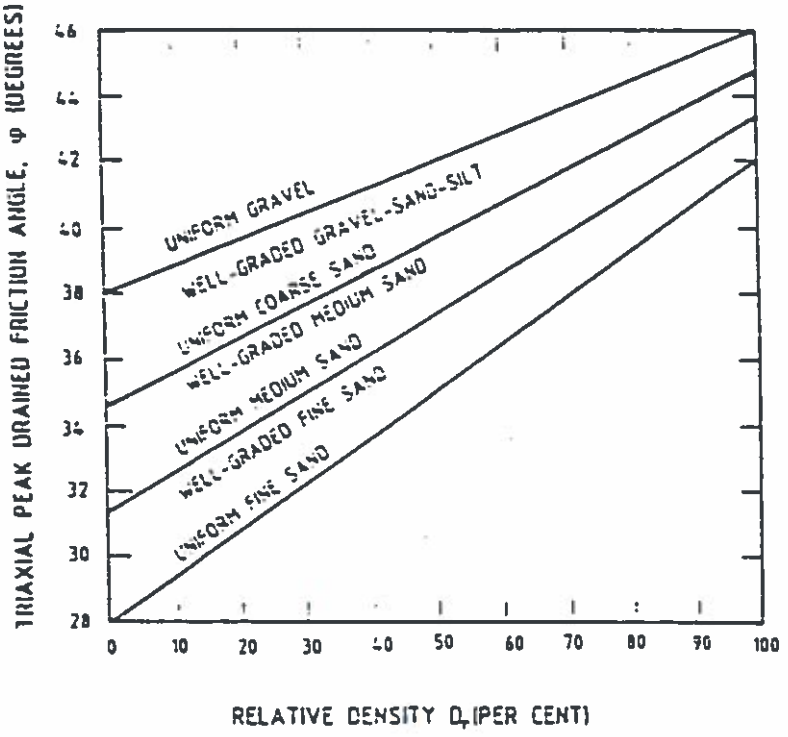

Relationship between φ' and D_r suggested by Schmertmann.

Fig. 16

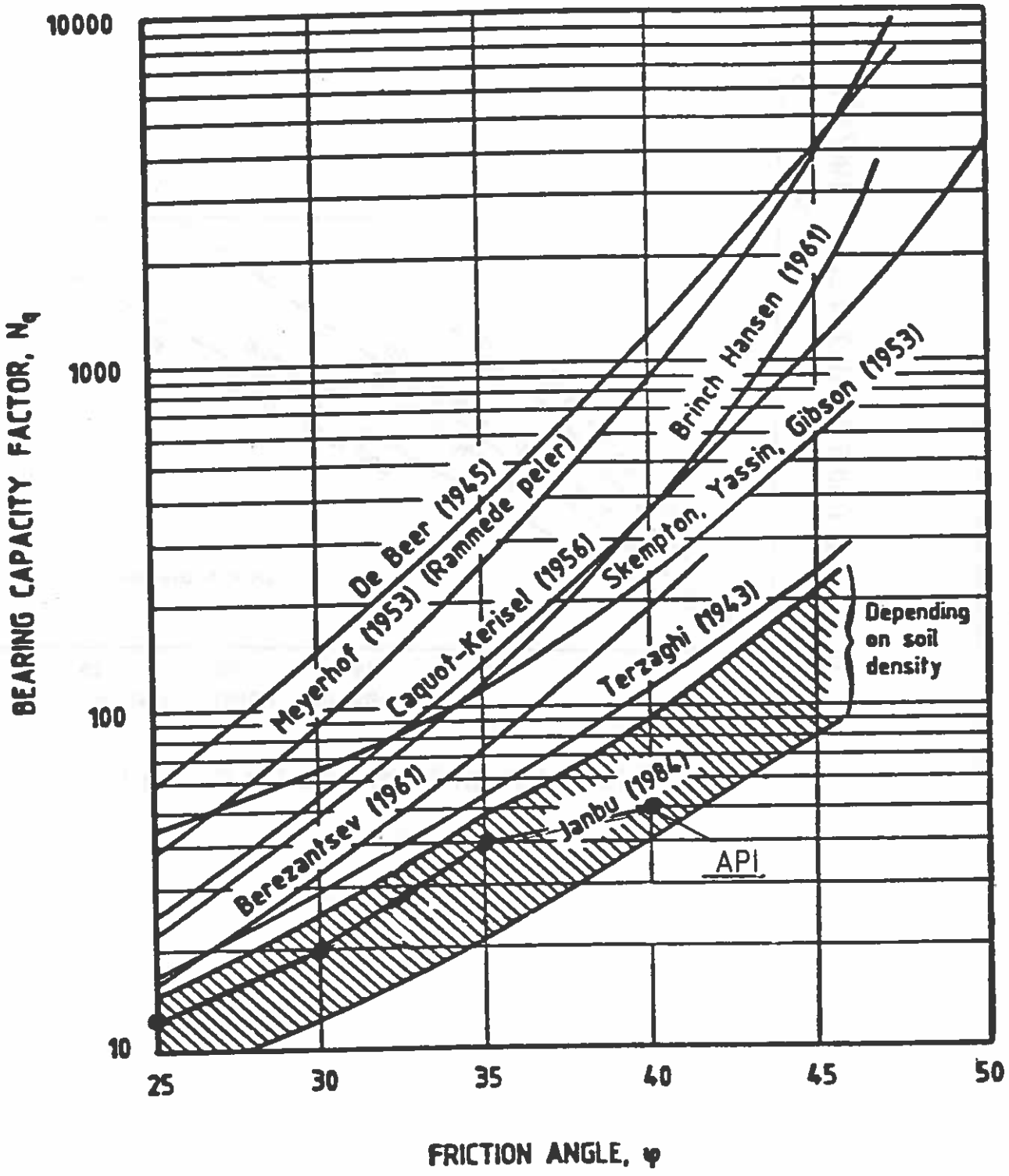
10000
1000
100
10
BEARING CAPACITY FACTOR, N_q
25
30
35
40
45
50
FRICTION ANGLE, φ
De Beer (1945)
Meyerhof (1953) (Rammede peler)
Brinch Hansen (1961)
Caquot-Kerisel (1956)
Skempton, Yassin, Gibson (1953)
Terzaghi (1943)
Berezantsev (1961)
Janbu (1984)
API
Depending on soil density

Fig. 17

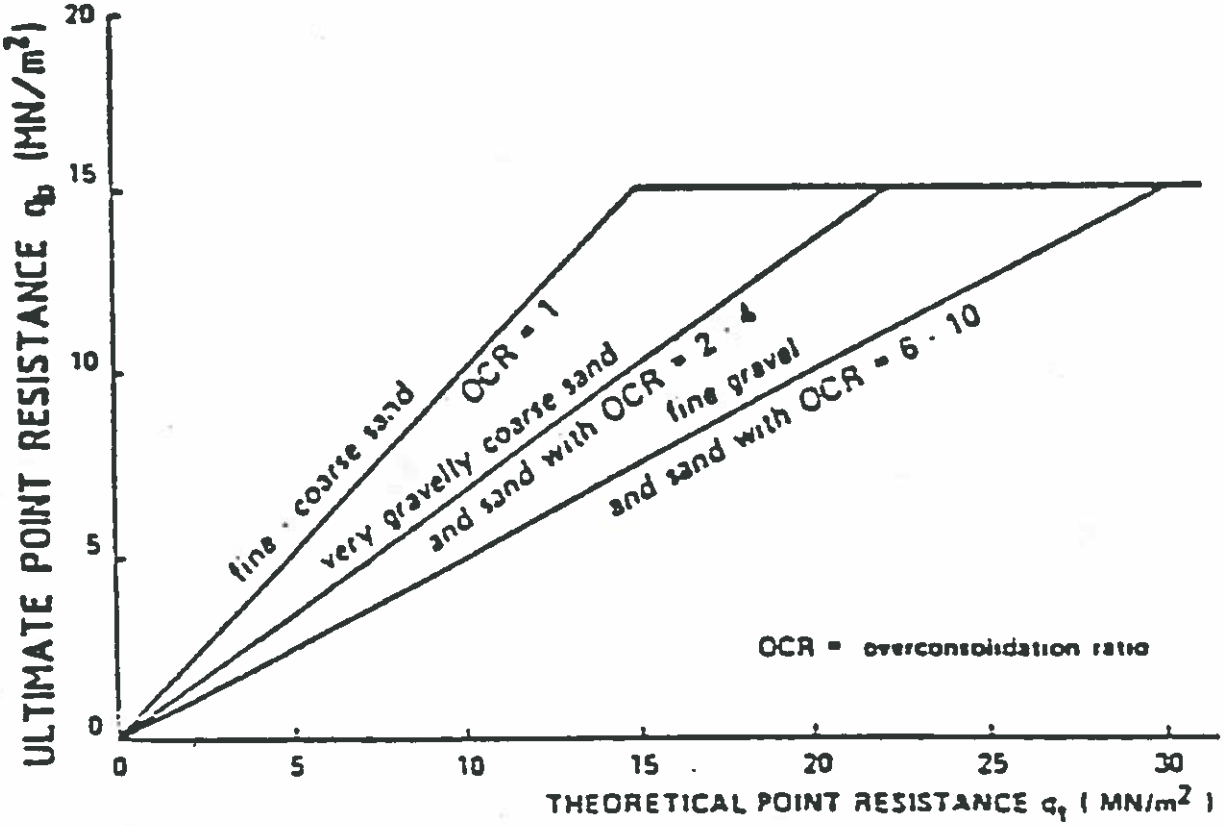

Limit Values of Point Resistance for Driven Piles.

Fig. 18

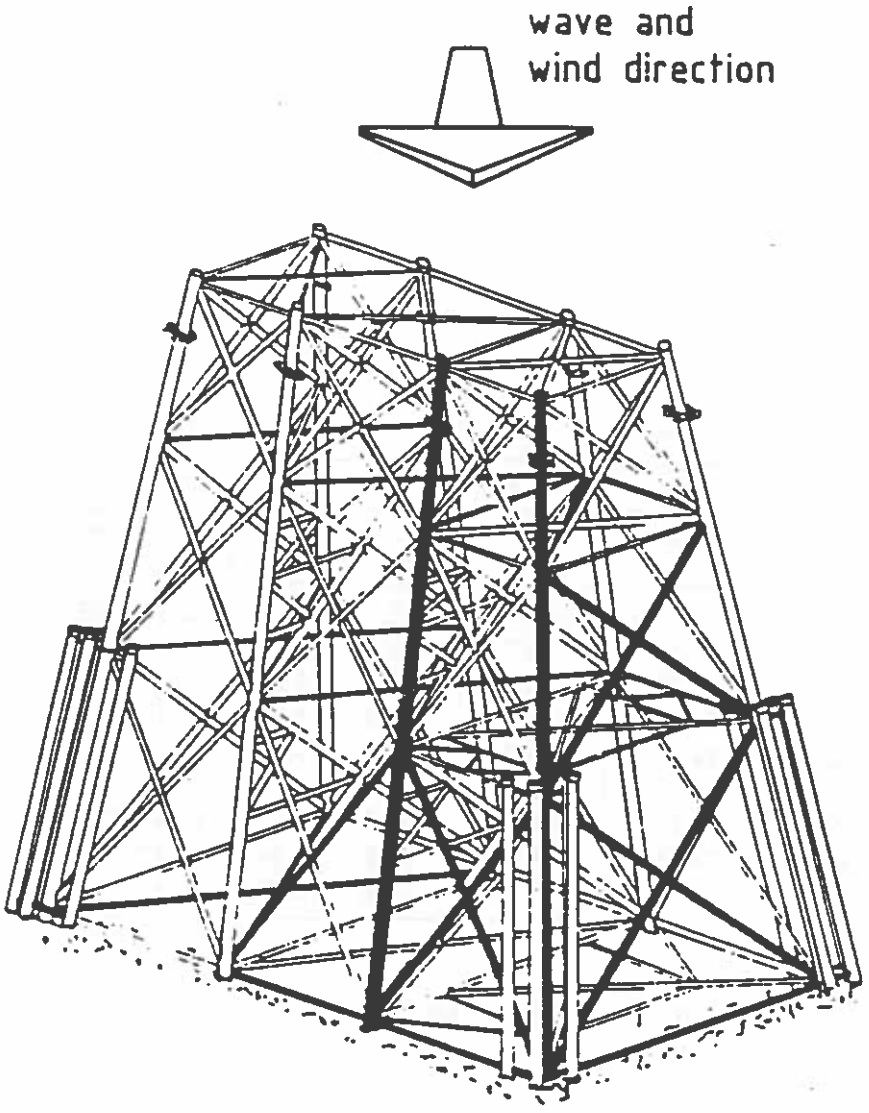

Fig. 19

Summary of Results, Foundation.

Case	Comment	Axial forces, MN			Max shear MN	Max moment MNm	Max stress MPa	Max lateral displacem. mm	Change in pile weight tons
		Max	Min	Sum max group					
0	Basic Case	$25.5^{3*)}$	-10.5^{23}	92.9	3.55^{6}	10.5^{7}	263^{3}	73.3	0
1	No Scour	25.5^{3}	-10.3^{23}	92.2	3.85^{6}	9.8^{6}	245^{3}	62.0	- 228
2	4 m Scour	25.5^{3}	-10.8^{23}	93.8	3.22^{6}	13.5^{5}	290^{3}	96.4	+ 340
3	Strong Top Sand	25.5^{3}	-10.4^{23}	92.4	3.85^{6}	10.7^{6}	257^{3}	66.2	- 79
4	Soft t - z Data	24.9^{3}	-9.3^{23}	93.9	3.56^{6}	11.1^{6}	259^{3}	74.9	- 44
5	Neglect Group	21.9^{3}	-9.9^{23}	96.0	3.01^{6}	10.6^{4}	238^{4}	56.1	- 311
6	Neglect S.O.M.	25.5^{3}	-10.5^{23}	92.9	3.51^{6}	10.4^{7}	259^{3}	72.8	- 49
7	ESTEEL/1.44	24.9^{3}	-10.1^{23}	93.8	3.44^{6}	11.5^{6}	265^{3}	93.8	+ 27
8	Rigid Jacket	23.8^{3}	-8.9^{22}	99.6	3.58^{6}	17.6^{6}	307^{3}	42.8	+ 594

*) Exponent gives pile number

S.O.M. = second order moments

Fig.20

UNRELIABILITIES IN THE LOAD RESPONSE OF JACKET STRUCTURES

by Jens Døssing, M.Sc., Civ.Eng.
Rambøll & Hannemann, Consulting Engineers and Planners A/S, Copenhagen.

Abstract

Some of the more important sources of unreliable predictions of the load response of a jacket structure are localized in the joints of the structure. These unreliabilities concern the stiffness as well as the strength of the jacket.

The field of internal forces, commonly determined by static (as opposed to dynamic) analyses, depends considerably on the local flexibility of the tubular chord members.

The evaluation of the strength of the joints is based on simple principles and empirical equations, not covering the phenomenon of interaction between several bracings framing into the same joint, and not satisfactorily covering the conditions by combined loadings.

The present section deals mainly with joint excentricities and flexibilities and the influence of these on the load response of the structure; further with the unreliabilities in the evaluation of the ultimate strength of simple as well as complex tubular joints subjected to pure or combined loads.

Introduction

As commonly known by designers of fixed offshore structures, the far most important unreliabilities in the load response are related to the foundation, where the continuous change in magnitude and direction of the load causes the mechanical properties of the soil to be time-dependent and thus complicates the establishment of these properties further. Also, group effects of and scour around piles influence significantly the response of the foundation and consequently also the jacket structure itself.

These problems are, however, thoroughly discussed elsewhere in these proceedings. In this section, the word "jacket structure" is taken literally, focusing on those sources of uncertain predictions of the structure's load response, found in the joints of the jacket.

Figure 1 shows an example of a typical wellhead platform in the Danish Sector of the North Sea. In the original and simplest design - as seen in the Gulf of Mexico - a jacket structure is a pre-fabricated, 3-dimensional lattice, which is hung on the main piles by site welded connections (in Figure 1 in level (+)8.000). The main piles are driven through the legs of the jacket, and the lattice prevents a stability failure of these main piles.

For jacket structures in the North Sea, an additional pile foundation is required for the structures to resist the horizontal loads. In these structures, the dead weight of the jacket is not only supported by the above-mentioned connections, but also, in shear, by sleeves shear-locked to the extra piles, the skirt piles.

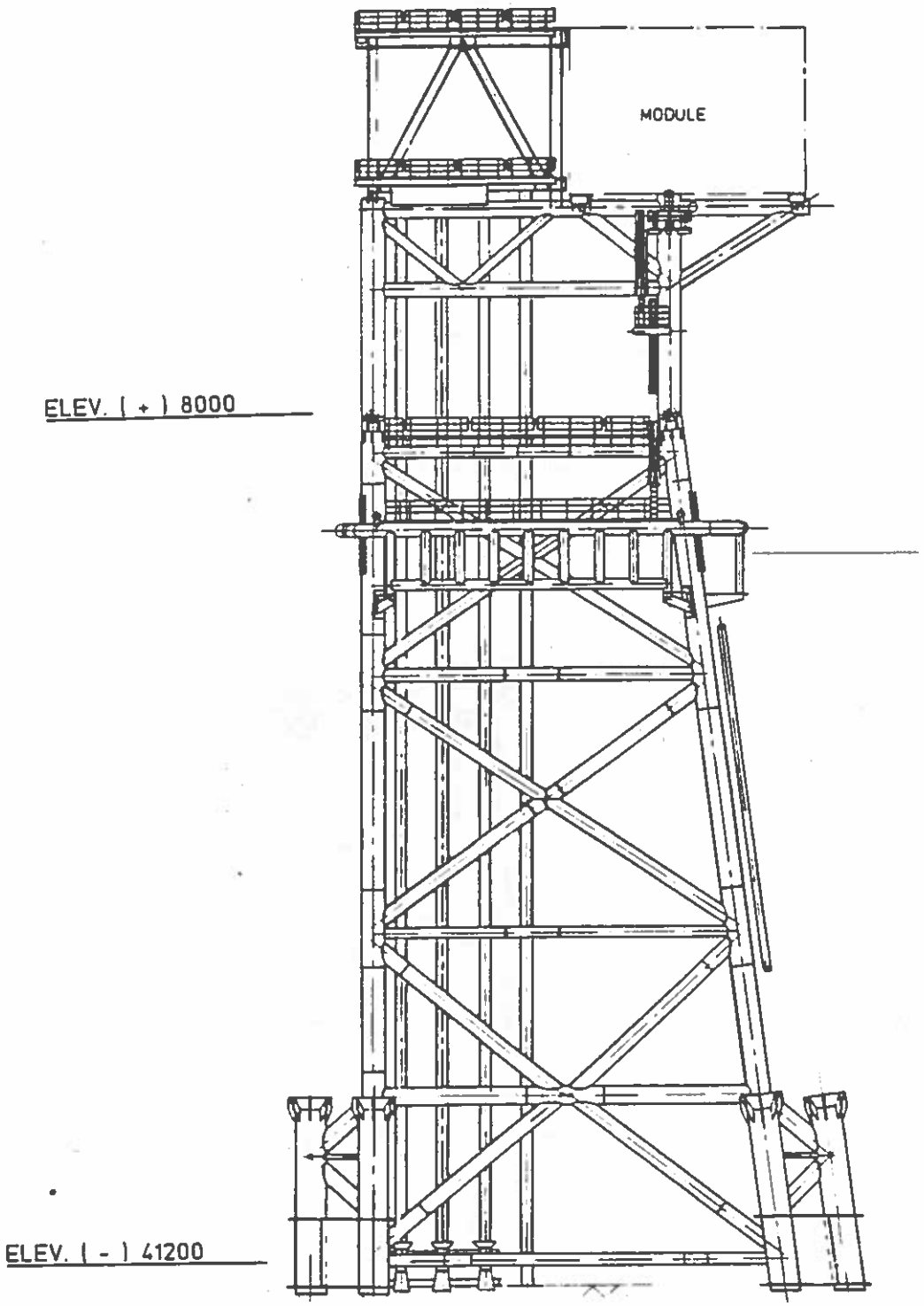

Figure 1

In newer designs, the function of the jacket is not only that of a bracing, in that some (but never all) of the deck columns are supported directly by the jacket. Part of the dead and live loads on the decks are in such structures led indirectly, through the jacket, to the foundation. However, in what follows, reference is made to the type of structure shown in Figure 1.

Unreliabilities in Determinations of Internal Forces

The jacket structure itself is traditionally modelled as an essentially linear framework of beams and columns. Figure 2 shows a plot of such a model.

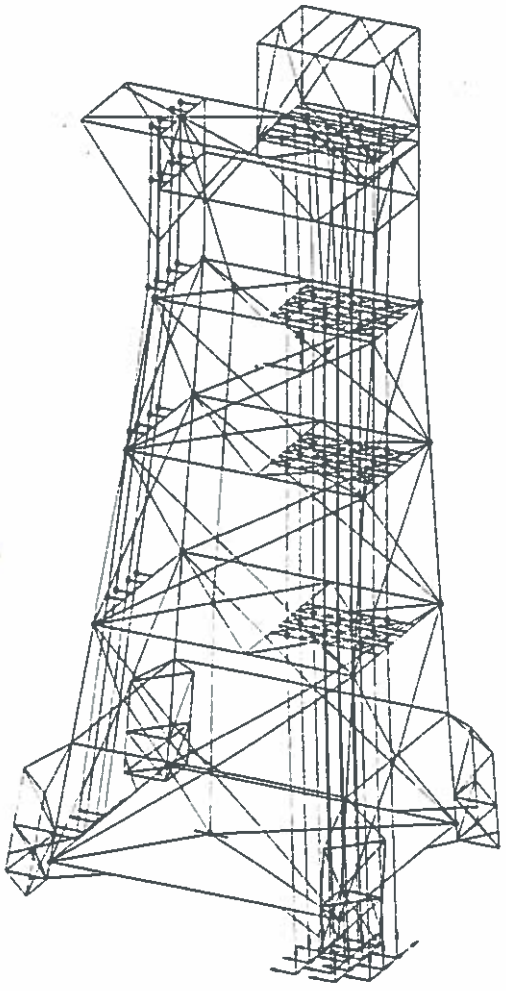

Figure 2

Considering the nature of the loads, it seems obvious to analyse the structure by means of the theory of dynamics. The load response is, however, commonly determined by considering the total structure statically loaded. The reasoning behind this common practice is that the lowest natural frequencies of the structure are considerably higher than the frequencies of the loads controlling the design. A reasoning which is theoretically correct, provided the structure's load response is linear, cfr the principles of modal analysis.

It is a fact, though, that the load response of an offshore structure is non-linear, primarily caused by the foundation, secondarily by the load transfer between the main piles and the jacket, taking place in the joints of the jacket legs. This load transfer is discussed later.

However, for loadings in that interval of frequencies, where the necessity of a theoretically correct consideration of dynamic amplification is of highest importance, the assumption of a linear load response also has its best justification. This concerns in particular the foundation.

By neglecting the dynamic response in the overall analysis of the structure, a theoretical error is introduced. But based on the arguments stated, and by comparison with other aspects of unreliabilities in the structural analysis, this error should - without detailed studies - be considered a minor one.

A dynamic analysis is, nevertheless, required for certain parts of the jacket structure. For example the horizontal framing in the upper part of the jacket, where wave slamming is present, and also conductors, casings and risers, for which vortex shedding may introduce significant dynamic amplifications of the internal forces. A common method of analysis of wave slamming is to undertake an equivalent static analysis with amplified loads, cfr (83.2), section B.1.5.

In the following, three sources of unreliable determinations of the field of internal forces in the jacket structure are discussed. These sources, all localized in the tubular joints, are:

1) the load transfer between main piles and jacket legs,

2) joint excentricities and

3) joint flexibilities.

Load Transfer Between Main Piles and Jacket Legs

The ideal installation of a jacket structure is one, in which main piles and jacket legs are co-axial. In the joints of the jacket legs, on the inside of the tubulars, so-called spacer-plates are welded, whereby an annular space of width d is established. Typically, d = ½", see Figure 3. The main piles are then supported by the joints of the jacket legs, whenever the difference between the horizontal displacements of pile and jacket leg, Δd, equals d. Commonly, this support is considered of the simplest kind, i.e. friction is neglected.

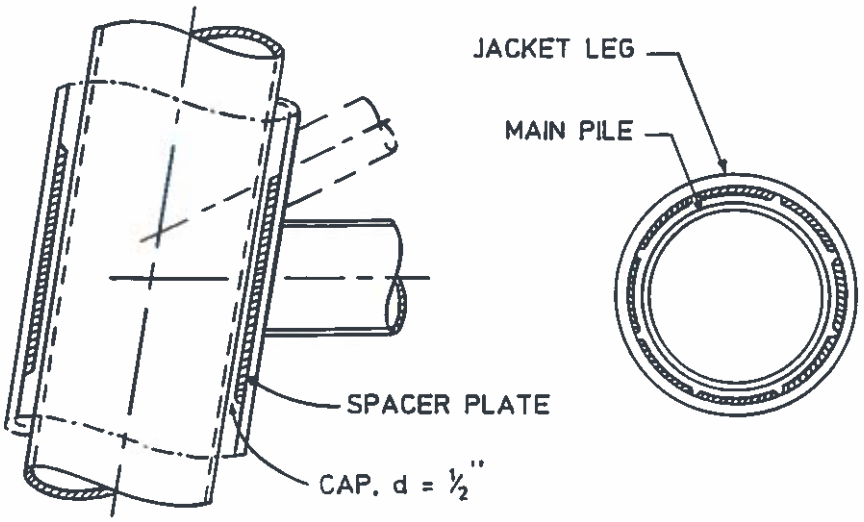

Figure 3

In a typical computer model (Figure 2), regardless of the magnitude of the horizontal loads, Δd is assumed equal to d in all jacket leg joints, except the ones in the lowest level (in Figure 1, level (-)41.200). In the upper joints, the contact between main pile and jacket leg is then always taken fully effective. In the lowest level, right above the mudline, a non-linear link is coded; this link constitutes a main pile support, whenever $\Delta d = d$ (storm conditions), but is otherwise forceless.

The assumption, the correctness of which can be checked by coding non-linear links in all joint levels, turns out to be in accordance with reality for a typical jacket structure in the Danish North Sea Sector, provided that main piles and jacket legs are truly co-axial.

More likely, a main pile is not driven co-axially with the jacket leg, but is supported by the jacket leg, even when the structure is not subjected to horizontal loads. The magnitude and direction of the difference in displacements of pile and jacket leg is then controlling, whether or not the pile is supported, and the above-mentioned assumption is in some load cases doubtful.

Naturally, these conditions, which cannot be accounted for in the design phase in any reasonable way, constitute a source of uncertain prediction of the structure's load response, not just for the jacket structure itself, where the uncertainty mostly affects the loading of horizontal bracings, but also for the foundation, because a shear loading of the main piles, in the mudline level, has a significant influence on the bending of the upper 5-10 diameters long pile section below the sea bed.

Joint Excentricities

In order to prevent complicated cuttings and weld preparations of brace endings, welds on welds and concentrations of stresses (implying large reductions of fatigue lives), most tubular joints are designed with excentricities in the intersections of the chord and brace centerlines. The different codes of practice require that the distance between adjacent bracings, as measured on the face of the chord, is not less than a = 2". Only in such cases where this requirement is impossible to meet, a tubular joint is designed with overlapping brace elements.

Two types of joint excentricities occur:

1) all brace centerlines intersect the chord centerline, but not in the same point (see Figure 4a), and
2) the certerlines of chord and brace do not intersect (see Figure 4b).

It is characteristic of offshore-codes that although they require joints designed with excentricities whenever possible, they do not require these excentricities accounted for in the analysis of the structure, unless they exceed a certain fraction of the chord diameter, D. Typically, joint excentricities of type 1 are neglected for values of a up to one fourth of D.

In practical design work, excentricities, for which $a \geq D/4$, are commonly introduced in the structural model by coding secondary nodes in the actual intersections between the chord and brace centerlines. These secondary nodes are all connected to the primary node by means of very stiff members, and prior to the stiffness analysis of the total structure, all degrees of freedom related to the secondary nodes are eliminated from the model.

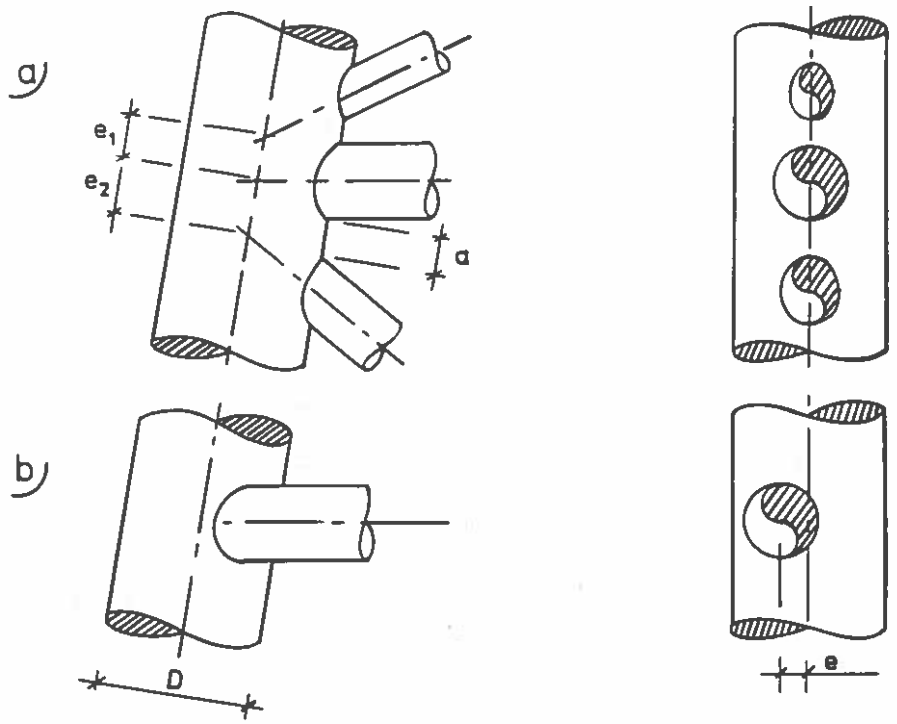

Figure 4

The stiff member between the primary and secondary nodes is unfortunate and does not reflect the true behaviour of the tubular connection:

Even simple, non-complex, tubular joints are very flexible, and for a complex joint, be it plane or 3-dimensional, it is obvious that the larger the actual joint excentricities, the larger the extension of the joint and, further, its flexibility.

The missing or deceptive consideration of joint excentricities can add considerably to an unreliable prediction of the internal forces in the lattice of the jacket. An evaluation of this unreliability, which obviously is closely related to the unreliability caused by disregarding the joint flexibilities, is given later.

Joint Flexibilities

It is, in general, relatively easy to design connections in ordinary structural framework so that all assumptions of analysis regarding stiffness (hinges etc.) are complied with. On this background, joint flexibilities have been rather disregarded.

In framework constructed of tubulars, the joints between the members are, however, rather poorly described by beam theory, if they - as it is common - are designed as unstiffened. This is due to the large deformations of the chord wall, occuring around a brace connection, even when this is subjected to moderate loadings.

Figure 5 shows typical load-displacement curves for an unstiffened T-joint subjected to pure loadings. The abscissae denote local deformations of the chord wall, only, and thus the curves illustrate how flexible this, the simplest of all tubular joints, really is. Note that the curves are non-linear virtually from the point of no loading, implying that an assumption of proportionality between load and displacement would be reasonable only within rather narrow limits.

A thorough consideration of joint flexibilities in the analysis of a jacket structure requires that also the interaction between different braces framing into the same joint is described. For a tubular joint with a total of n brace connections, a linear description of the joint flexibilities is given by the equation

$$\begin{bmatrix} \delta_1 \\ \phi_{1,IPB} \\ \phi_{1,IPB} \\ \vdots \\ \delta_n \\ \phi_{n,IPB} \\ \phi_{n,OPB} \end{bmatrix} = \begin{bmatrix} a_{11} & a_{12} & a_{13} & \cdots & a_{1,3n-2} & a_{1,3n-1} & a_{1,3n} \\ a_{12} & a_{22} & a_{23} & & & & \\ a_{13} & a_{23} & a_{33} & & & & \\ \vdots & \vdots & \vdots & & & & \\ a_{1,3n-2} & & & & & & \\ a_{1,3n-1} & & & & & & \\ a_{1,3n} & \cdots & \cdots & \cdots & \cdots & \cdots & a_{3n,3n} \end{bmatrix} \begin{bmatrix} P_1 \\ M_{1,IPB} \\ M_{1,OPB} \\ \vdots \\ P_n \\ M_{n,IPB} \\ M_{n,OPB} \end{bmatrix} \quad (1)$$

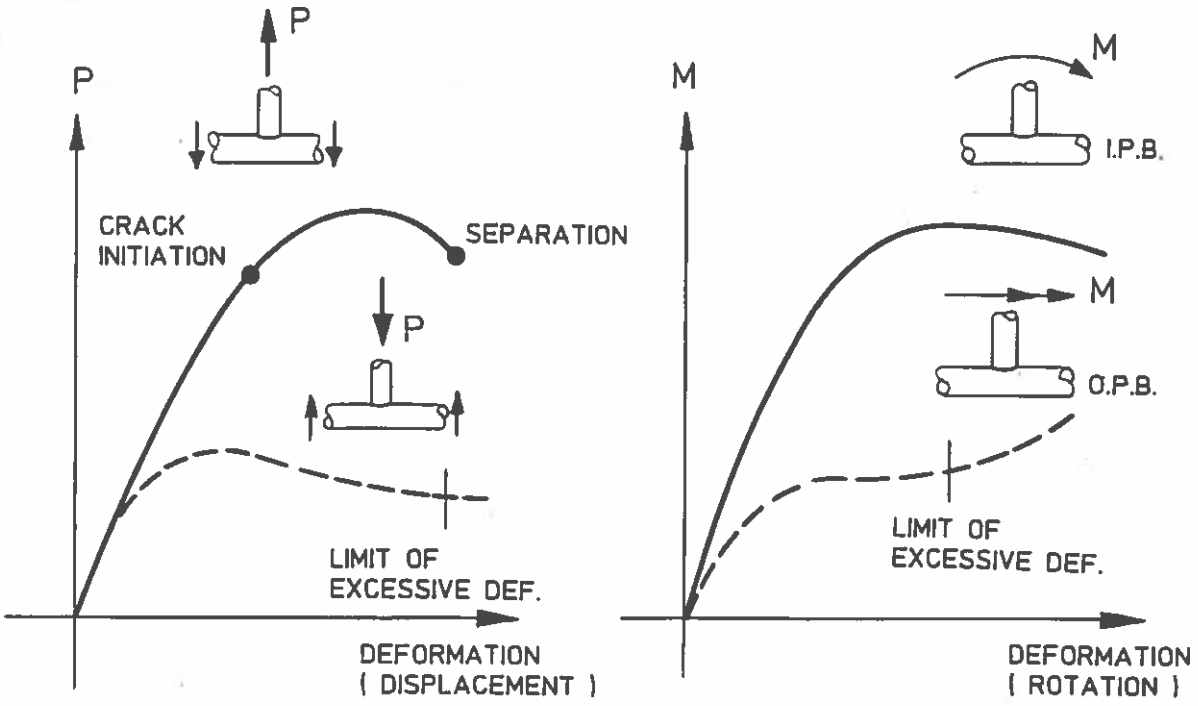

Figure 5.

in which

δ_i denotes the axial desplacement,

$\phi_{i,IPB}$ the rotation in the plane, π, defined by the chord and the brace element considered,

$\phi_{i,OPB}$ the rotation out of π,

P_i the axial loading,

$M_{i,IPB}$ the in-plane bending moment,

$M_{i,OPB}$ the out-of-plane bending moment,

all of brace element "i".

a_{ij} are the coefficients of flexibility.

Note that Eq. (1) does not include shear and torsion of the braces. There is, of course, nothing wrong in taking account of these types of loading and deformation, too. They can, however, a priori be regarded as being of secondary importance, because they affect the chord wall to a state of membrane action, mainly, and so do not give reason to deformations of an order of magnitude, comparable to the one following the local chord wall bending.

One obvious way to establish relation (1) is, in a separate finite element analysis, to model the entire tubular joint in shell elements, point out those boundary nodes, in which the chord and the braces (considered as beam elements) are connected, and later, before inclusion in the computer model of the total structure, eliminate all degrees of freedom related to the internal nodes. In other words: To create a macro element. It is

important, that such a macro element includes sections of the chord and braces, sufficiently long for the presumptions of beam theory to be complied with on the boundary.

In this application, the method of macro elements will inevitably imply solutions of very large systems of equations and consequently be relatively expensive. And without any facilities to automatically generate nodes and elements, the method will be too time consuming to be of practical interest.

Finite element analyses of joint details have been offered a still growing interest, especially regarding element types. In this context, it should only be noted that the best results are reached by applying thick shell elements, because the concentrated loadings of the chord wall introduce large stress concentrations; in some cases singularities, which can only be described by special types of elements. The so-called Ahmad element, a thick isoparametric shell element, is commonly used. Also, reference is made to (80.2) and the literature about the Finite Element Method.

Obviously, the macro element method described is applicable for plane as well as 3-dimensional tubular joints, and also, the method accounts for joint excentricities in a direct way.

Alternatively, joint flexibilities can be included in linear analyses by coding simple, linear springs between the principal node and the intersections between the brace centerlines and the chord wall, see Figure 6a. If also the actual intersections between the chord and brace centerlines are coded as secondary nodes, thereby including joint excentricities in the model, this method is equivalent to only considering the diagonal elements in the matrix of Eq.(1) and a priori putting all other flexibility coefficients equal to zero. See Figure 6b.

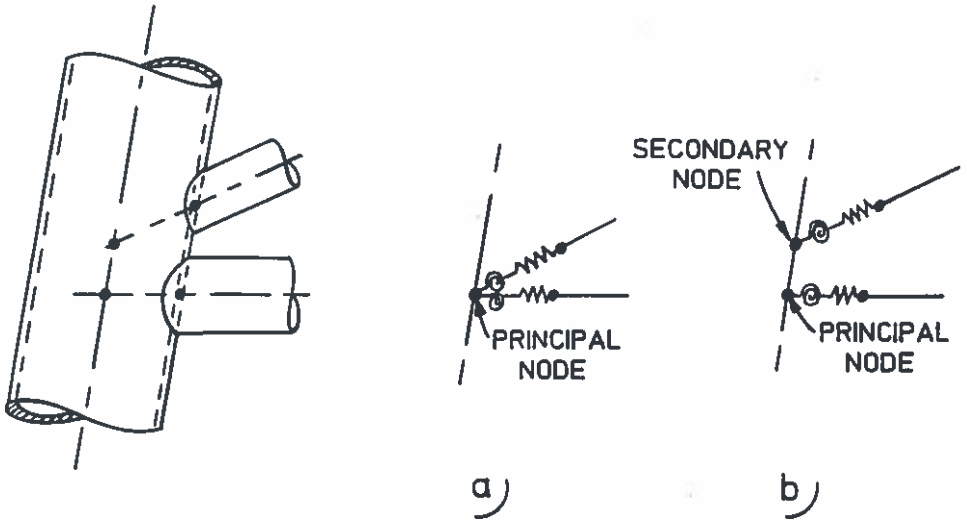

Figure 6

The philosophy behind this spring method, which, as it is seen, does not account for brace interactions, is familiar to the one, traditionally used in the classification of the connections in a given, 3-dimensional, tubular joint prior to an evaluation of ultimate and/or fatigue strengths. This principle of classification is discussed later.

Fessler has, based on 24 tests with plane, unstiffened T/Y-joints, stated the following parametric equations for the flexibility of the equivalent springs:

$$a_{axial} = 2.3\gamma^{2.3}e^{-3.3\beta}\,ED\,(\sin\theta)^{3} \qquad (2)$$

$$a_{IPB} = 171\gamma^{1.65}e^{-4.6\beta}ED^{3}\,(\sin\theta)^{1.7} \qquad (3)$$

$$a_{OPB} = 48.1\gamma^{2.5}e^{-3.7\beta}\,ED^{3}\,(\sin\theta)^{3}\ , \qquad (4)$$

(81.1). The definition of the parameters is the usual, shown in Figure 7. There are no limits given for the applicability of (2)-(4).

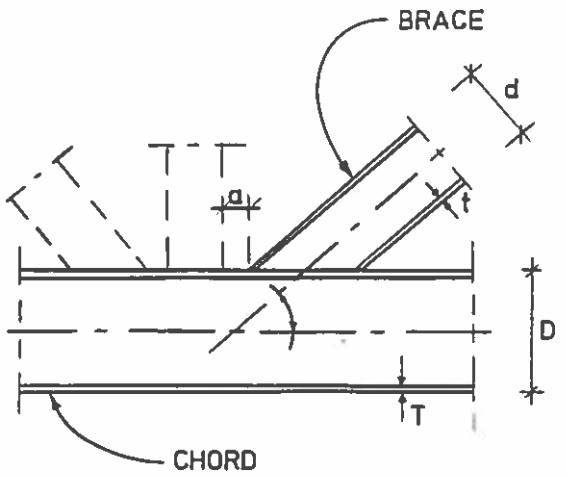

$$\beta \equiv \frac{d}{D}$$

$$\gamma \equiv \frac{D}{2T}$$

$$\tau \equiv \frac{t}{T}$$

$$\zeta \equiv \frac{a}{d}$$

Figure 7

For comparison, the DnV-equations for a_{IPB} and a_{OPB}, valid for unstiffened T-joints, only, are

$$a_{IPB} = 18.6\left[\gamma^{-1} - 0.01\right]^{-(2.35-1.5\beta)} ED^3 \qquad (5)$$

$$a_{OPB} = 5000\left[\gamma^{-1} - 0.20\right]^{-(2.45-1.5\beta)} \left[215-135\beta\right]^{-1} ED^3 \qquad (6)$$

for which β and γ should be within the limits

$\beta \in [0.33, 0.8]$ and $\gamma \in [10, 30]$,

see (77.1).

It is remarkable that neither experimental nor theoretical results regarding other types of joints, especially 3-dimensional joints, have been reported. After all, lots of (destructive) tests of ultimate capacity have been performed, and data regarding flexibility could easily have been extracted from these tests.

Evaluation of Unreliabilities Related to Disregarding Joint Excentricities and Joint Flexibilities

A study of a plane structure, conducted by the Underwater Engineering Group, (84.1), applied the spring method without consideration of joint excentricities, and concluded by comparison with the results of a traditional analysis the following:

- Axial forces in brace elements change insignificantly.
- Deflections increase up to 13%.
- Critical axial loads of brace elements are reduced by 10%.
- The distribution of bending moments (IPB) in braces of K-, KT- and TY-joints changes considerably.

The results of the study are also given in (85.1), section C6.

The significance of also considering joint excentricities are illustrated in a study by Bouwkamp et al., (80.1). Again, a plane structure was analysed, but, different from the UEG-study, this study applied the macro element method. By comparison with results of traditional analysis, this study concluded:

- Axial forces in brace elements are reduced up to 20%.
- Deflections increase up to 30%.
- Bending moments in chord elements are increased up to 400%.

Unfortunately, Bouwkamp et al. state no results regarding bending moments (IPB) in the braces. In a traditional design, based on structural models with rigid joints, the braces often include thick-walled end sections, stubs. There are reasons to presume that the elastic connections between the braces and the chord are so flexible and thereby moment-reducing that such stubs could be omitted, provided, naturally, that the flexibilities are accounted for in the analysis.

Additionally, this presumed reduction of bending moments would beneficially affect the fatigue strength of the tubular joint. The aspects of unreliabilities in fatigue life assessment of offshore structures are, however, the subject of a later section in these proceedings and shall not be discussed in detail here.

Bouwkamp's conclusion regarding bending moments in chords (jacket legs) is remarkable. However natural it is to be sceptic to a five-fold increase in these moments, it is important to note that the local bending and ovalization of the chord section can be considerable, both in magnitude and in extension, the latter due to the singly curved geometry of the circular cylindrical element. Because of the ovalization of the chord section, the presumption of beam theories (Bernouilli, Timoshenko), regarding sections being non-deformable, cannot be complied with within large parts of the members, cfr the previously noted importance of including sufficiently long sections of chord and braces in macro elements. The ovalization causes an increase in curvature and also in bending moments.

For obvious reasons, the two studies of plane structures do not state any results regarding the effects of considering OPB-flexibilities too. In traditional analyses, presuming rigid joints, out-of-plane bending of brace elements (principally caused by wave and current loadings of the brace itself) is transferred by torsion of the chords, and since the chords' stiffness against this kind of deformation is indeed very large, the out-of-plane rotation of a brace/chord-connection is virtually restrained in such analyses. But, as it is seen in Figure 5, the OPB-flexibilities are typically larger than the IPB-flexibilities, and a study of the effects of including OPB-flexibilities would therefore, most likely, conclude a considerable reduction of the bending moment in the joints coupled with an increase in the field moment. Such a study has, however, not been reported.

The previous remarks regarding stubs and beneficial influence on fatigue strength applies, naturally, also to out-of-plane bending.

Generally, it is tempting to neglect the effects of joint flexibilities as long as all static conditions can be complied with by using only the simplest structural models. The basis of this argumentation is obviously the lower bound theorem of classical theory of plasticity. Anyhow, this basis fails, because in far the most cases the controlling failure criterion of the lattice of the jacket structure is one of instability, and, as stated, due consideration of joint flexibilities can influence considerably actual as well as critical axial forces in the brace elements.

Unreliabilities in Evaluations of Ultimate Strengths of Tubular Joints

After the determination of the jacket structure's internal forces follows the evaluation of the structure's strength, in particular the strength of the joints.

In the following, two sources of unreliable evaluation of the static strength of tubular joints are discussed:

1) the principle of joint classification and

2) the establishment of the failure criterion.

The Principle of Joint Classification

In the classification of given, generally 3-dimensional, tubular joints, reference is made to basic types of plane, unstiffened, connections without excentricities or overlappings.

Such basic types of joints, of which the most important are the T-, Y-, K- and X-joints, are shown in Figure 8. Determining the type of any of these joints is not only the overall geometry, but also the nature of the load transfer between the braces and the chord (K- and X-joints).

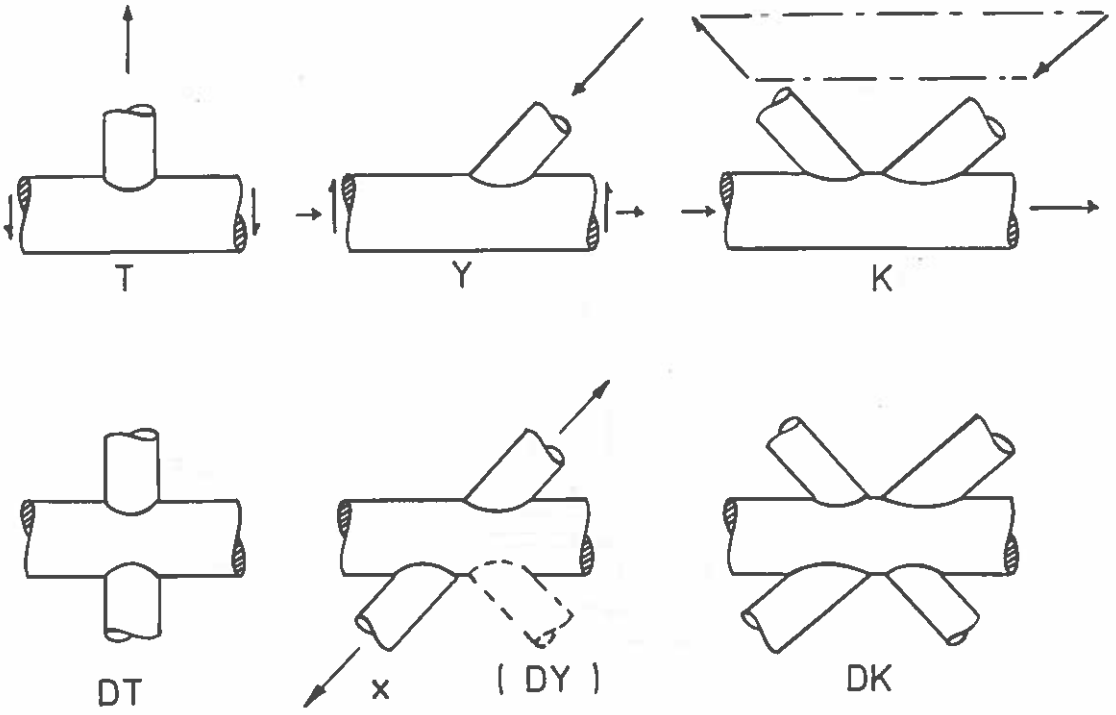

Figure 8.

The common procedure for classification of given tubular joints is:

- The chord is identified.
- The connections between the braces and the chord are considered one by one; each connection defines a plane, π. (In case the centerlines of chord and brace do not intersect, the excentricity is ignored.)
- The joint is classified with reference to the basic types of joints, depending on how the axial forces, only, in the brace elements in π are transferred, mutually and/or with the chord.

Figure 9 shows a simple example of a classification of a plane joint.

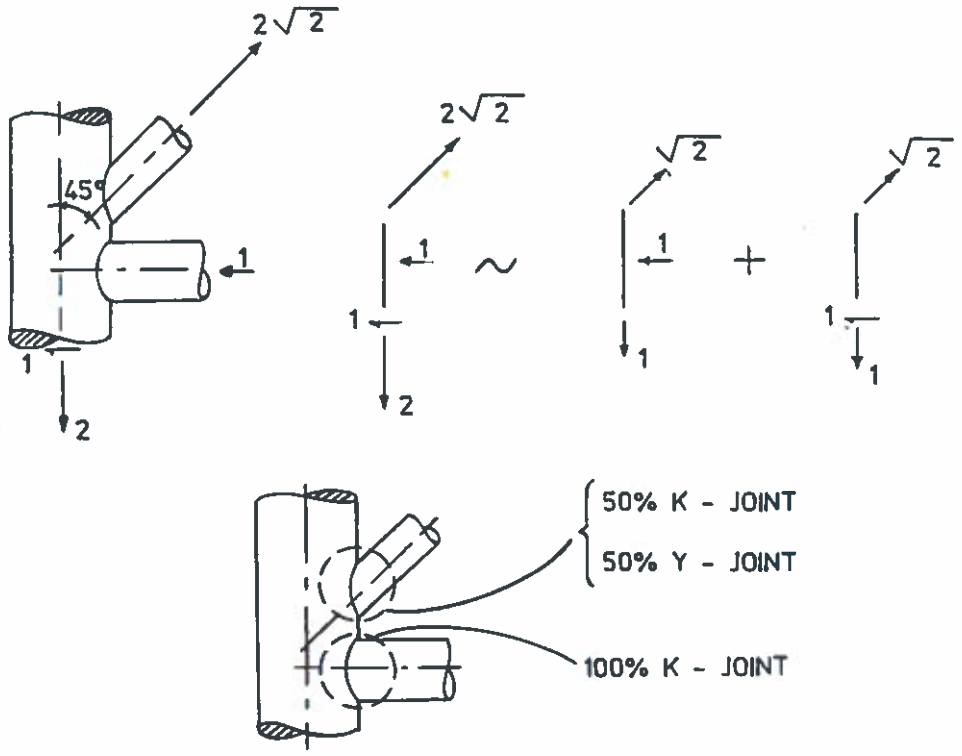

Figure 9.

Several aspects of uncertainty characterize this principle:

Firstly: Following the principle, the classification of a given joint depends not only on the geometry of the connection, but also - in an unfortunate way - on its loading. This implies that classifications in some cases are (theoretically) ambiguous.

Secondly: By referring to plane joints, all interaction with out-of-plane braces, beneficial or not, is neglected in the evaulation of the strength of a given joint.

Thirdly: The classification's dependence on loading is a dependence on axial forces, only, in the brace elements. Naturally, this is unfortunate in such cases, where a joint is predominantly subjected to bending moments.

The two last mentioned aspects of uncertainties in joint classifications are closely related to earlier applications of tubulars in structures and also to the experimental results, regarding strength of tubular joints.

Earlier, tubulars in structures were almost exclusively seen in plane trussworks. It is therefore natural, that classifications and evaluations of static strength of tubular joints refer to 2-dimensional types of connections, and also, that the classification's dependence on loading is a dependence on axial forces, only.

As of today, the amount of evidence, be it theoretical or experimental, regarding interaction between different out-of-plane bracings framing into the same joint, is insufficient for the unreliability related to neglecting this interaction to be evaluated.

Ultimate Strength of Simple, Basic Types of Tubular Joints

The static strength of tubular joints is today evaluated by means of empirical equations, based on test results for the types of joints, shown in Figure 8.

Due to large deformations, strain hardening, crack-initiation and -propagation together with typical local yielding, a theoretical determination of the strength is extremely cumbersome. Only few elastic-plastic finite element analyses of tubular joints have been performed. These analyses can be characterized as numerical simulations of laboratory tests and offer as such

no opportunity to more clearly define the meaning of "ultimate strength". Also, they turn out to be rather elaborate and time consuming, both in relation to establishing the structural model and in relation to CPU-time. There is, however, no doubt that the future will show a still growing number of theoretical determinations of ultimate capacities of tubular joints.

The oldest - and for many years mostly applied - set of empirical strength equations are fitted to the punching shear principle, according to which an equivalent punching shear stress in the actual connection must be less than or equal to the allowable value of this shear stress. The original basis of the formulae of the Punching Shear Method were the results of about 25 tests with tension-loaded T-joints of tubulars with only small or moderate dimensions. The type of failure for these joints is a separation of chord and brace (Figure 5).

Later, the equations of the Punching Shear Method were modified almost every year in order to incorporate the results of the latest research. Today, application of the principle can only be described as laborious. This follows naturally from the fact, that the principle in its origin does not include results of tests other than tension-loaded T- and Y-joints, not even connections subjected to bending, and that types of failure, different from the separation of chord and brace, have been adjusted to an unfortunate (wrong) format.

Most codes of practice now recommend the static strength of tubular joints be evaluated by a method referring to total loads in stead of stresses. This also includes the Danish offshore code, DS 449, the equations of wich were first published and documented in (80.3). Also see (83.2), annex D2.

The basis of the equations, recommended in DS 449, is a database including the results of a total of 137 tests, and the formulae all draw lower bounds of the observed capacities. This database

is a reduction of an originally larger one, including the results of some older test with joints of small dimensions. For these tests, the scale effect, introduced by the relatively large weldings, has been considered too significant for the results to be applied in the analysis of offshore structures, where the dimensions of the tubulars typically are ten-fold those of common pipe sections.

The scale effect mentioned is principally related to the fact, that the large deformations in a broken tubular joint are localized in the chord, whereas the brace element, including the welding between the brace and the chord, virtually undergoes a rigid-body displacement during the process of deformation. Test results for joints of small dimensions, in which the weldings are relatively heavy, would therefore be registered under deceptive diameter ratios, β.

As already mentioned, the equations of strength all draw lower bounds of the observations, and so, one cannot speak of significant unsafeties when applying them. However, it should be noted that the ratio of computed to measured capacities show a relatively large scatter, typically some 25%, for tension loaded T-, Y- and DT-joints as high as 60%.

The scatter is caused by one or more of the following circumstances:

Firstly, the definition of ultimate load changes from "the load at crack initiation" over "maximum loading possible" to "the load at excessive and unacceptable deformations", see Figure 5. Especially in such cases, where failure is defined by "the load at crack initiation" (predominantly tension-loaded connections and connections subjected to in-plane bending), a large scatter is to be expected, because crack-initiation and -propagation strongly depends on the actual, detailed shaping of the weld. Also, see the following section on weldings. Regarding a definition of "excessive deformations", see (80.3).

Secondly, only few test reports state the actual yield strength of the applied steel, but refer in stead to the guaranteed minimum value of this.

Thirdly, the number of free parameters in the empirical equations have been kept on a minimum, including primarily the diameter ratio, β , and the thinness γ , whereas the actual capacities most probably also depend on other parameters, for instance the ratio τ of the wall thicknesses of brace and chord.

In its philosophy, the principle of ultimate loads must, nevertheless, be considered more rational than the punching shear principle. The scatter discussed is actually less than that found in the Punching Shear Method. Again, see (80.3).

Ultimate Strength of Generally 3-dimensional Tubular Joints Subjected to Combined Loadings

Once a given tubular joint has been classified according to the principle previously described (i.e. as a combination of the basic types of joints), the ultimate strength of each connection is - for each of the components of the loading - in practical work of analysis computed as a weighed average of the strengths of the basic types of joints. The weights in this average are those determined by the classification.

This common practice, which obviously can be characterized by superposition, is theoretically wrong, since it is applied in the solution of a non-linear problem. Still, a theoretically correct determination of the ultimate capacity of each joint in the jacket structure for each load combination must a priori be considered unfeasible, and the question is, whether principles more rational than the traditional can be devised as long as the computation of the ultimate strength is based on empirical equations.

It is not possible to evaluate the uncertainties involved when following the common practice. Again, no investigation has been made, which could confirm or reject the sense in this practice.

For a joint subjected to combined loadings, the yield criterion, used in the principle of ultimate loads, is:

$$\frac{P}{P_u} + \frac{2}{\pi} \text{Arcsin} \left[\sqrt{\left(\frac{M_{IPB}}{M_{u,IPB}}\right)^2 + \left(\frac{M_{OPB}}{M_{u,OPB}}\right)^2} \right] = 1.0, \qquad (7)$$

in which the force and bending moments with lower index "u" are loads of reference, the ultimate capacities of the joint, subjected to pure loadings, cfr. (83.2), section D2.5.

The yield locus, represented by (7) and shown in Figure 10a, is the same as the one, valid for a circular cylindrical member, subjected only to an axial force N and a bending moment $M = \sqrt{M_x^2 + M_y^2}$. The method of ultimate loads thus applies the same yield criterion for the members and for their connections, naturally because neither experimental nor theoretical results regarding joints subjected to combined loadings have been available.

Consequently, the sense in applying this yield criterion can hardly be criticized. There is, however, a priori reason to doubt the sense in the vectorial addition of $M_{IPB}/M_{u,IPB}$ and $M_{OPB}/M_{u,OPB}$, because the capacities of the tubular joint, when subjected to these two types of bending, are considerably different. This is contrary to what governs the M_x, M_y -loading of the circular cylindrical member. Also, see Figure 5.

A yield criterion alternative to (7) is one, for which the yield locus lies in a $(\frac{P}{P_u}, \frac{M_{IPB}}{M_{u,IPB}}, \frac{M_{OPB}}{M_{u,OPB}})$- coordinate system, Figure 10b. Without reference to any tests or analyses of tubular joints subjected to combined loadings, one could suggest a number of yield loci, represented by convex surfaces, in this coordinate system, for instance a sphere, a paraboloid of revolution or a cube.

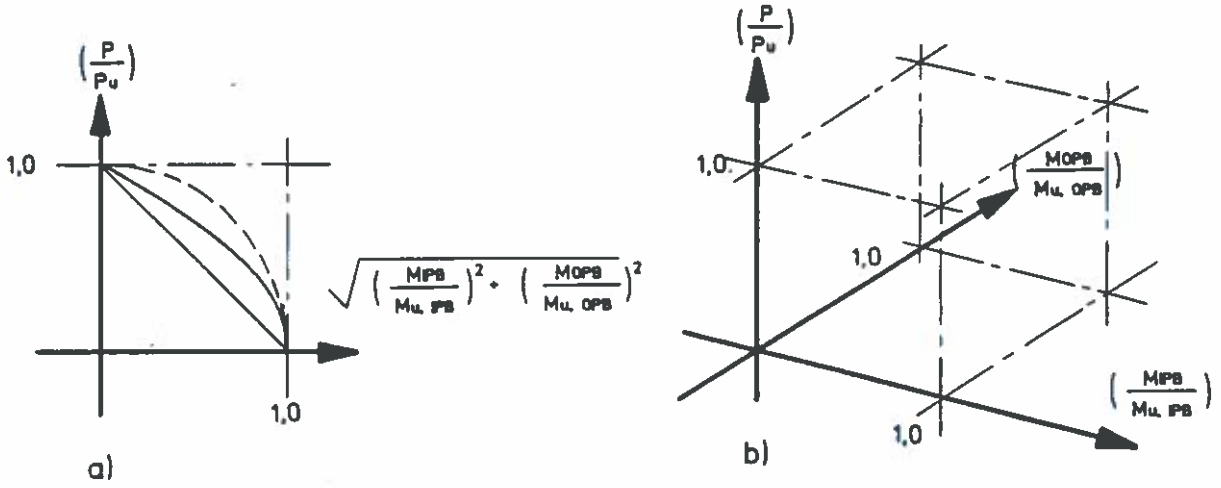

Figure 10.

Hoadley has in 1984 proposed an alternative to (7) based on the results of a test programme including 12 tests with DT-joints. The tests are reported in (84.2) and also referred to in (85.2). In all the tests, the diameter ratio $\beta = 2/3$ and the thinness of the chord $\gamma = 25.2$. In 9 of the 12 tests, the joints were subjected to combined loadings.

The alternative, which is an inner bound of the observed points on the yield locus, is

$$(\frac{P}{P_u}) + (\frac{M_{IPB}}{M_{u,IPB}})^{2.1} + (\frac{M_{OPB}}{M_{u,OPB}})^{1.2} = 1.0, \qquad (8)$$

in which P_u, $M_{u,IPB}$ and $M_{u,OPB}$ are capacities of reference, as measured in the tests.

The largest observed value of the left hand side of (8) is 1.15. The observed values of the left hand side of (7) all lie in the interval $[0.84, 1.12]$ with only two values larger than 1.0.

Based on these raltively few test results, the Arcsine-equation must therefore be considered as being some 15% unsafe.

If, however, the reference-capacities of the DT-joint are computed by the empirical equations, (83.2) annex D2, (7) and (8) turn out to be very conservative. The observed values of the left hand side of (8) then all lie in the interval $[1.67, 2.83]$. In other words: The empirical equations, which themselves draw lower bounds of observed capacities, obviously underestimate the capacity of the joints in this test series.

A modification of (8) has been suggested:

$$\left(\frac{P}{P_u}\right) + \left(\frac{M_{IPB}}{M_{u,IPB}}\right)^2 + \left(\frac{M_{OPB}}{M_{u,OPB}}\right) = 1.0 \qquad (9)$$

Applying this criterion, the capacities of reference should be computed by the ordinary equations. With the results of Hoadley's tests, the observed values of the left hand side of (9) lie in the interval $[1.00, 1.19]$.

The test programme initiated by Hoadley was later continued with tests of DT-joints of diameter ratios equal to 1/3 and 1. The results of these tests have not yet been reported, but may be expected to conclude a proposal of modification of (8), in which the powers of each term are β-dependent.

Conclusion

Many aspects of uncertainties in the analysis of a jacket structure's load response originate in the complex behaviour of the tubular joints.

Due to the considerable local flexibility of the chord wall and due to the excentricities, commonly designed in tubular joints, the presumptions of traditional analyses, regarding rigid

bility caused by disregarding joint excentricities and joint flexibilities affect the field of internal forces in all the elements of the structure; for actual as well as critical axial forces in the bracings it is of the order 15%, and the moment loading of same elements turn out to be reduced and differently distributed in reality as compared to the results of the traditional analysis. Uncertainties regarding deflections are of the order 30%.

A theoretical analysis of the ultimate capacity of a given tubular joint is, because of large deformations, strain hardening, crack initiation and propagation as well as local yielding, very cumbersome. In stead, the ultimate capacity of tubular joints is evaluated by means of empirical equations, based on the results of laboratory tests with simple types of plane joints. The empirical equations all draw lower bounds of the capacities observed in tests. However, the ratio of predicted to measured capacities show a relatively large scatter, in some cases up to 60%.

As a consequence of the empirical equations, covering only 2-dimensional connections, common methods of analysis disregard the influence of the interaction between several out-of-plane bracings, framing into the same joint, on ultimate behaviour. Uncertainties related to these circumstances have, so far, not been investigated. Also, the commonly applied yield criterion for tubular joints subjected to combined loadings is rather poorly based. The results of newer test programmes, regarding this problem, indicate the need for a better yield criterion to be established.

References

(77.1) Det norske Veritas:
Rules for the Design, Construction and Inspection of Offshore Structures, 1977.

(80.1) Bouwkamp, J.G. et al.:
Effects of Joint Flexibility on the Response of Offshore Towers.
OTC-paper No 3901, 1980.

(80.2) Hoffmann, R.E., and Sharifi, Parviz:
On the Accuracy of Different Finite Element Types for the Analysis of Complex, Welded Tubular Joints.
OTC-paper No 3691, 1980.

(80.3) Yura, J.A., Zettlemoyer, N. and Edwards, I.F.:
Ultimate Capacity Equations for Tubular Joints.
OTC-paper No 3690, 1980.

(81.1) Fessler, H. and Spooner, H.:
Experimental Determination of Stiffness of Tubular Joints.
Paper No 28, Symposium on Integrity of Offshore Structures, Glasgow, 1981.
Also reproduced in (85.1).

(82.1) Jaap Wardenier:
Hollow Section Joints.
Delft University Press, 1982.

(83.1) Dansk Ingeniørforening's Code of Practice for Pile Supported Offshore Steel Structures, 1. edition, 1983.

(83.2) Annexes A-F and Supplementary Guide to (83.1), 1983.

(84.1) Node Flexibility on the Behaviour of Jacket Structures.
UEG, Underwater Engineering Group.
Report No UR/22, 1984.

(84.2) Hoadley, P.W., and Yura, J.A.:
Ultimate Strength of Tubular Joints Subjected to Combined Loads.
Phil. M. Ferguson Structural Engineering Lab.
The University of Texas at Austin, 1984.

(85.1) Design of Tubular Joints for Offshore Structures, Volume 1-3.
UEG, Underwater Engineering Group.
Publication No UR33, London, 1985.

(85.2) Hoadley, P.W., and Yura, J.A.:
Ultimate Strength of Tubular Joints Subjected to Combined Loads.
OTC-paper No 4854, 1985.

Uncertainties in fitness for purpose assessments of welds

Birger Hansen

Abstract:

The application of quality criteria, based on fitness for purpose assessments, would have many benefits to the manufacture and application of welded products. Less repair and lower costs in addition to better information on the true level of safety obtained are essential benefits. The application of fitness for purpose criteria is hindered mainly by imperfect inspection procedures, characterized by large inherent uncertainties. The paper gives an overview of inspection uncertainties in conventional inspection systems and outlines trends, which may result in greatly ameliorated inspection systems in the not so distant future.

UNCERTAINTIES IN FITNESS-FOR-PURPOSE ASSESSMENTS OF WELDS

Birger Hansen

FITNESS FOR PURPOSE

Any product should be designed and manufactured in such a way, that premature failure does not occur when the product is being used for the intended purpose. Also, the product should function satisfactorily. Fitness for purpose means, that the strength and other properties of the product are adequate to withstand the loads, environmental factors and other actions on the product during use.

A product should be fit for the purpose. This is true for any product, from sewing machines to supertankers, from toys to tanks. Experience has shown, however, that fitness for purpose not always is obtained. Codes and regulations and mandatory inspections are precautions enforced by the society as a safeguard against failures resulting in loss of human life, pollution, large economical losses or other unacceptable consequences.

The nature of the problem of fitness for purpose must be understood in order to take efficient and reasonable precautions. When a product finally is scrapped, it is known if that particular product was fit for the purpose. Nature gives a final answer to the question of fitness for purpose, or not. The real problem is entirely different, however. The real problem is that the parties concerned: Designer, manufacturer, end user, insurance companies, authorities etc. need to know if a particular product will be fit for the purpose, or not, and they should know before the product is being used by the end user. In brief, they would like to know the future. According to conventional science, exact information on future events can not be obtained. What can be obtained, however, is an estimate of the probability of various events. The probability of failure and the degree of assurance of the fitness for purpose of the new product can be estimated. Fitness for purpose assesments must, for that reason, be based on probabilistic considerations. This is not always realised, mainly because design codes often appear "deterministic"; the probabilistic considerations are inherent to the code rules, however.

The designer has to estimate the loads, environmental factors and other actions likely to occur during the use of the product. Wind speeds during storms, maximum snow loads, extreme wave loads and other environmental loads have been observed for several decades, if not centuries. The designer should use conservative, code values. Other live loads may be more difficult to estimate. Even loads specified in codes are not absolutely "safe". From time to time loads surpassing anything previously observed do occur. Even centuries of observation does not prevent even larger loads tomor

row. The uncertainties are, of course, substantial when the designer has to estimate laod under unusual events, earthquakes e.g. Some loads are directly influenced by the end user. What is the limit between normal use and misuse?

The designer should determine and specify all relevant properties of the product. Determination often involves stress analysis and other calculations. Several formulas used during stress analysis are empirical and based on a limited amount of tests and observations.

The manufactured product should fulfil all requirements, specified by the designer. This is far from guaranteed; several factors may cause deviations. The properties of the welds depend critically on the procedure for welding actually used by the welder. The performance of the welding engineers an technicians planning the fabrication of the welded product and the skill and care of the welders largely determine the mechanical properties of the welds.

The existance of a large number of uncertainties in design and fabrication of welded products is a well known fact. The uncertainties are compensated by various means. First of all, safety factors of various kinds are mandatory for all "code products". Similar safety factors are applied on a voluntary basis for "non code" products.

The consequence af using safety factors is not always realised. Safety factors do not assure fitness for purpose of all products. Safety factors merely reduce the risk (probability) of failure to an acceptable level.

There is a price to be paid for the use of safety factors. The average product will presumably be correctly designed, the welders will adhere reasonably well to the (correctly) specified welding procedures and the product is not going to be exposed to unforeseen storms or earthquakes or misuse. The average product therefore should be fit for the purpose even if designed without any safety factor (safety factor equal to one). A mandatory safety factor makes all products stronger and therefore augments the weight and the cost of all products. On the other hand, a large safety factor means, that a product may deviate significantly from the "average" product and still be fit for the purpose, even if overloaded somewhat. Code committees have to consider the extra expences for all products, but also the consequences of the remaining few failures likely to occur.

Inspection during manufacture, inspection of the final product and in service inspection all provide information on the properties of the actual product. Information on the properties reduces some of the uncertainties and consequently permits reduced safety factors. Inspection is a necessity for many welded products in order to

reduce the uncertainties and the safety factor to a reasonable level.

Inspection may be rather expensive; the reduced manufacturing costs (due to reduced product weight permitted by lowered safety factors) may be offset by the costs of inspection.

Inspection has for some years partially been superseded, partially supplemented by formalised quality systems encompassing design as well as manufacture of welded products. Rules and regulations for quality systems hav been standardised. General international standards for quality systems are in an advanced stage of preparation. The philosophy behind the rules and regulations is to assure a "perfect" performance of design offices and workshops, or at least that any mistake or deviation is disclosed in time so that a faulty product is not passed on to the end user. The philosophy is sound, but a bureaucratic and expensive system may be the result, if the manufacturer does not take great care in implementing a quality system.

WELDED PRODUCTS

The question of fitness for purpose is most pertinent for welded products. Many, potentially dangerous, products are welded: Offshore platforms, storage tanks for inflammable or poisoneous fluids, critical pressurised components in nuclear and conventional power plants etc. The welds frequently determine the strength and resistance to brittle fracture of the product. Finally, inspection of welded products is expensive; it involves rather costly qualification of welding procedures and welders, welding inspection and nondestructive examination of the finished welds. The nondestructive examination has been subject to much discussion, analysis, but also development for some years. It has now been confirmed by several research projects that nondestructive examinations may be characterised by rather large uncertainties. These uncertainties are compensated by imposing stringent acceptance criteria for the nondestructive examinations. The design safety factors are often kept at a minimum for critical products; weight may be a problem and heavier materials may actually diminish the resistance against brittle fracture. The cost of welding and inspection also grows faster than the resistance, when heavier materials are used. Uncertainties in nondestructive examinations of welds are, for these reasons, compensated by safety factors on defect size, that is by stringent acceptance criteria. The price is paid by the welding workshops. Productivity is lowered and welds are frequently rejected and repaired or scrapped even though it can be shown that the imperfections do not impair the fitnes for purpose of the product. Many researchers and welding engineers in the workshops are striving to obtain more economical, more efficient and less uncertain procedures for nondestructive examination of welds, permitting relaxation of the conventional acceptance criteria.

Figure 1. Collapsed storage tank

A spectacular example of a failure caused by an imperfection not disclosed during inspection.

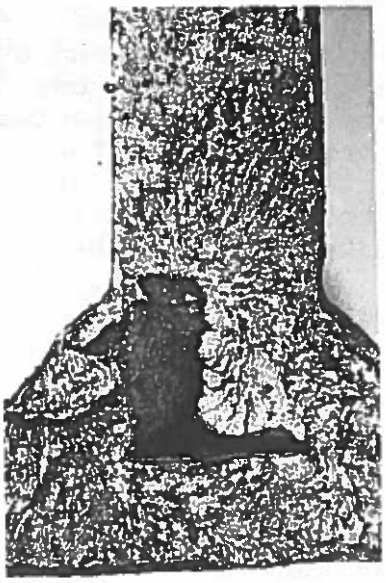

Figure 2. Initiating defect
The failure occurred a cold winter night and initiated from a cracklike imperfection in the lowest edge of the wall of the storage tank.

UNCERTAINTIES IN NONDESTRUCTIVE EXAMINATIONS

Nondestructive examination of welds is performed by a number of methods: Radiographic examination, ultrasonic examination, magnetic particle examination, penetrant examination and last, but not least, visual examination. All methods rely on the skill of a human inspector to interpret the results. Human errors certainly add to the uncertainties. The methods do, in addition, have severe limitations, which further adds to the uncertainties. The significance of an imperfection depends critically on the height of the imperfection, in addition to imperfection type and orientation. All these parameters are difficult to measure accurately by nondestructive methods.

A workstation in a workshop performing nondestructive examinations of welds may be imagined as a sorting machine, which sorts the welds (and consequently the products) into two categories: Accepted and rejected. Hopefully, all accepted products are fit for the purpose, rejected products unfit. Unfortunately this is not the case. Inspection uncertainty makes the examination "fussy" and the outcome unpredictable to a degree. Some products, which are likely to fail prematurely during service may be accepted. By using stringent acceptance criteria, this risk is reduced to an acceptable level. However, at the same time the probability of rejecting welds with only small defect will, inevitably, augment. The workshop can not consistantly repair a high proportion of the manufactured products; welding procedures resulting in only a limited amount of small imperfections and a reasonable rate of acceptance must be applied. Production and subsequent acceptance of products with grave imperfections in one or more welds will thereby be reduced to a very low level (acceptable considering the normal design safety factors, which further diminish the risk of failure). The rejection rate is reduced and the costs related to repair are acceptable to the manufacturer. However, the unavoidable reduction of the productivity may be less obvious .

The performance of a procedure for nondestructive examination may be analysed in the following way: A fairly large number of test specimens is prepared. Each test specimen holds a weld and in each weld is an imperfection of a well known type, size, position and orientation. The test specimens are passed through the normal examination procedure. The operators must, of course, have no opportunity to obtain information on the imperfections prior to the examination. The outcome of the examination is analysed statistically. The results are plotted so that the probability of acceptance is shown as a function of imperfection size. An sigmoidal curve will be the result (Figure 3). Even though the test specimens represent a rather artificial type of product, the result gives important information on the performance of the examination.

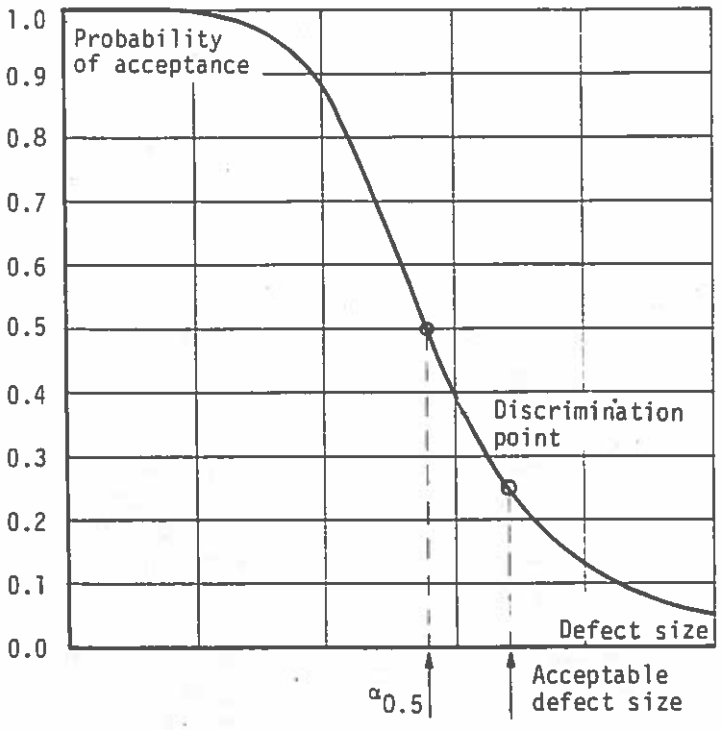

Figure 3. Schematical acceptance curve for nondestructive examination

In the range of large imperfections - grave imperfections making the product unfit for purpose - the probability of acceptance should be negligible. Actually, nondestructive examinations are far from perfect and there is a certain risk of overlooking imperfections, even very large imperfections. Part of this uncertainty may be due to human errors, but the method as such also have limitations, which may cause acceptance of even very large imperfections.

In the range of small imperfections, the probability of acceptance should be equal to one. However, due to several factors, one of which is human errors, spurious indications do occur, causing rejection of perfectly sound welds.

In the intermediate range, the probability of acceptance diminish as a function of imperfections size. The ideal examination procedure would have a very abrupt change from 100 % to 0 % probability of acceptance. An analysis of conventional nondestructive procedures shows a very gradual transition from high to low probabilities of acceptance. The slope of the acceptance curve in the intermediate range is determined mainly by the measuring uncertainties (scatter) inherent to the nondestructive procedure.

The experiment described is difficult to perform. Production of welds with well defined imperfections is far from easy (in contrast to naturally occurring, random imperfections which come easily). A slight change of the experimental procedure is necessary. The straightforward solution is to determine imperfection size, type and orientation after the nondestructive examination has been performed. The test pieces are manufactured in such a way, that they may be assumed to represent the quality variations likely to occur during actual production. Actually, they may be production samples. After nondestructive examinations have been terminated, the specimens are destructed by slicing, whereby defect configuration can be measured accurately. An even more direct way is to determine the fitness for purpose directly by e.g. fatigue testing. The probability of acceptance may then be determined as af function of fatigue strength.

Experiments of this type represent the only way to obtain reliable information on the uncertainties inherent to nondestructive examinations. The experiments are bound to be complicated and lengthy and often very costly. Large scale international cooperation is the rule in such experiments.

An acceptance curve shows the outcome of a nondestructive examination of welds holding only one defect, using a specified procedure for the nondestructive examination and specified acceptance criteria.

An acceptance curve should, in principle be determined for each type of defect and may even have to be determined for a number of defect orientations. Such a set of curves may be determined from a single experiment, provided the examined welds represent a complete range of imperfection sizes, types and orientations.

A set of acceptance curves have to be determined for each set of acceptance criteria. The acceptance criteria form part of the inspection procedure. Fortunately, the examination data may, in certain cases, be re-evaluated using different acceptance criteria. Radiographs may easily be re-evaluated by a new team of inspectors, using new acceptance criteria. Re-evaluation is straigtforward for ultrasonic examinations where full information on echo heights, echo source location etc is reported. Computerised ultrasonic procedures such as P-scan and similar procedures permit complete re-evaluation as a matter of course.

The basic information on a nondestructive procedure consists of a set of acceptance curves. The acceptance curves do not completely determine the outcome of an inspection. Several other factors are significant for the outcome. Welded product frequently are examined, using a sampling procedure. Only a certain proportion of a bach of identical products may be examined. The welds in large, welded products are far from always examined in their entire length. The chief inspector designates certain welds to be examined. These welds are assumed to be representative of all welds. Sampling is related to unavoidable uncertainties. These uncertainties can be analysed by statistical methods. Important factors in sampling examinations are the rules for actions to be taken in case some welds are rejected. The usual precaution is to demand examination of a much larger sample.

Another factor, which is important for the outcome of the examination is, of course, the original population of imperfections in the products as manufactured. If the welds are near perfect and holds only very few and small imperfections, any examination will be adequate. The welds are fit for the purpose anyway. Welds holding several gross imperfections are likely to be rejected even by rather uncertain examination procedures. The performance of the inspection procedure really counts for welds holding a reasonable number of imperfections of which only one or at mo most a few are critical and compromising the fitness for purpose. The statistical distribution of defect then becomes essential. Conventional examination procedures can not reliably reject such few critical imperfections. The procedures are not suitable for a "needle in a haystack" inspection. The welds must be rejected on the basis of observations of much more common large (but not critical) imperfections. This is an other way of demonstrating the need for a safety factor on imperfection size.

Even though many factors interfere it is possible, at least in theory, to calculate the performance of the entire inspection system provided the basic acceptance curves have been determined.

Several investigations of the uncertainties in nondestructive examinations have been published (cf. ref 1). The results confirm the relatively large uncertainties in nondestructive examinations of welds. Figures 5 and 6 show representative acceptance curves.

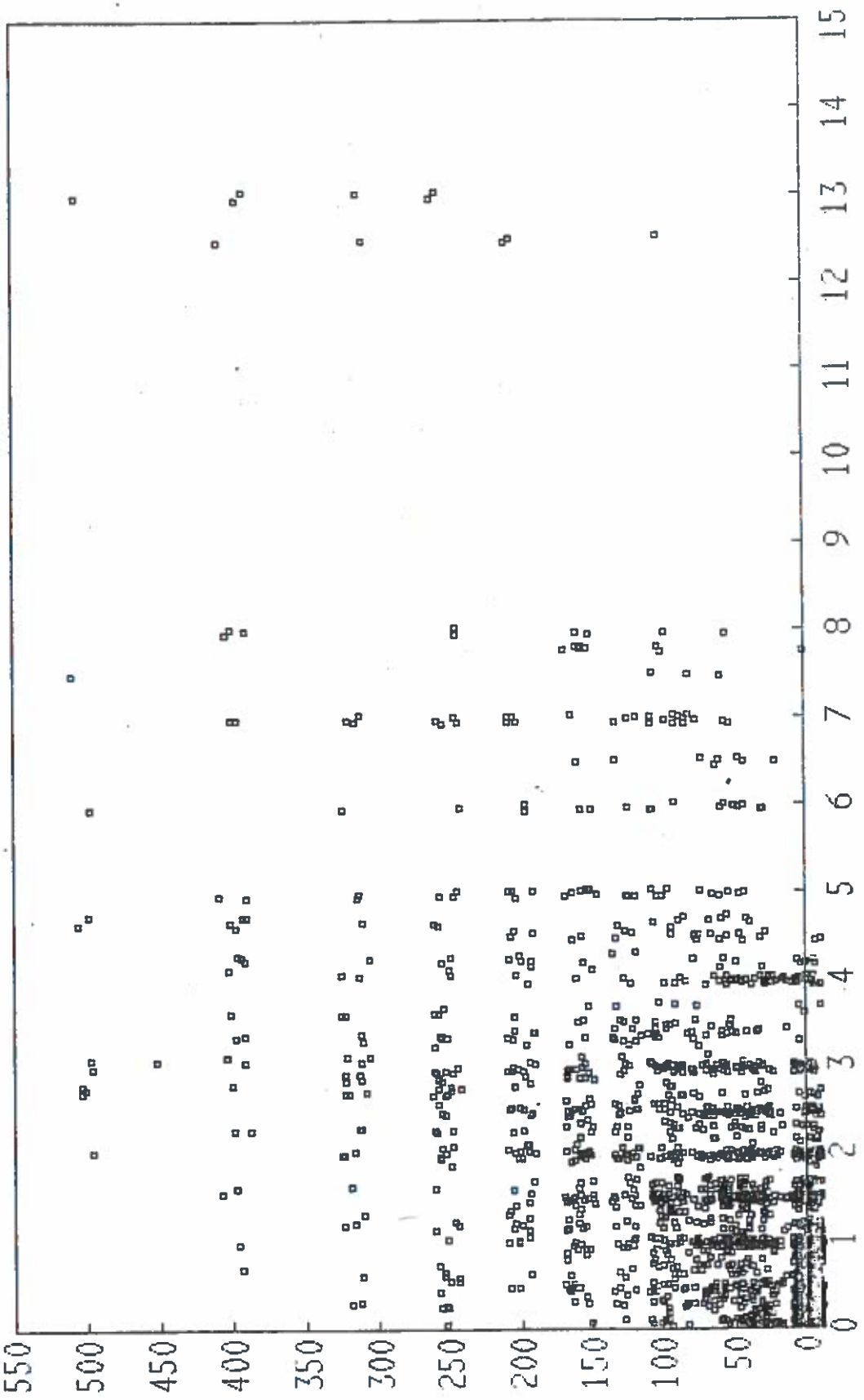

Figure 4 Scatter in ultrasonic examinations

The figure shows ultrasonic echo amplitude height versus imperfections height for imperfections examined by a conventional ultrasonic technique. From ref 1.

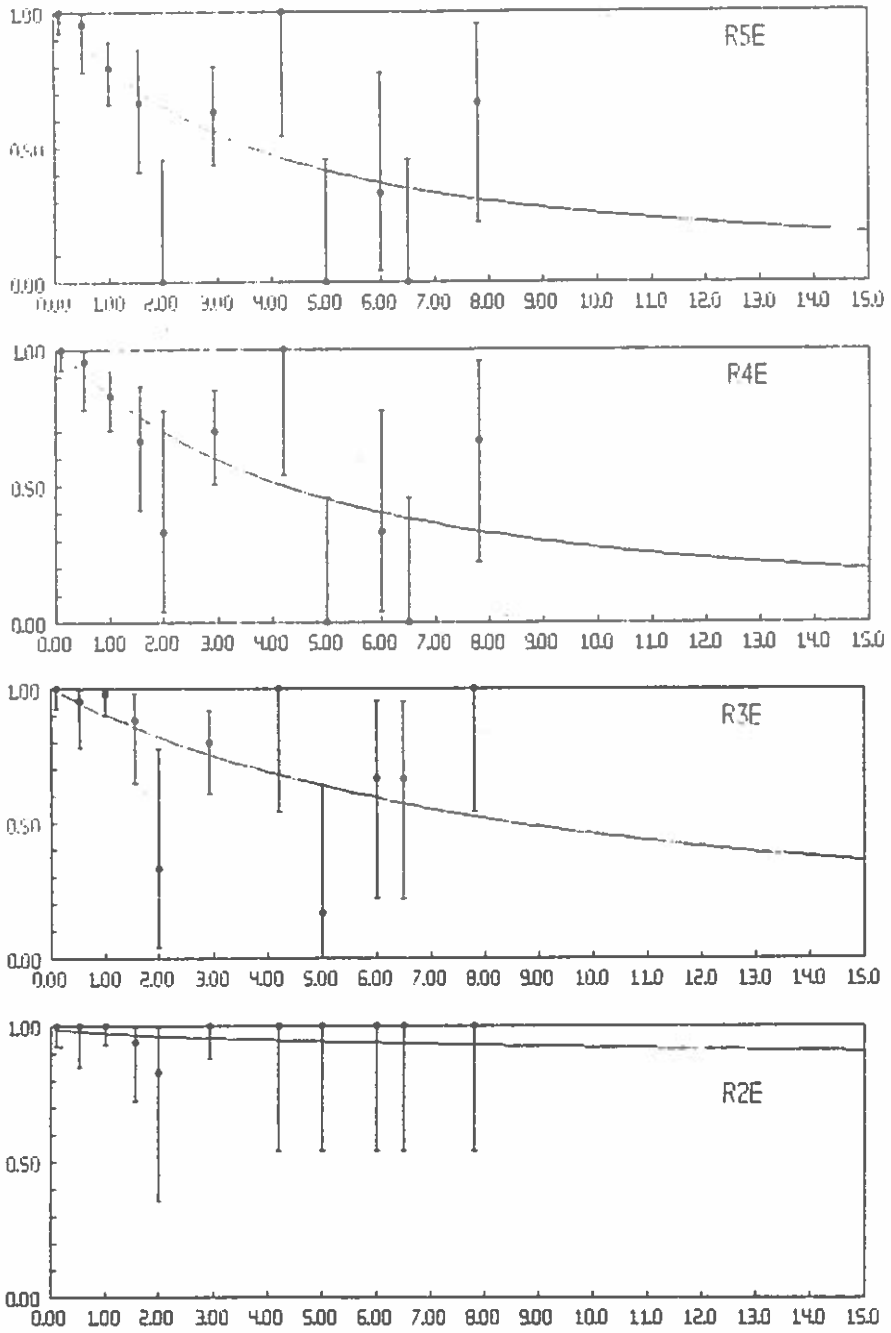

Figure 5 Acceptance curves for radiographic examination. Cracks.

The acceptance curves relate to conventional radiographic examination of butt welds in the thickness range 10 to 20 mm. The acceptance criteria correspond to IIW degree black (upper curve), blue, green and brown (lowest curve). Codes usually specify acceptance criteria roughly corresponding to IIW degree blue for highly stressed welds and critical applications. From ref 1.

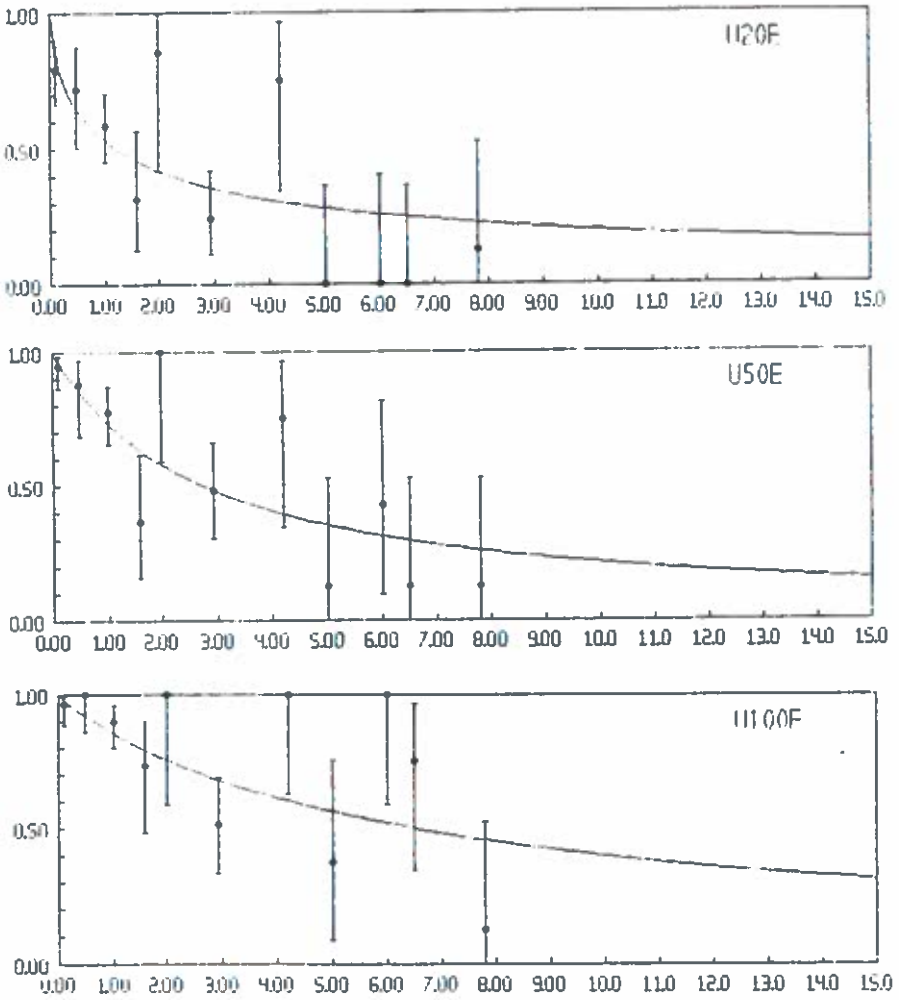

Figure 6 Acceptance curves for ultrasonic examination. Cracks.

The acceptance curves relate to conventional ultrasonic examinations, carried out manually and evaluated by the ultrasonic operator during the examination. The figures 20, 50 and 100 refer to percentage of reference echo height. 50% is specified by some codes for critical applications.

Figure 6 Acceptance curves for ultrasonic examination. Cracks.

The acceptance curves relate to conventional ultrasonic examinations, carried out manually and evaluated by the ultrasonic operator during the examination. The figures 20, 50 and 100 refer to percentage of reference echo height. 50% is specified by some codes for critical applications.

FITNESS FOR PURPOSE LIMITS

Determination of the fitness for purpose limits is essential for the application of more rational inspection procedures. Many imperfections i welds, in particular dangerous imperfections are crack-like imperfections (planar imperfections). The stress field near the tip of a crack-like imperfection is difficult to analyse using conventional stress analysis. Singularities where stresses are infinite occur at the tip of the imperfections. Special tools , collectively known as fracture mechanics have been developed for the analysis of fractures initiated from crack-like imperfections. Fracture mechanics are becoming accepted tools for the designer. Tentative standards have emerged, for examble the document from British Standard, PD xxxxx. (ref 2). The International Institute of Welding (IIW) is presently preparing a draft for an international standard on fitnes for purpose assesment of welds. Sound technical solutions for determination of inspection uncertainties and calculation of safety factors on defect size necessary are problems, which have to be solved before the IIW document can be operational.

REVISION OF EXAMINATION PROCEDURES

The data for inspection uncertainties obtained so far leaves a strong impression of a need for large compensating safety factors. There is little hope of relaxing the safety factors and consequently the acceptance criteria, unless examination procedures having essentially reduced uncertainties, can be developed and implemented in everyday inspections of welds. A number of strategies may be followed.

Fast and cheap examination procedures would permit augmented sample sizes and consequently reduced uncertainties due to sampling. Nondestructive examinations of welds are carried out manually to a very large extent. Costs are related to salaries. Mechanization, automation or robotication of nondestructive examinations would be a solution, but has largely remained a theoretical possibility so far.

An important part of the inspection procedure is evaluation of the results from the nondestructive examinations. Computers are becoming smaller, cheaper and more powerfull; they offer a possibility of computerized evaluation of the results from nondestructive examinations. Ultrasonic examination is in many cases the preferred procedure for determination of imperfection sizes. Ultrasonic examinations is characterized by a large amount of information, which previously has been evaluated by the inspector during the actual examination. An elaborate evaluation under the often adverse conditions in a welding workshop is hardly to be expected and bound to be lengthy and expensive. Computerized registration and evaluation of all essential information obtained during the ultrasonic examination has proved to permit an essential reduction of the examination uncertainties.

CONCLUSION

The application of fitness for purpose criteria in welding would diminish costs and reduce waste and permit higher productivity in the welding workshop.

A serious hindrance to the application of fitness for purpose criterial is the large uncertainty and the relatively high costs inherent to conventional examination procedures. The development of computerized ultrasonic examinations, combined with mechanized, automated og robotized scanning of the welds by the ultrasonic probe provides a hope for faster and much more reliable inspections of welds, permitting widespread application of fitness for purpose criteria in a not too distant future.

Another hindrance is the lack of codes for determination of critical defect sizes and acceptance criteria. Present work going on within the IIW should provide the basis for such documents witin a reasonable future.

REFERENCES

1 Olav Førli, Birger Hansen, Sven Kjellander, Bjørn Petterssen, Thomas Åstrøm: A Comparison of Radiographic and Ultrasonic NDE. Nordtest 72-76. SVEJSEcentralen, Brøndby, 1983.

2 Guidance on some methods for the derivation of acceptance levels for defects in fusion welded joints. PD 6493:1980. British Standards Institution (BSI).

FATIGUE UNCERTAINTY ANALYSIS OF TUBULAR JOINTS

Henrik O. Madsen (1)

ABSTRACT

The fatigue limit state is governing the structural dimensions in several parts of offshore structures and in particular anticipated deep water structures. Prediction of fatigue life of tubular joints and other structural elements is subjected to large uncertainty arising from the environmental forces, the global and local response of the structure and the fatigue strength and damage accumulation. Modern reliability methods provide a tool for efficient and accurate uncertainty analysis. Nominal failure probabilities are computed which allow a comparison between reliability levels for different joints or different designs. Important sources of uncertainty are determined and at the same time, the sensitivity of the reliability to various design parameters is determined. The paper provides examples of uncertainty modeling relevant for fatigue strength of tubular joints, and the application of a probabilistic fatigue analysis is demonstrated for a tripod tower platform example.

1. INTRODUCTION

For many offshore structures and anticipated deep water structures in particular, the fatigue limit state is often governing the structural dimensions in several parts of the structure. In addition, these structures often have little redundancy, and the consequences of element failure due to fatigue are more severe with respect to loss of facilities and human lives than for traditional jacket structures in more shallow waters. The possibility of carrying out repair is also very limited for these structures. The emphasis in this paper is on fatigue of tubular joints, but the analysis method is applicable to other welded structural elements such as anchoring chains or tethers.

At present most fatigue analyses consist of simple checking of safety according to some code. Computed life times are checked to be larger than the anticipated life time by a certain factor. The relative magnitudes of computed life times are also used to define inspection programs. It is well accepted that there is little correspondence between computed and observed life times. When fatigue is the governing ultimate limit state and the consequences of fatigue failure can be dramatic, more confident information about fatigue life must be produced. Also, the fatigue limit state must be treated in the same way as other limit states, i.e.,

(1) A.S.Veritas Research, P.O.Box 300, 1322 Hovik, Norway.

by use of principles of limit state analysis and by calibration of partial safety factors by a reliability method on a higher level. Conceptually, the fact that time is an explicit parameter does not make the use of limit states design any different. In most present design codes all parameters are taken at their expected values except for a conservative choice of fatigue strength. To verify that such a simple format is sufficient also for new structural concepts can only be done if an advanced reliability analysis is available.

The analysis model must be based on physical and mechanical models of the loading, the fatigue strength and the damage accumulation. These models need not necessarily be state-of-the-art models but they must provide a satisfactory compromise between accuracy in description and simplicity in use. The models are 'randomized' by replacing various parameters with random variables. It is important that the probabilistic model also contains model uncertainty variables which explicitly account for the shortcomings of the physical and mechanical models due to a lack of knowledge and due to simplifications in the modeling. Reliabilities are computed by first- or second-order reliability methods. The computed reliabilities are measures of the confidence in the structural reliability. The reliability is not a property of the structure and may change as more information becomes available. Although the computed reliabilities can therefore not be interpreted as expected failure frequencies, they are ideal measures for comparing reliabilities of different possible designs; and they are very efficient in identifying important sources of uncertainty and in identifying cost optimal ways of improving the reliability. The application of the results of the reliability analysis in a sensitivity study is illustrated in an example, but first a description of uncertainty modeling in relation to fatigue strength and of the reliability calculation are presented.

2. UNCERTAINTY MODELING FOR FATIGUE STRENGTH OF TUBULAR JOINTS

Two models for fatigue strength are presently being used. For design purposes it is customary to use so-called $S-N$-curves, expressing the number of stress cycles of a certain stress range and with a certain mean stress necessary to cause failure. For welded details it is a common practice to ignore the mean stress, implying that the welding procedure sets up residual stresses of yield value. $S-N$ curves are generally linear or piecewise linear in a double-logarithmic mapping, [1], i.e., of the form

$$N\,S^m = A\,, \quad S>0 \tag{1}$$

or, as e.g., the T-curve from Department of Energy [2,3],

$$N = \begin{cases} A\,S^{-3}, & N<10^7 \\ A_1 S^{-5}, & N\geqslant 10^7 \end{cases} \tag{2}$$

where the constants A and A_1 are uniquely related as the $S-N$ curve is continuous. The constant A depends on the wall thickness. Uncertainties in the $S-N$ curve parameters are described in a subsequent section.

For variable amplitude loading a damage accumulation model is needed and a damage indicator D is introduced. The damage indicator increases from an initial

value of 0 to the value 1 at failure. The increment in damage for a stress cycle of stress range S_i is taken as

$$\Delta D_i = \frac{1}{N(S_i)} \tag{3}$$

This is the Miner damage hypothesis and damage is summed over all stress cycles. The order in which the stress cycles occur is thus ignored, which is a source of model uncertainty.

In a fitness-for-purpose analysis carried out when a defect has been detected, the fatigue analysis is generally based on a fracture mechanics approach. In this approach the fatigue crack growth from an initial size a_0 to a critical size a_C is modeled. The crack increment in one cycle is described by the equation of Paris and Erdogan, [4]

$$\frac{da}{dN} = C\ (\Delta K)^m, \quad \Delta K > 0 \tag{4}$$

where a is the crack size, N is the number of stress cycles, C and m are material parameters, and K is the stress intensity factor. The stress intensity factor is computed by linear fracture mechanics and is expressed in the form

$$K = \sigma\, Y(a)\, \sqrt{\pi a} \tag{5}$$

where σ is the far-field stress and $Y(a)$ is the so-called geometry function. This function depends on the overall geometry including the possible presence of a weld. Eqs. (4) and (5) can be generalized to a two-dimensional description of the crack and to combined loadings.

Eq.(5) is inserted in (4) and for constant amplitude loading with stress range $S=\Delta\sigma$ the differential equation (4) is solved as

$$\Psi(a) = \int_{a_0}^{a} \frac{dx}{Y(x)^m\ (\sqrt{\pi x}\ )^m} = C\ S^m\ N \tag{6}$$

With failure taking place when the crack size exceeds the critical size, the following relation is valid at failure

$$N\ S^m = \frac{1}{C} \int_{a_0}^{a_C} \frac{dx}{Y(x)^m\ (\sqrt{\pi x}\ )^m} = A \tag{7}$$

An $S-N$-curve similar to (1) thus follows from this approach.

For variable amplitude loading the order in which the stress cycles appear in the stress history is ignored. Solution of (4) leads in this case to

$$\Psi(a) = \int_{a_0}^{a} \frac{dx}{Y(x)^m\ (\sqrt{\pi x}\ )^m} = C \sum_{i=1}^{N} S_i^m \tag{8}$$

A damage indicator can be defined as

$$D = \frac{\Psi(a)}{\Psi(a_C)}, \quad 0 \leqslant D \leqslant 1 \tag{9}$$

In this case that damage is related to a physically measurable quantity crack size.

The damage increment in a stress cycle with stress range S_i becomes

$$\Delta D_i = \frac{CS_i^m}{\int_{a_0}^{a_c} \frac{dx}{Y(x)^m (\sqrt{\pi x})^m}} = \frac{1}{N(S_i)} \tag{10}$$

and the damage accumulation model is thus in agreement with the Miner damage hypothesis. There is thus a close agreement between the $S-N$-based and the fracture mechanics based fatigue analysis for design. In connection with updating based on inspection results only the fracture mechanics approach is, however, useful. The uncertainty in the parameters in the fracture mechanics approach is not discussed here.

2.1. Uncertainty Modeling of Fatigue Strength from Code Based S-N Curves

The T-curve from Department of Energy [2,3] and given in (2) was based on test results shown in Fig.1.

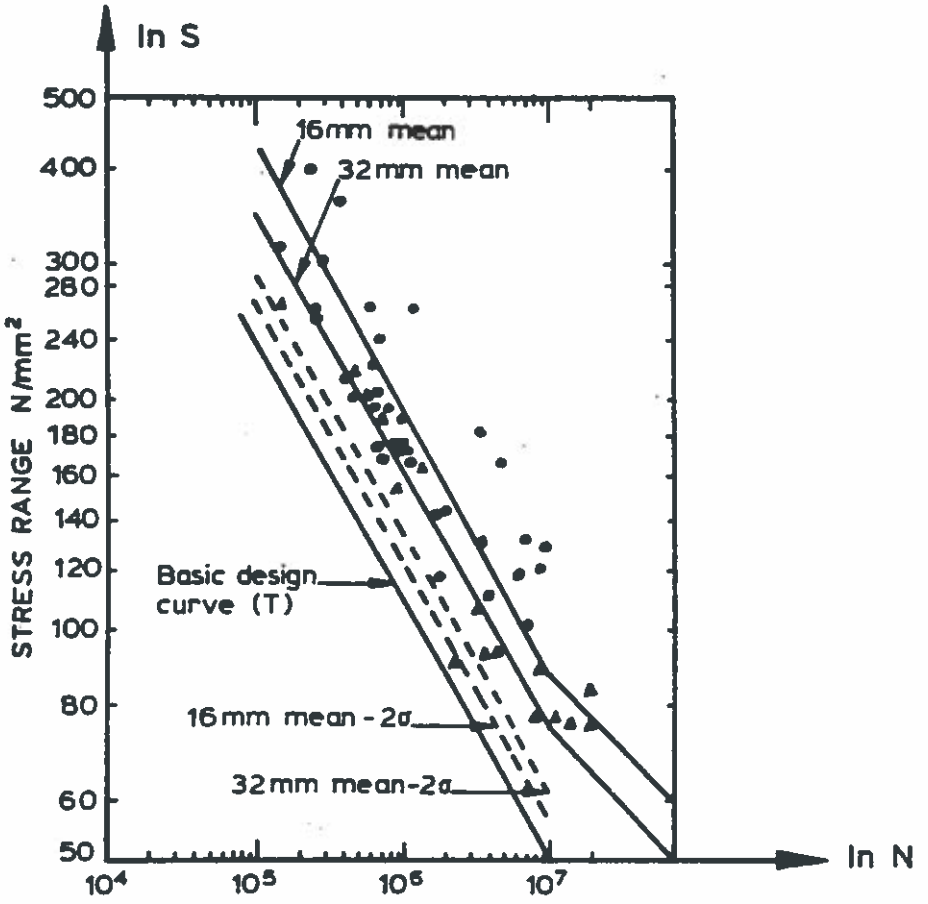

Figure 1 T-curve and fatigue test results.

The upper part of the T-curve is the result of a linear regression analysis. The distribution of $\ln N$ for a fixed value of S is taken as normally distributed with mean value varying linearly with $\ln S$ and with a standard deviation $\sigma_{\ln N}$ independent of S. The mean value of $\ln N$ is estimated as

$$E[\ln N] = 29.152 - 3.0 \ln S \tag{10}$$

and the standard deviation $\sigma_{\ln N}$ is estimated as 0.572. $\ln N$ is thus expressed as

$$\ln N = 29.152 - 3.0 \ln S + 0.572U \tag{11}$$

where U has a standard normal distribution. The slope $m=3$ for $N<10^7$ is justified from fracture mechanical considerations. The change in slope to $m_1=5$ at $N=10^7$ is not well justifiable and to account for this the slope m_1 is modeled as a random variable.

$$m_1 = 3+M \tag{12}$$

where M is a positive random variable. The thickness reduction factor is also subject to uncertainty and therefore modeled as a random variable.

2.2. Uncertainty Modeling for Fatigue Strength from Statistical Analysis of Test Results

The statistical analysis aims at determining the constants K and m in an S-N curve of a form corresponding to (1). A detailed description with examples of a Bayesian statistical analysis of fatigue data is presented in Madsen [5] and is briefly summarized. Test results are transformed as $(x,y) = (\ln s, \ln n)$ and a linear normal regression model with constant variance is formulated with x as the independent and y as the dependent variable. This choice of statistical model is in accordance with (1). The value of Y for a given value $X=x_t$ is written as

$$Y_t \mid X=x_t] = \alpha - \beta(x_t - \bar{x}) + \sigma U_t \tag{13}$$

where U_t is a standardized normal variable

$$U_t \in N(0,1) \tag{14}$$

The mean value and variance of $Y_t \mid X_t=x_t$ are

$$E[Y_t \mid X=x_t] = \alpha - \beta(x_t - \bar{x}) \tag{15}$$

$$Var[Y_t \mid X=x_t] = \sigma^2 \tag{16}$$

respectively, where $\bar{x}$ is the average x-value for the r test results

$$\bar{x} = \frac{1}{r}\sum_{t=1}^{r} x_t \tag{17}$$

Due to the limited number of tests the parameters α, β and σ cannot be determined with certainty. Rather, α, β and σ must be considered as outcomes of random variables A, B and Σ. The distributions of A, B and Σ are obtained by combining prior knowledge with the results of tests. The resulting posterior distribution is obtained by use of Bayes' theorem stating that, Lindley [6],

$$f_{AB\Sigma}(\alpha,\beta,\sigma \mid x_1,..,x_r,y_1,..,y_r) = \tag{18}$$

$$C\ f_{Y_1..Y_r}(y_1,..,y_r \mid x_1,..,x_r,\alpha,\beta,\sigma)\ f_{AB\Sigma}(\alpha,\beta,\sigma)$$

The left hand side is the posterior probability density function. It is proportional to the product of the likelihood function and the prior probability density function. The constant of proportionality C is a normalizing factor.

The random variables U_i are assumed mutually independent corresponding to independent tests and the likelihood function becomes

$$f_{Y_1..Y_r}(y_1,..,y_r \mid x_1,..,x_r,\alpha,\beta,\sigma) \propto \tag{19}$$

$$\frac{1}{\sigma^r} \exp[-\frac{1}{2\sigma^2}(Q^2+r(a-\alpha)^2+S_{xx}(b+\beta)^2)]$$

where '$\propto$' means 'proportional to'. The constants a, b, S_{xx} and Q are determined as

$$a = \bar{y} = \frac{1}{r}\sum_{i=1}^{r} y_i \tag{20}$$

$$S_{xx} = \sum_{i=1}^{r}(x_i-\bar{x})^2 = \sum_{i=1}^{r} x_i^2 - r\,\bar{x}^2 \tag{21}$$

$$S_{xy} = \sum_{i=1}^{r}(x_i-\bar{x})(y_i-\bar{y}) = \sum_{i=1}^{r} x_i y_i - r\,\bar{x}\,\bar{y} \tag{22}$$

$$S_{yy} = \sum_{i=1}^{r}(y_i-\bar{y})^2 = \sum_{i=1}^{r} y_i^2 - r\,\bar{y}^2 \tag{23}$$

$$b = \frac{S_{xy}}{S_{xx}} \tag{24}$$

$$Q^2 = S_{yy} - \frac{S_{xy}^2}{S_{xx}} \tag{25}$$

The prior probability density function for (A, B, Σ) is assumed to correspond to mutually independent variables, i.e.

$$f_{AB\Sigma}(\alpha,\beta,\sigma) = f_A(\alpha) f_B(\beta) f_\Sigma(\sigma) \tag{26}$$

The selection of prior distribution involves a compromise between accurate representation of prior knowledge and the desire to have a simple posterior joint distribution. Simple posterior distributions arise if the prior distributions are diffuse (no prior knowledge), concentrated at one value (complete prior knowledge) or are conjugate distributions. The prior knowledge for A, B and Σ in relation to offshore joints is from test series with joints of different geometry. Although some information is available on A it is convenient and sufficient to select a diffuse prior. The value of B is not known completely in advance but can, in general, be rather narrowly bounded. If a diffuse prior is chosen the resulting fatigue life predictions are unnecessarily pessimistic. A uniform prior in an interval $[m_1;m_2]$ is therefore selected for B. The standard deviation Σ is nonnegative. When many test series can be pooled the value of Σ can sometimes be assumed completely known. For a diffuse prior for $\ln\Sigma$ the resulting prior probability density is

$$f_{AB\Sigma}(\alpha,\beta,\sigma) \propto \frac{1}{\sigma} \quad , \quad \sigma>0, \quad m_1 \leqslant \beta \leqslant m_2 \tag{27}$$

where $1/\sigma$ represents the asymptotic limit density shape of a sequence of prior densities of (A,Σ) that approaches uniform density on the entire $(\alpha,\ln\sigma)$ plane.

The posterior distribution function is

$$f_{AB\Sigma}(\alpha,\beta,\sigma \mid x_1,..,x_r,y_1,..,y_r) \propto \tag{28}$$

$$\propto \frac{1}{\sigma^{r+1}} \exp[-\frac{1}{2\sigma^2}(Q^2+r(a-\alpha)^2+S_{xx}(b+\beta)^2)], \quad \sigma>0, \quad m_1 \leqslant \beta \leqslant m_2$$

The joint posterior distribution is thus somewhat complicated. Simplification is achieved by introducing random variables T_1, T_2 and T_3 as

$$T_1 = \frac{\sqrt{r}\,(A-a)}{\Sigma} \tag{29}$$

$$T_2 = \frac{\sqrt{S_{xx}}(B+b)}{\Sigma} \tag{30}$$

$$T_3 = \frac{Q^2}{\Sigma^2} \tag{31}$$

The joint posterior distribution of these variables is

$$f_{T_1T_2T_3}(t_1,t_2,t_3) \propto \exp(-\frac{1}{2}t_1^2)\exp(-\frac{1}{2}t_2^2)\,t_3^{\frac{r-2}{2}-1}\exp(-\frac{1}{2}t_3) \tag{32}$$

$$-\infty<t_1<\infty, \quad 0<t_3<\infty, \quad \frac{\sqrt{S_{xx}t_3}(m_1+b)}{Q}<t_2<\frac{\sqrt{S_{xx}t_3}(m_2+b)}{Q}$$

From this equation follows that T_1 is independent of (T_2,T_3), with

$$T_1 \in N(0,1) \tag{33}$$

It further follows that

$$T_3 \in \chi^2(r-2) \tag{34}$$

where $\chi^2(r-2)$ denotes a chi square distribution with $r-2$ degrees of freedom. The probability density function of T_2 conditional upon T_3 is a truncated normal distribution on the interval $\sqrt{S_{xx}t_3}(m_1+b)/Q<t_2<\sqrt{S_{xx}t_3}(m_2+b)/Q$

The material parameters m and K can now be expressed as

$$m = B = -b + \frac{Q\,T_2}{\sqrt{S_{xx}T_3}} \tag{35}$$

$$K = \exp[A + B\bar{x} + \Sigma U] = \exp[a + \frac{Q\,T_1}{\sqrt{rT_3}} + (-b + \frac{Q\,T_2}{\sqrt{S_{xx}T_3}})\bar{x} + \frac{Q\,U}{\sqrt{T_3}}] \tag{36}$$

where T_2 is set equal to zero and Q is replaced by Q_1 if the value of B is fixed. As mentioned earlier the distribution of U is a standardized normal distribution.

A statistical analysis for 10 test results for various tubular joints under constant amplitude loading has been performed. Test joints and results are shown in Table 1, from Gibstein [7].

TABLE 1 Test data				
Joint type	Test environment	Strain range	S [MPa]	N
T	air	$1740 \cdot 10^{-6}$	348.0	206000
T	air	$1390 \cdot 10^{-6}$	278.0	580000
T	air	$1085 \cdot 10^{-6}$	217.0	866000
T	air	$1100 \cdot 10^{-6}$	220.0	1600000
T	air	$960 \cdot 10^{-6}$	192.0	1070000
T	sea water	$1307 \cdot 10^{-6}$	261.4	591200
T	sea water	$715 \cdot 10^{-6}$	143.0	3900000
Y	air	$834 \cdot 10^{-6}$	166.8	1220000
K	air	$829 \cdot 10^{-6}$	165.8	1490000
K overlap	air	$804 \cdot 10^{-6}$	160.8	4600000

These results are shown in Fig.2 from Gibstein [7]. The stress range has been obtained by multiplying the strain range by Youngs modulus $2.0 \cdot 10^5$ MPa.

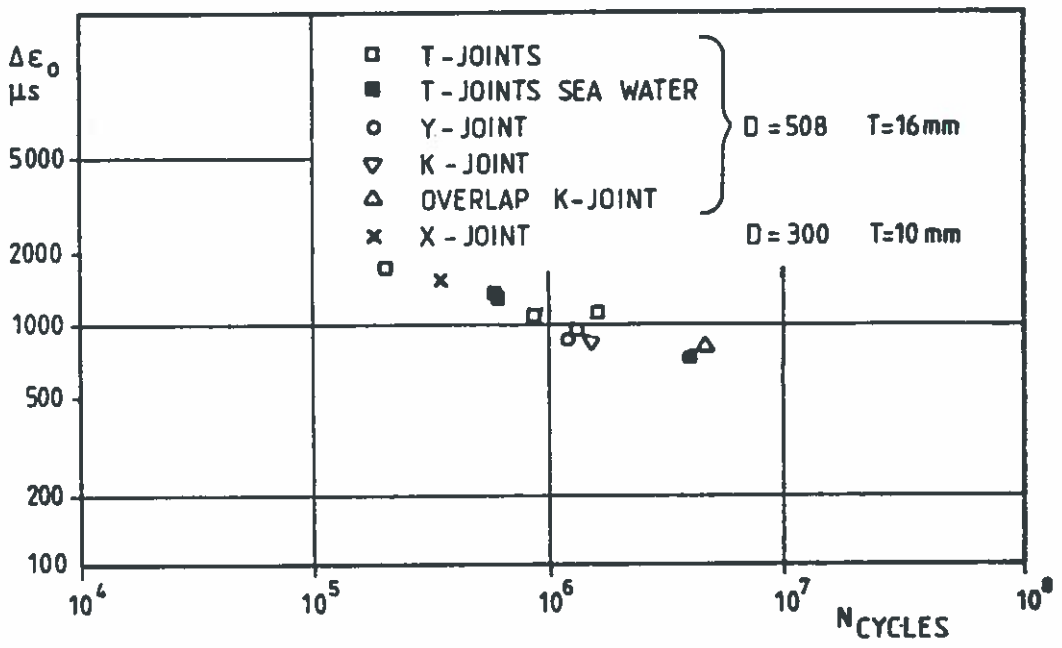

Figure 2 DnV fatigue test results, based on DnV's SCF and hot spot strain definition.

The constants r, $\bar{x}$, a, b, Q and S_{xx} are computed,

$$r=10,\ \bar{x}=5.335,\ a=13.938,\ b=-2.934,\ Q=1.164,\ S_{xx}=0.719 \qquad (37)$$

The estimate $\hat{\sigma}$ of the standard deviation becomes

$$\hat{\sigma} = \frac{Q}{\sqrt{r-2}} = 0.41 \qquad (38)$$

This is somewhat smaller than for the T-curve, where tests of different details

have been pooled together without a detailed stress analysis for each case.

3. RELIABILITY ANALYSIS

The failure criterion is expressed as

$$\Delta - D \leqslant 0 \tag{39}$$

where the damage D is computed according to the Miner damage hypothesis and the value at failure Δ is taken as a random variable, to account for the model uncertainty. A summary of experimental results in Wirsching [8] has indicated a lognormal distribution for Δ with median 1 and coefficient of variation of 0.3. Both the 'resistance' Δ and the 'loading' D are thus uncertain. The failure probability is computed by a first- or second-order reliability method as explained in detail in Madsen et al.[9]. The resulting approximation to the failure probability P_F is for a first-order reliability method

$$P_F \approx \Phi(-\beta) = \Phi(-|\mathbf{u}^*|) \tag{40}$$

where β is the first-order reliability index, and $\mathbf{u}^*$ is the design point. The design point written as $\beta\boldsymbol{\alpha}$, where $\boldsymbol{\alpha}$ is a unit directional vector and its components are called the sensitivity factors. α_i^2 can be interpreted as the fraction of total uncertainty which is caused by uncertainty in basic variable i. The sensitivity of the first order reliability index to changes in distribution parameters for the uncertain parameters can also be expressed in terms of the sensitivity factors. For a normally distributed variable with mean value μ_i and standard deviation σ_i is shown, Madsen et al.[9]

$$\frac{\partial \beta}{\partial \mu_i} = -\frac{\alpha_i}{\sigma_i} \tag{41}$$

$$\frac{\partial \beta}{\partial \sigma_i} = -\frac{\beta \alpha_i^2}{\sigma_i} \tag{42}$$

4. AN EXAMPLE

As the example structure is chosen an early version of a tripod tower platform, Michelsen and Meek [10]. The tripod tower platform is shown in Fig.3. For this platform concept fatigue strength is a governing design criterion in many cross sections and joints. The tripod tower platform consists of a piled foundation, three legs and a center column which supports the top-side facilities. The center column is laterally supported by the three inclined legs. There are several fatigue critical areas in the structure and this analysis is for a cross section just below the top node on one of the inclined legs. Four points around the circumference have been selected as also shown in Fig.3 and results are presented for Point 4. The wave loading is computed by diffraction theory for the top node and the column above it and by Morison's equation for the structure below the node. The structural response from regular waves is obtained by a forced vibration method using the mode superposition principle after the natural frequencies and the mode shapes have been determined. Axial stresses due to the axial force and the bending moment are computed and the stress transfer functions are thereby determined.

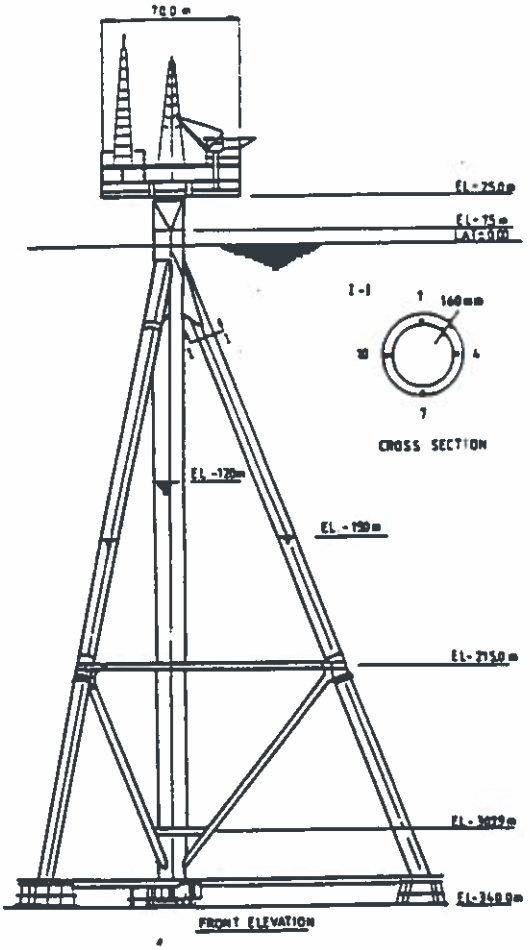

Figure 3 Tripod tower platform concept.

This is done for two wave directions 90 degrees apart. Transfer functions for waves of opposite directions have the same moduli due to symmetry. For this illustration the stress transfer functions are assumed deterministic.

Uncertainties included in the analysis are modeled as explained in Madsen et al [11]. The uncertainties refer to

- main wave direction probabilities (Z_1)
- distribution of significant wave height (Z_2)
- distribution of mean wave period (Z_3)
- wave energy spreading function (Z_4)
- stress concentration factor (Z_5)
- T-curve, position (Z_6), slope (Z_7), thickness effect (Z_8)
- value of Miner's damage index at failure (Z_9)

Figure 4 shows the reliability index and corresponding first order approximation to the failure probability for various life times. Reliabilities are computed for a stress concentration factor with a mean value of five and a standard deviation of 0.5. The purpose with the analysis is to provide an allowable stress concentration factor for the detailed design of the top node.

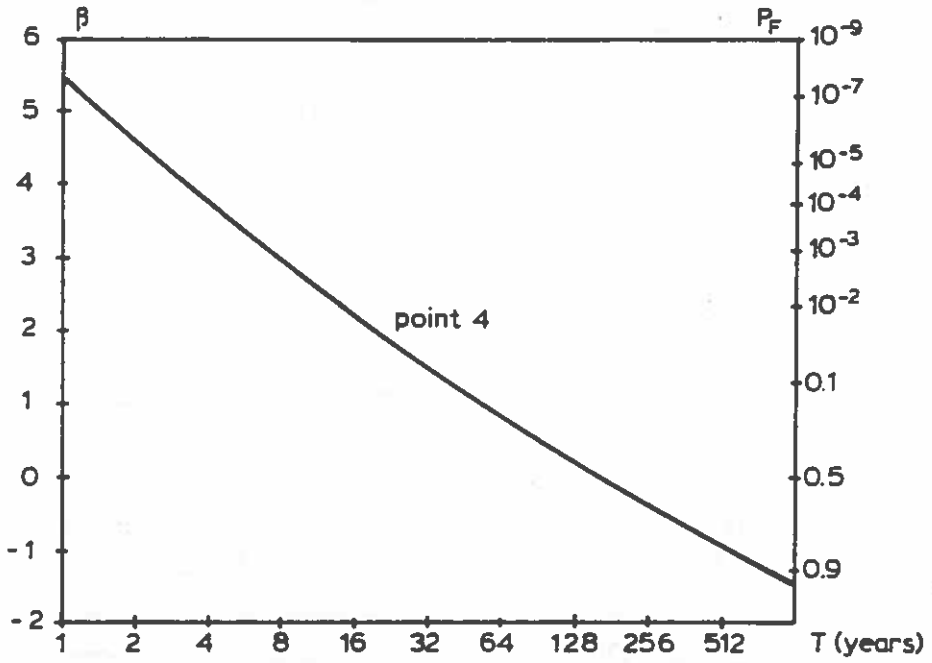

Figure 4 Reliability index and nominal failure probability.

Table 2 shows the sensitivity factors for $T=32$ years.

TABLE 2 Sensitivity factors

Reliability index $\beta = 1.42$
Nominal failure probability $P_F = 7.7 \cdot 10^{-2}$

Variable Number	Source of Uncertainty	Distribution Type	Sensitivity Factor
Z_1	Main wave direction	normal	0.064
Z_2	Sea scatter diagram H_S	lognormal	0.255
Z_3	Sea scatter diagram T_Z	lognormal	-0.205
Z_4	Wave energy spreading	lognormal	-0.143
Z_5	SCF	normal	0.382
Z_6	S-N curve position	lognormal	-0.773
Z_7	S-N curve slope	lognormal	-0.192
Z_8	S-N curve thickness reduction	lognormal	-0.223
Z_9	Miner's damage index at failure	lognormal	-0.195

The total uncertainty is divided between uncertainty in loading Z_1—Z_5, 28%, uncertainty in S-N curve Z_6—Z_8, 68%, and model uncertainty in the damage accumulation model Z_9, 4%. It further follows that if the mean value of the stress concentration factor can be reduced by one, then the reliability index is increased by approximately 0.382/0.5=0.764 to 2.18. The corresponding change in the nominal failure probability is from $7.7 \cdot 10^{-2}$ to $1.5 \cdot 10^{-2}$.

5. SUMMARY AND CONCLUSIONS

A summary of sources of uncertainty for the fatigue strength of welded joints has been presented. Two different formulations based on $S-N$-curves and on a fracture mechanics approach are described together with their similarities and differences. Some statistics are presented for the T-curve and for tubular joint experiments from DnV. The effect of fatigue strength uncertainty has been compared to the effect of other uncertainties in a probabilistic fatigue analysis of a joint in a tripod tower platform.

6. REFERENCES

1. Det norske Veritas: 'Rules for the Design, Construction and Inspection of Offshore Structures, Appendix C Steel Structures', Reprint with Corrections, 1982.
2. Department of Energy: 'New Fatigue Design Guidance for Steel Welded Joints in Offshore Structures', Recommendations, 1982.
3. Guerney, T.R.: 'The Basis for the Revised Fatigue Design Rules in the Department of Energy Offshore Guidance Notes,' in Proceedings, Second International Conference on Offshore Welded Structures, The Welding Institute, London, 1982.
4. Paris, P.C. and F. Erdogan: 'A Critical Analysis of Crack Propogation Laws,' Journal of Basic Engineering, ASME, Vol. 85, 1963, pp.528-534.
5. Madsen, H.O.: 'Bayesian Fatigue Life Prediction', in, Probabilistic Methods in the Mechanics of Solids and Structures, Springer Verlag, 1985, pp.395-406.
6. Lindley, D.V.: Probability and Statistics 2, Inference. Cambridge University Press, 1965.
7. Gibstein, M.: 'Fatigue Strength of Welded Tubular Joints Tested at Det norske Veritas Laboratories,' in Proceedings, International Conference Steel in Marine Structures, Paris, October 1981.
8. Wirsching, P.: 'Fatigue Reliability for Offshore Structures,' Journal of Structural Engineering, ASCE, Vol. 110, No.10, 1984, pp. 2340-2356.
9. Madsen, H.O., Krenk, S. and N.C. Lind: Methods of Structural Safety, Prentice-Hall Inc., Englewood Cliffs, New Jersey, 1986.
10. F.C.Michelsen and J.Meek: 'Development of the Tripod Tower Platform Design', in Proceedings, Boss'82, MIT, Cambridge, 1982, pp.847-863.
11. Madsen, H.O., Skjong, R. and M. Moghtaderi-Zadeh, 'Experience on Probabilistic Fatigue Analysis of Offshore Structures,' in Proceedings, OMAE Conference, Tokyo, Japan, 1986, Vol.II, pp.1-8.